# Submarine mass movements on continental margins

HOMA J. LEE*, JACQUES LOCAT†, PRISCILLA DESGAGNÉS†, JEFFREY D. PARSONS‡, BRIAN G. McADOO§, DANIEL L. ORANGE¶, PERE PUIG**, FLORENCE L. WONG*, PETER DARTNELL* *and* ERIC BOULANGER†

**United States Geological Survey, 345 Middlefield Road, Menlo Park, CA 94025, USA (Email: hjlee@usgs.gov)*
*†Département de Géologie et de Génie Géologique, Laval University, Québec G1K 7P4, Canada*
*‡School of Oceanography, University of Washington, Seattle, WA 98195, USA*
*§Department of Geology and Geography, Vassar College, Poughkeepsie, NY 12604, USA*
*¶AOA Geophysics, Inc., Moss Landing, CA 95039, USA*
***Institut de Ciències del Mar, Barcelona 08003, Spain*

**ABSTRACT**

Submarine landslides can be important mechanisms for transporting sediment down sloping seabeds. They occur when stresses acting downslope exceed the available strength of the seabed sediments. Landslides occur preferentially in particular environments, including fjords, active river deltas, submarine canyons, volcanic islands and, to a lesser extent, the open continental slope. Evaluating the relative stability of different seabeds requires an understanding of driving stresses and sediment strength. Stresses can be caused by gravity, earthquakes and storm waves. Resisting strength can be reduced by pore water and gas pressures, groundwater seepage, rapid sediment deposition, cyclic loading and human activity. Once slopes have become unstable or have failed, strength may continue to decrease, leading to sediment debris flows and possibly turbidity currents. Recent submarine landslide research has: shown that landslides and sediment waves may generate similar deposits, which require careful interpretation; expanded our knowledge of how strength develops in marine sediment; improved techniques for predicting sediment rheology; and developed methodologies for mapping and predicting the medium- to large-scale regional occurrence of submarine landslides.

**Keywords** Landslides, earthquakes, rheology, shear strength, Humboldt Slide, sediment waves.

## INTRODUCTION

This paper considers **submarine mass movements**, which result when marine sediment or rock is loaded by the environment until it fails. These events are also referred to as **landslides**, although not all involve actual sliding of one mass of material over another. Mass movements can result either from an increase in the environmental loads, a decrease in the strength of the sediment/rock, or a combination of load increase and strength decrease. The resulting types of gravity-driven sediment transport events differ from such processes as fluid-mud migration in that the moving sediment has previously been formed into consolidated material possessing strength and stiffness. Submarine landslides can subsequently transform into debris flows or even turbidity currents (Hampton, 1972), but such transformations do not always occur. Likewise, turbidity currents and sediment flows can occur by means other than an initial landslide (e.g. hyperpycnal flows from rivers, Mulder & Syvitski, 1995). Parsons *et al*. (this volume, pp. 275–337) review flows including fluid mud, debris flows and turbidity currents, and this paper focuses on submarine landslides: how and when these events produce subsequent flows. This paper also focuses on how shear strength develops in marine sediment, because knowledge of shear strength is essential in predicting slope stability.

## HISTORIC DEVELOPMENT OF UNDERSTANDING

Knowledge about submarine landslides extends back at least to the 1929 Grand Banks incident (Heezen & Ewing, 1952), when a magnitude 7.2 earthquake set off a sequence of events that led to an orderly progression of submarine cable breaks south of Newfoundland. Following the event, the scientific community began a discussion that has continued to the present concerning exactly what caused the cable breaks and how the resulting processes related to the initial earthquake loading. Terzaghi (1956) proposed a mechanism that is now known to be almost certainly false: that the cable breaks resulted from an advancing front of liquefaction within the seafloor sediment. That is, the sediment did not move but rather a liquefaction wave passed through the sediment. Heezen & Ewing (1952) presented the more convincing argument that the earthquake 'jarred the continental slope and shelf, setting landslides and slumps in motion'. These mass movements 'raced downward, and by the incorporation of water, the moving sediment was transformed into turbidity currents'. The currents started in different submarine canyons; as the flows down each canyon joined, the currents grew larger. Ultimately the combined current covered the floor of a 300-km-wide bight. The currents easily snapped the cables and proceeded toward the south for at least 600 km.

The model suggested by Heezen & Ewing (1952) has generally withstood the test of time, but the details of the event are not yet fully understood. At one point scientists thought that the initial failure might have been one or two very large landslides. Heezen & Drake (1964) found what appeared to be a 500-m-thick displaced block on the upper part of the Laurentian Fan, and Emery *et al*. (1970) found a similar scale feature 40 km to the west. Later investigations (Piper & Normark, 1982) showed that these features were not displaced blocks at all, but were parts of eroded terrain that only appeared to be blocks when viewed along individual tracklines. Recent studies involving high-resolution sidescan sonar and sub-bottom profiles show there were probably many small failures in the source region having a variety of scales and morphologies. These include rotational, retrogressive slumps that passed downslope to form debris flows that carried blocks and formed channels. Piper *et al*. (1999) inferred that the debris flows, in turn, transformed into turbidity currents (Fig. 1). A problem that has still not been fully resolved is the difference in sediment types between that of the

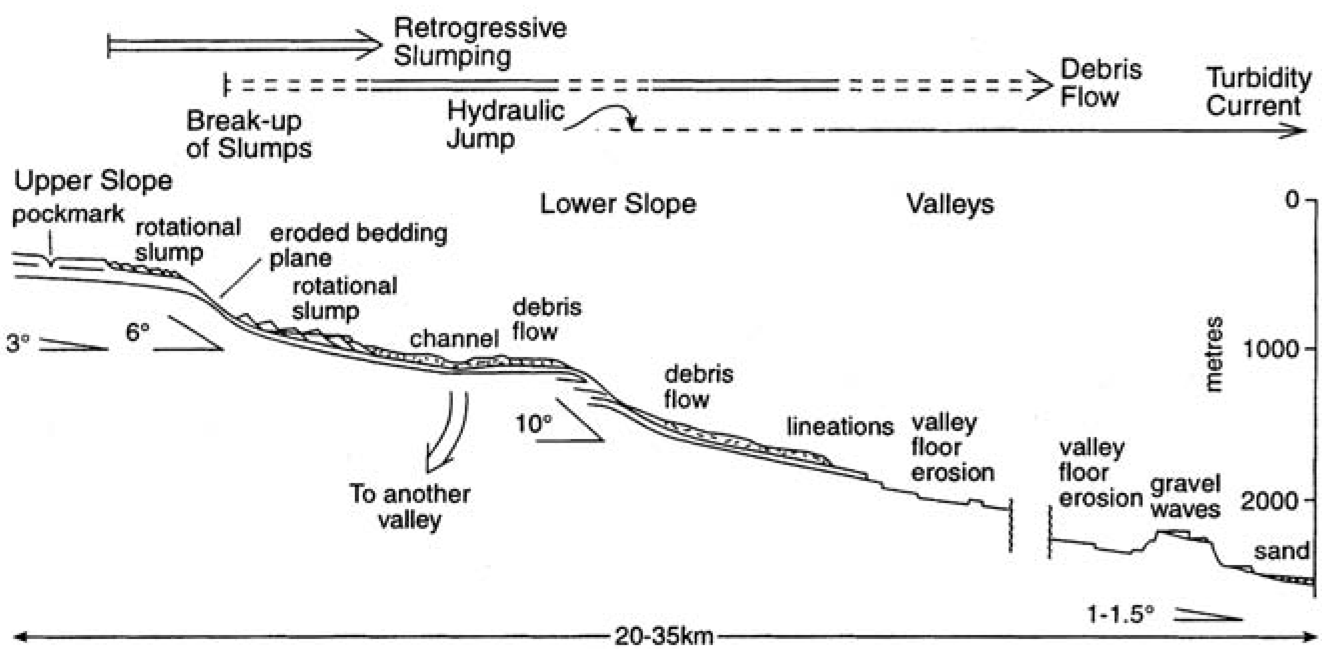


**Fig. 1** Interpretative drawing from Piper *et al*. (1999) showing the sequence of sediment facies developed downslope of the Grand Banks margin.

source region, where the sediment is dominantly fine grained, and that of the Sohm Abyssal Plain, where the massive turbidite deposited in 1929 is predominantly sand (Piper & Aksu, 1987). The continuing discussion of the Grand Banks event, which occurred 75 yr ago, is an indication of the difficulty in understanding events that occur out of sight and in an environment that has similarities to the subaerial world but displays many differences.

Another burst of interest in submarine landslides occurred in 1969 when Hurricane Camille struck the coast of Louisiana. Wave heights of 21–23 m were recorded near the South Pass portion of the Mississippi Delta, and three offshore drilling platforms were badly damaged or destroyed. One of the platforms was found, half-buried in mud and displaced 30 m downslope. Investigations after the hurricane showed that bottom relief had changed by as much as 12 m. The mode of damage to the platforms (piles bent rather than pulled out) led investigators to believe that sediment failure was a primary cause for the platform damage (Sterling & Strohbeck, 1973; Bea *et al*., 1983). A period of active research followed, leading to models of storm-wave-induced slope failure. There also was renewed interest in the deltaic sediment strength, which resulted in a new appreciation for the role of rapid sediment accumulation in generating low strength and excess pore-water pressures, the importance of weak layers, and the development of instrumentation to measure excess pore pressures (Garrison, 1977).

In the late 1980s (Moore *et al*., 1989; Holcombe & Searle, 1991), following improvements in seafloor mapping techniques (e.g. long-range sidescan sonar system GLORIA), the marine community became aware that the largest landslides on Earth occur under water. These giant landslides, having run-out distances over 200 km and volumes exceeding 5000 $km^3$, occur most commonly off volcanic islands, and are particularly well displayed off Hawaii and the Canary Islands. However, giant landslides also occur on continental margins and include the massive Storegga landslide complex off Norway (Bryn *et al*., 2003). The mechanics are not well understood of how these landslides are triggered; however, strength development in active volcanoes and gas hydrate dissociation on continental margins appear to play a part (Kayen & Lee, 1991).

The role of submarine landsides in producing **tsunamis** has recently received attention following the 1998 magnitude 7.0 earthquake that occurred off the northern coast of Papua New Guinea. Two thousand people died from tsunami waves that washed ashore after the earthquake. This event sparked considerable discussion and debate (Tappin *et al*., 1999; Geist, 2000), but the majority of scientists presently believe that the large sea waves were not generated directly by the earthquake motions but rather by a large underwater landslide initiated by seismic shaking. Marine surveys have identified an amphitheatre-shaped region and complex topography, which have been interpreted, respectively, as the erosion scar and a series of large, displaced blocks having a thickness of up to 700 m (Tappin *et al*., 2003).

Landslide-induced tsunamis also were observed during the 1964 Alaska earthquake in Resurrection Bay and Port Valdez and many other locations off the southern coast of Alaska (Coulter & Migliaccio, 1966; Lemke, 1967). Coastal and submarine slope failures caused loss of shoreline and coastal facilities. Tsunamis generated by the landslides repeatedly inundated the coastal areas, causing many fatalities and considerable property damage to the communities. In addition to earthquake-induced landslides, fjords are susceptible to slope failures, particularly those caused by low tides. The coastline and seafloor of Kitimat Arm, British Columbia, failed in 1975 just after a low tide. The deposits remaining after the failure were mapped by Prior *et al*. (1982a) and these images showed a wide range of recognizable features, including outrunner blocks that probably raced ahead of the rest of the landslide debris through a process of hydroplaning. Similar failures occurred in Skagway Alaska in 1994 (Rabinovich *et al*., 1999) and Howe Sound, British Columbia in 1955.

## CLASSIFICATION

The discussion above provides a background for the scale, importance and continuing debate related to the field of submarine landslides. However, a classification system is needed to consider these events in greater detail. This paper follows the terminology recommended by Varnes (1958) with some modification (Fig. 2). Other classification

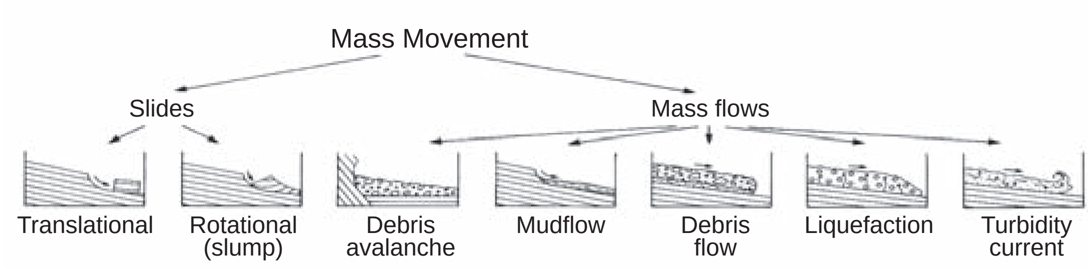


**Fig. 2** General landslide classification. See text for further details. (Modified from Varnes, 1958.)

schemes have been provided by Prior (1984), Norem *et al*. (1990) and Mulder & Cochonat (1996). **Slope failure** occurs when the downslope driving forces acting on the material composing the seafloor are greater than the forces acting to resist major deformations. Following slope failure, the failed mass moves downslope under the influence of gravity and possibly other forces. Thus, **mass movement** is defined as the movement of the failed material driven directly by gravity or other body forces, rather than tractive stresses associated with fluid motion. If the moving sediment takes a form that resembles a viscous fluid, the feature is termed a **mass flow (gravity flow)**. Such a failure has considerable internal deformation with innumerable invisible or short-lived internal slip surfaces. **Slides** are movements of essentially rigid, internally undeformed masses along discrete slip planes. In the literature, all forms of mass movement are occasionally referred to as **slumps**. Correctly, slumps are a kind of slide in which blocks of failed material rotate along curved slip surfaces. The other kind of slide involves movement on a planar surface and is referred to as a **translational slide**. In each of these types, movement can be fast or slow. Extremely slow movement is called **creep**.

Submarine slides can become mass flows (gravity flows) as the failed mass progressively disintegrates and continuous downslope movement occurs (Morgenstern, 1967; Hampton, 1972). End-member products of disintegrating slides have been given special names. **Debris flows** are flows in which the sediment is heterogeneous and may include larger clasts supported by a matrix of fine sediment. **Mud flows** involve predominantly muddy sediment. **Turbidity currents** involve the downslope transport of a relatively dilute suspension of sediment grains that are supported by an upward component of fluid turbulence (Parsons *et al*., this volume, pp. 275–337). Turbidity currents are often generated by the disintegration and dilution of slides or debris flows, although they also may be generated independently of other mass wasting events. **Liquefaction flows** occur when a loosely packed sediment collapses under environmental conditions such as cyclic loading from earthquakes or waves. The grains temporarily lose most contact with one another, and the particle weight is temporarily transferred to the pore fluid, producing excess porewater pressures. The material may flow downslope under the influence of gravity or spread laterally under the influence of stresses induced by earthquakes or perhaps storm waves.

As discussed above, recent surveys have revealed giant submarine landslides that involve the failure of thousands of cubic-kilometres of rock and sediment (Moore *et al*., 1989). When these landslides have disintegrated into smaller pieces (which may still be quite large) and have clearly moved very rapidly without a channel, they are referred to as **debris avalanches** (Varnes, 1958).

## ENVIRONMENTS

Submarine landslides are not distributed uniformly over the world's oceans, but instead they tend to occur commonly where there are thick bodies of soft sediment, where the slopes are steep, and where the loads exerted by the environment are high. These conditions are met in fjords, deltas, submarine canyons and on the continental slope.

### Fjords

Fjords with high sediment accumulation rates are one of the environments most susceptible to failure, both in terms of the proportional areal extent of deposits that can become involved in mass movement and also in terms of the recurrence interval of slope failures at a given location. **Fjords** are glacially eroded steep-walled valleys that have been inundated by the sea and are typically fed by sediment-laden rivers and streams that drain glaciers. These factors lead to environmental conditions that are highly conducive to slope failure. There is typically a delta at the head of the fjord, formed by streams draining the remnant of the glacier that initially eroded the valley, with foreset beds that dip at 5° to 30° between 10 m and 50 m water depth. Below this, the prodelta dips at angles of 0.1° to 5° to the flat basin floor, typically at depths between 100 m and 1000 m (Syvitski *et al*., 1987).

The glacial streams feeding fjord deltas carry both rock flour and coarse sediment, which form deposits that easily lose strength when shaken by an earthquake. In addition, the sediment may be deposited so rapidly that pore-water pressures cannot dissipate completely, resulting in an under-consolidated state and abnormally low strength. Abundant organic matter brought down with the glacial debris also can decay and produce bubble-phase gas within the seabed that can lead to elevated pore-water pressure and low strength. Some fjord-delta deposits are so near instability that they fail during greater than average low tides, during which the supporting forces of the fjord waters themselves are temporarily removed from the sediment. Many of these steep slopes are composed of weak sediment that is susceptible to cyclic loading, and may fail seasonally or semi-continuously via numerous small-scale slope failures. Slope failures of a seasonal or semi-continuous nature have been reported in many Canadian fjords, including Bute Inlet (Syvitski & Farrow, 1983; Prior *et al*., 1986a), Knight Inlet (Syvitski & Farrow, 1983) and North Bentinck Arm (Kostaschuk & McCann, 1983). In some situations, fjord-head delta slopes may fail infrequently and produce catastrophic effects, such as occurred in Valdez (Coulter & Migliaccio, 1966), Seward (Lemke, 1967) and Whittier (Kachadoorian, 1965) during the 1964 Alaska earthquake or in Kitimat Arm, Canada (Prior *et al*., 1982a, 1982b).

In addition to the fjord-delta deposits, the side-wall slopes of fjords also can be unstable. Deposition of suspended sediment on the steep (10° to 90° overhangs) submerged valley sides can frequently lead to small slope failures (Farrow *et al*., 1983). Even more important are slope failures on side-entry deltas that build out rapidly onto the side-wall slopes (e.g. Howe Sound, Canada; Terzaghi, 1956; Prior *et al*., 1981).

Finally, the deep fjord basins, which tend to have slopes of less than 0.1°, commonly receive failed sediment masses and flows from the side walls and fjord-head deltas. If these landslides incorporate enough water during their movement, they can evolve into gravity flows and turbidity currents. Submarine channels can feed these gravity flows and turbidity currents into and across the basins (Syvitski *et al*., 1987).

Fjords are commonly found in rugged mountainous terrain, and the unstable fjord-head deltas and side-entry deltas are commonly the only flat land available for coastal development. Not only do these developments become vulnerable to natural slope failure, but human activities also can lead to additional slope failures. For example, a river channel stabilization programme at Howe Sound (Terzaghi, 1956) caused rapid delta growth to be localized and probably contributed to ultimate slope failure on the delta.

#### Active river deltas on the continental shelf

Active river deltas are another likely site for slope instability. Rivers contribute large quantities of sediment to relatively localized areas on the continental margins. Depending upon a variety of environmental factors, including rate of sediment influx, wave and current activity, and the configuration of the continental shelf and coastline, thick deltaic deposits can accumulate fairly rapidly. These sediment wedges can become the locations of sediment instability and landsliding. To create large, deep-seated landslides, a thick deposit containing comparatively low-strength sediment or containing weak zones is needed. Most of the continental shelves were subaerially exposed during the last glacial cycle, so most sediment on the shelves from that time or before has been eroded, desiccated or otherwise diagenetically altered. Accordingly, the strengths of these older deposits are commonly high enough to resist downslope gravitational stresses on the gentle shelves, and all but the very greatest storm- and earthquake-induced stresses. As a result of rapid sedimentation, young deposits tend to have relatively low strength. In addition, decaying organic matter can produce bubble-phase gas that can further reduce strength. These locations may fail under gravitational loading (due to the slope angle alone) or during storms or earthquakes.

The locations of the major sedimentary depocentres provide some information on where undersea landslides might be expected on the continental shelf. Glacially fed rivers debouching into the Gulf of Alaska or adjacent sounds and inlets contribute $450 \times 10^6$ tons of sediment per year (Milliman & Meade, 1983). Slope failures have been identified in modern sediment all along the margin including within the Kayak Trough (Molnia *et al.*, 1977) and Alsek prodelta (Schwab & Lee, 1983; Schwab *et al.*, 1987). Also included are major landslides on the Copper River prodelta (Reimnitz, 1972), off Icy Bay and the Malaspina Glacier (Carlson, 1978; Lee & Edwards, 1986) and off Yakutat (Schwab & Lee, 1983). The high incidence of landsliding arises because of the intensity of earthquake and storm-wave loading (Schwab & Lee, 1983), the thickness of modern sediment, and the tendency of glacial rock flour to lose strength when cyclically loaded.

The Mississippi River contributes the most sediment to the sea of any single river within North America ($2.1 \times 10^8$ tons of sediment per year; Milliman & Meade, 1983). Most of this sediment is deposited in front of the modern bird-foot or Balize delta, a delta-lobe that has been in existence for only 600–800 yr (Fisk *et al.*, 1954). The distributary mouths of the modern delta build seaward at rates varying from 50 to 100 m yr$^{-1}$ depending on the particular distributary. Seaward of these distributaries, the sediment accumulation rates are very high, reaching 1 m yr$^{-1}$ or more (Coleman *et al.*, 1980). The sediment consists mostly of clay-sized particles, rich in organic matter that is rapidly degraded to gas (mainly methane and carbon dioxide). Rapid sedimentation and gas charging lead to high excess pore-water pressures and a state of extreme underconsolidation. Although the gradients of the delta front are very low (ranging from 0.2° to 1.5°), evidence of slope failure is widespread, including submarine gullies (Shepard, 1955) and extensive fields of sediment instability features all along the delta front (Coleman *et al.*, 1980). Another subaqueous delta that displays considerable landslide activity is the Huanghe (Prior *et al.*, 1986b), where the gradient is so gentle that the sediment collapses upon itself (collapse depression) rather than deforming downslope.

#### Submarine canyon-fan systems

Submarine canyon-fan systems serve as conduits for passing large amounts of sediment from the continental shelf to the deep sea. The presence of extensive, thick sediment fans and abyssal plains off the coasts of many areas testifies to the importance of mass-movement mechanisms associated with these systems, which are capable of bringing sand-size and even coarser particles to locations hundreds of kilometres from shore. Landsliding appears to be an element that allows the formation of massive submarine fans. According to one model (Hampton, 1972), sediment accumulations in canyon heads begin to move as coherent landslide blocks following some triggering event, such as an earthquake or storm. As the blocks move downslope, the resulting jostling and agitation causes disintegration and subsequent incorporation of water. The debris flow that is produced displays increasingly fluid-like behaviour. As the debris flow continues on its path, further dilution by surrounding water occurs, particularly as sediment is eroded from the front of the flow. Ultimately, a dilute turbulent cloud is created that has a density below 1.1 g cm$^{-3}$. The resulting turbidity current can flow for long distances (up to hundreds of kilometres) at moderate to high velocities (Parsons *et al.*, this volume, pp. 275–337).

Landsliding, particularly within submarine canyons, appears to be an important, if not essential, part of the process of building deep-sea fans, which are among the most extensive sedimentary features of the Earth's surface. However, the circumstances surrounding these slope failures and their subsequent conversion into turbidity currents are poorly understood. Storms cause sediment movement in canyons, perhaps by inducing failure near the canyon heads (Marshall, 1978; Puig *et al.*, 2003) or perhaps by introducing or resuspending enough sediment to form a gravity current directly (Shepard & Marshall, 1973; Reynolds, 1987). Earthquakes also cause landslides in canyon heads and subsequent turbidity-current flow (Malouta *et al.*, 1981; Adams, 1984), but details of this process are lacking. Major earthquakes and other shocks do not always cause canyon-head landslides (Dill, 1964). However, landslides can occur under aseismic conditions (Shepard, 1951). Landsliding in canyon heads and turbidity-current mobilization were probably more common during glacial stages (Nelson, 1976; Barnard, 1978) because of increased sediment supply, proximity of river sediment source to steep canyon slopes, and possibly increased storm-wave loading resulting from lowered sea level.

#### The open continental slope

A final common environment for undersea landsliding is the intercanyon area of the continental slope. Landslides have been reported all around the globe along continental slopes removed from submarine canyon-fan systems. Included are slopes off southern California (Buffington & Moore, 1962; Haner & Gorsline, 1978; Field & Clarke, 1979; Nardin *et al*., 1979a,b; Ploessel *et al*., 1979; Field & Edwards, 1980; Field & Richmond, 1980; Hein & Gorsline, 1981; Thornton, 1986), central and northern California (Field *et al*., 1980; Richmond and Burdick, 1981), Alaska (Marlow *et al*., 1970; Hampton & Bouma, 1977; Carlson *et al*., 1980), Gulf of Mexico (Lehner, 1969; Woodbury, 1977; Booth & Garrison, 1978; Booth, 1979), and Atlantic coast (Embley & Jacobi, 1977; McGregor, 1977; Knebel & Carson, 1979; McGregor *et al*., 1979; Malahoff *et al*., 1980; Cashman & Popenoe, 1985; O'Leary, 1986).

The COSTA (Continental Slope Stability) Project (Canals *et al*., 2004) investigated large submarine landslides on the open continental slope around the European continent and off Africa. There are several very large features, particularly off Norway. The largest is the Storegga Slide, off central Norway, with a runout distance of 810 km and a volume of 2400 to 3200 km$^3$. Others off Norway include the Traenadjupet Slide, off northern Norway, and the Malenbukta Slide off Svalbard (Haflidason *et al*., 2004). The occurrence of these large landslides off Norway appears to be related to glacial stages. At Storegga, contrasting sedimentation conditions produced clay layers during interglacial stages overlain by glaciomarine layers produced during glacial stages. Owing to rapid sedimentation, some of these layers contain excess pore pressures. The resulting weak layers provide a plane along which failure can occur, although the failures are still probably triggered by earthquakes (Bryn *et al*., 2003; Canals, 2004). Large failures have occurred at the site of the Storegga Slide at semi-regular intervals over the past 500 kyr, but the most recent large failure occurred 8200 yr ago. Other large failures investigated by COSTA include the BIG 95 Slide off the east coast of Spain in the Mediterranean and the Canary Slide in the east-central Atlantic off Africa (Canals *et al*., 2004).

Open-continental-slope failures are found near river mouths and far removed from them, as well as in both arid and humid climates. Ages of the slope failures are seldom known (the Storegga Slide is one of the few exceptions), so investigators cannot determine whether they occurred under glacial or interglacial conditions. Many were probably seismically induced because the typical gradients of continental slopes are 5° or less and the seabed should be statically stable (unless very weak layers are present), and because storm-wave loading is seldom a major factor much below the shelf break (Lee & Edwards, 1986). Some failures appear to be related to the presence of relatively weak sediment layers. The occurrence of failures seems to correlate with sediment accumulation rate, bathymetric gradient, seismicity, and presence of bubble-phase gas and gas hydrate, but the relationships are complex (Field, 1981). The continental slope is an area of extensive mass wasting; however, estimating recurrence intervals for slope failures in this environment is often difficult. Predicting the likelihood of failure (Syvitski *et al*., this volume, pp. 459–529) at any specific location can be accomplished using three-dimensional seismics and deep sediment boreholes, but the process is very expensive. Landslides on the open slope are probably an important sediment-transport mechanism and pose hazards to offshore development.

## STATISTICS OF SUBMARINE LANDSLIDES

Booth *et al*. (1993) presented statistical information on a large suite of submarine landslides on the USA Atlantic margin. The Atlantic margin is representative of passive margins, as far as landslide prevalence is concerned, and includes both glaciated and non-glaciated sections. The authors reviewed the characteristics of 179 individually mapped landslides and prepared a map showing the location of each. The statistical information showed that the features in their study most commonly originated on a seafloor gradient of between

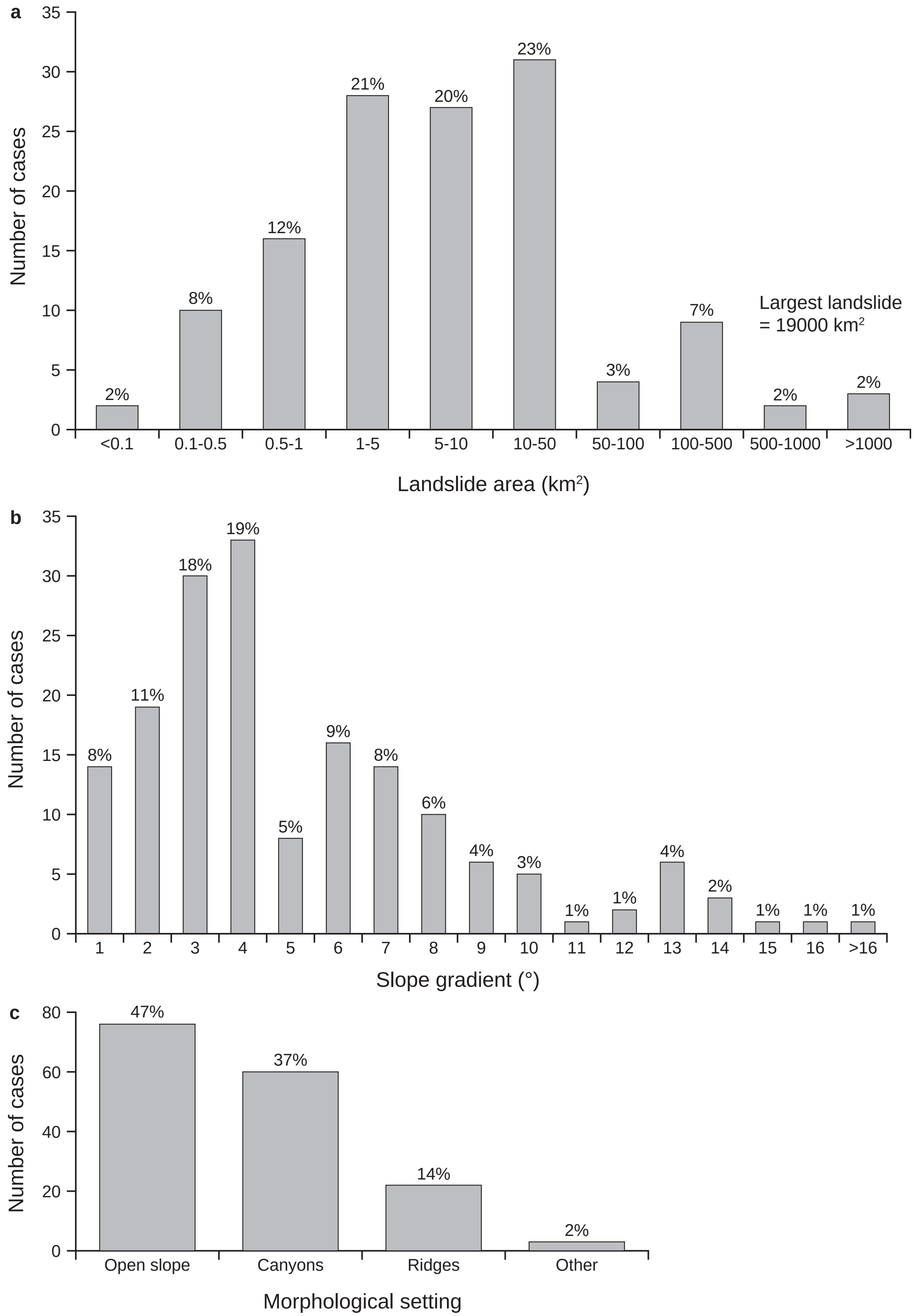


**Fig. 3** (a) Distribution of submarine-landslide area on USA Atlantic margin. (b) Distribution of bathymetric gradients at these sites. (c) Distribution of landslide locations for the same sites. (After Booth *et al.*, 1993.)

3° and 4° (Fig. 3b) and had an area of 1–50 $km^2$ (Fig. 3a); however, smaller landslides might have been missed in the survey because of a lack of complete data coverage. They found that most landslides occurred on the open slope (Fig. 3c), although almost as many occurred in submarine canyons. Given that canyons cover a smaller percentage of total area than do open-slope environments, frequency of landsliding per unit area is probably higher in canyons than the open slope.

Booth *et al*. (1993) observed that most of the landslides were disintegrative; that is, after initial slope failure, whether translational or rotational, most landslides tend to develop large strains, lose their internal structure, and flow, collapse, or generally break up into debris or rubble. This implies that the sediment tends to weaken considerably once it experiences stresses greater than its original strength can withstand (i.e. after initial failure).

## MECHANICS OF SLOPE FAILURE

To understand the mechanics involved in slope failure, it is necessary to consider the following factors: (i) driving stresses, (ii) strength and (iii) potential mobilization into flows.

### Driving stress

Generally, a landslide will take place in a given setting if the driving stresses exceed the shearing resistance of the sediment or rock mass. Gravity exerts a downslope driving stress as long as the seafloor is not flat. In fact, even on nearly flat surfaces, where the seafloor gradient is much less than 1°, debris flows continue to move downslope, sometimes for great distances. Bathymetric-map data can be used to give an estimate of this driving stress field, because the gravity-induced shear stresses vary with steepness. This is done by assuming that each point on the seafloor initially can be approximated as part of an infinite surface. In effect, most topographic complexities are ignored. For an infinite surface, the downslope gravitational **shear stress** at any point below the seafloor is then given by

$$\tau_s = \gamma' h \sin \alpha \qquad (1)$$

where $\tau_s$ is the downslope shear stress, $\gamma'$ is the average buoyant (submerged) density of sediment, $h$ is the depth below the seafloor (i.e. thickness of the failed layer) and $\alpha$ is the seafloor gradient. Therefore, if charts of bathymetric gradient and surface-sediment density can be made from multibeam and core data (Fig. 4), respectively, then the downslope driving stress can be calculated within the context of a geographical information system (GIS) by applying Eq. 1 to the slope and density spatial data (Lee *et al*., 1999).

Earthquake shaking also produces shear stresses that can cause the seafloor to fail. These stresses are related to accelerations and the dynamic response of the sediment column. Earthquake-induced stresses can add to the ambient gravitational stresses, causing a previously stable slope to deform, fail and potentially transform into a flow. **Earthquake-induced cyclic stresses** also can lead to the development of excess pore-water pressures, and then to a degradation in shear strength. The combination of enhanced stress and degraded strength causes earthquake loading to be a particularly effective mechanism for slope failure. A simple method to account for both earthquake and gravitational loads was presented by Morgenstern (1967), modified by Lee & Edwards (1986), and assumes an infinite surface and a pseudo-static earthquake acceleration.

In continental-shelf depths, large **storm waves** can induce a field of shear stresses on the seafloor. These result from the passage of alternating wave crests and troughs that differentially load the seafloor surface and produce the highest shear stresses halfway between crest and trough (Henkel, 1970). As discussed above, loading from hurricane waves has been known to cause failures in the Mississippi Delta and the subsequent loss of offshore drilling platforms on the shelf (Bea *et al*., 1983). A simplified method for predicting the shear stresses resulting from storm waves was presented by Seed & Rahman (1978). Storm-wave-induced shear stresses can combine with the ambient gravitational stresses on slopes and lead to failure (Lee & Edwards, 1986).

### Resisting stress (strength)

Submarine mass movements take place either in rock, in sediment or a mixture of both. At one end of the spectrum are hard rocks for which failure

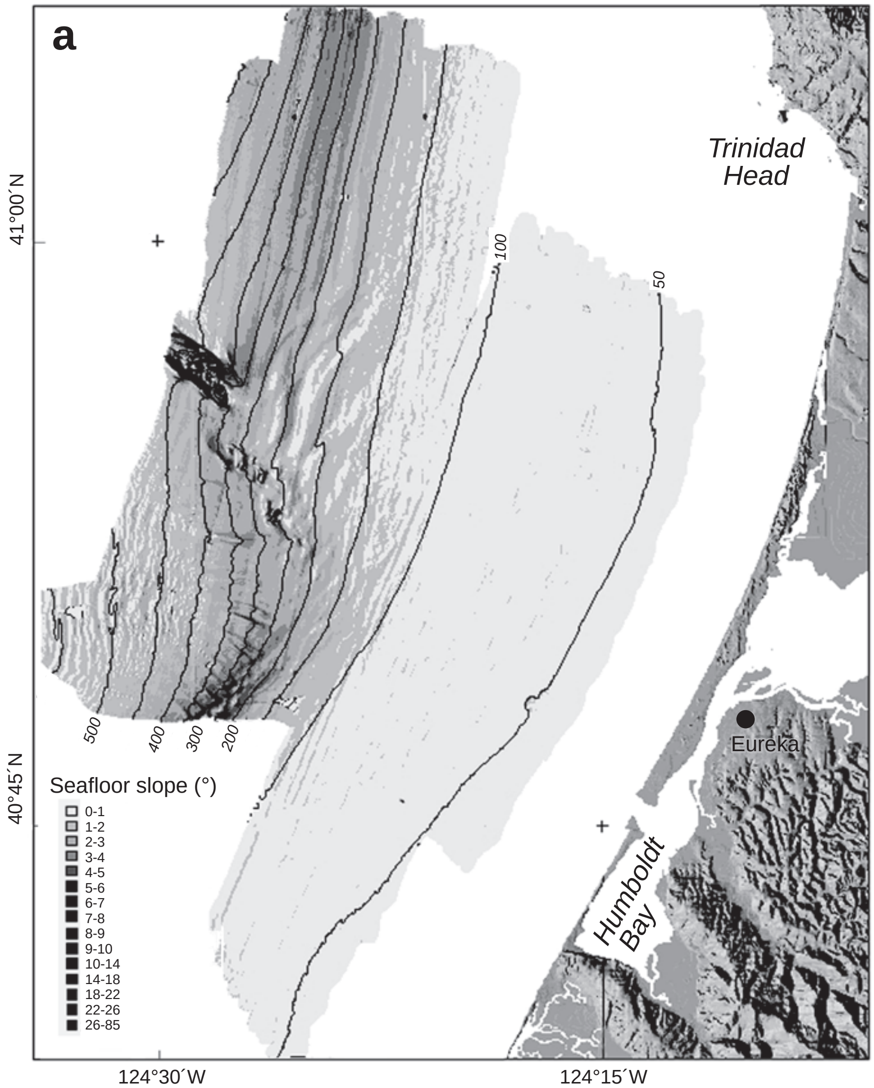


**Fig. 4** STRATAFORM study area. (a) Example of regional variability of seabed steepness from multibeam bathymetry. (b) Example of the regional variability of surface-sediment density obtained from cores. Isobaths in metres. (After Lee *et al.*, 1999.)

usually takes place along pre-existing discontinuities (e.g. bedding planes) so the shearing resistance of the intact rock is not mobilized. For soft sediment, the shearing resistance is mobilized throughout the full volume. For soft rocks or hard sediment, the shearing resistance is often mobilized along shear bands or within localized zones of failure.

Material strength may be measured either *in situ*, on shipboard, or in the laboratory. In the laboratory, the shearing resistance of a sediment or rock is obtained by geotechnical tests such as **direct shear**, **simple shear** or **triaxial shear** under confining pressures representative of *in situ* conditions. Simple tests, such as unconfined compression, vane or cone tests, are also useful (see Lee (1985) for details on measurement techniques and Lambe & Whitman (1969) for further details on shear strength).

The shear strength of sediment represents its ability to resist shear stress. As the shear stress applied to a sediment element steadily increases, the shear strain of the sediment element increases as well. At some point a limiting shear stress is reached and the sediment element strains by a large or unlimited amount. This limiting stress is taken as the **shear strength**. If sediment is considered to be a particular assemblage of grains, the shear strength of that sediment can vary dramatically depending on the way in which shear stresses are applied and the stress history of the sediment. If stresses are applied so rapidly that pore

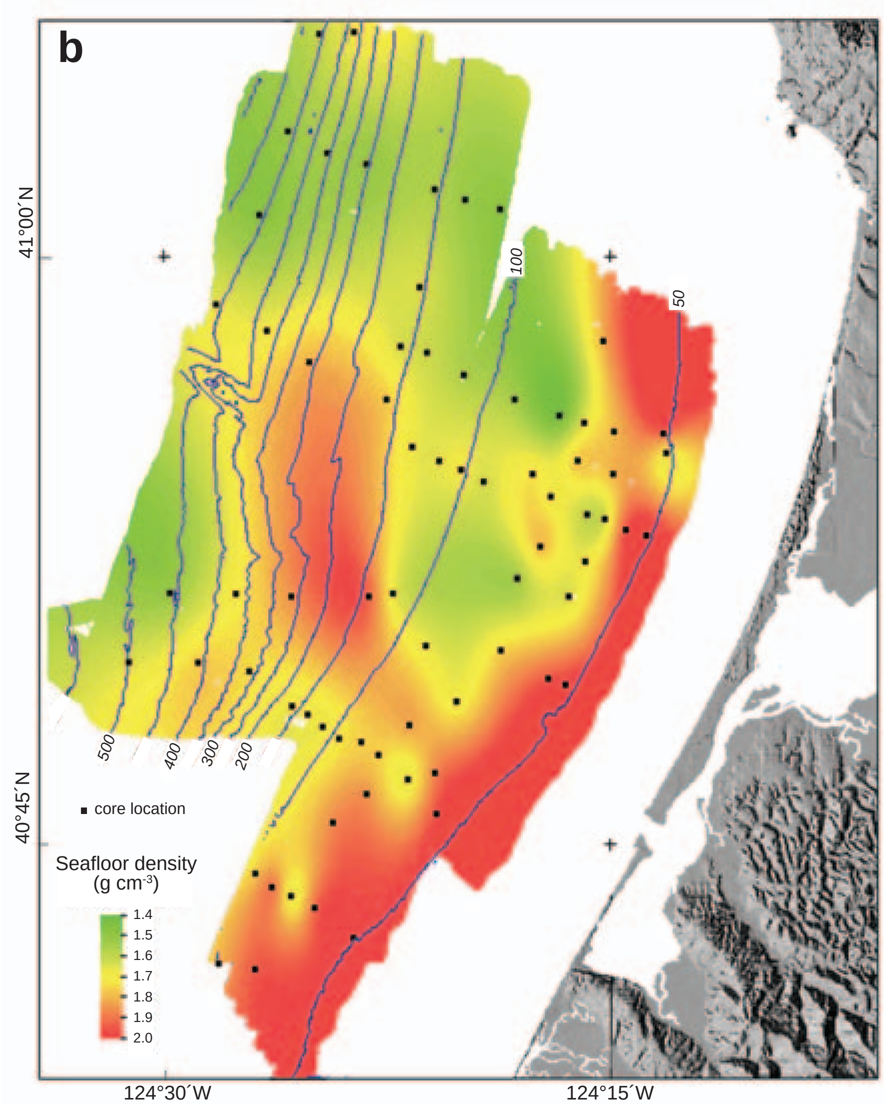


**Fig. 4** (*cont'd*)

water cannot leave or enter the sediment framework, conditions are said to be **undrained**. Under these conditions, pressures in the pore water, either positive or negative, commonly build up and have an influence on the strength. On the other hand, if stresses are applied so slowly that no excess pore pressures are developed, loading conditions are said to be **drained**. The rate of loading required to achieve either drained or undrained conditions is highly dependent upon the grain size, sorting and permeability of the sediment. Undrained failure of a sandy sediment commonly occurs during very rapid loading, such as one might encounter during an earthquake. Otherwise, slope failure in sandy sediment usually occurs under drained conditions. In contrast, clayey and silty sediment more commonly fails under undrained conditions. The critical case for slope stability in these sediments is the undrained one, because the undrained shear strength is commonly less than the drained shear strength.

The **stress history** of the sediment also is an important factor influencing shear strength. When sediment particles first come together in a flocculating environment and are deposited on the seafloor, the effective stress acting on them is very low. Here the effective stress, $\sigma'$, is taken to represent the total stress, $\sigma$, minus the pore-water pressure, $u$. On the seafloor the high **hydrostatic pressure**, corresponding to the overall water depth, contributes to both the total stress and the pore-water pressure. The difference between the total stress and the pore-water pressure is small and includes only the accumulated submerged weight per unit area of the overlying sediment particles (e.g. near the sediment surface the effective stress resulting from sediment overburden is practically zero). As deposition continues and the sediment element becomes buried to greater depths in the sediment column, the **effective overburden stress** increases nearly linearly with sub-bottom depth. Under these conditions, the sediment compacts and dewaters, and the shear strength increases. **Normal consolidation** occurs when sediment accumulation is slow and steady.

For normal consolidation, the shear strength measured under either drained or undrained conditions increases linearly with the increasing effective overburden stress. Such a response is distinctly frictional and for drained loading is represented by

$$\tau_f = \sigma' \tan \phi' \tag{2}$$

where $\tau_f$ is the shear stress at failure, $\sigma'$ is the effective stress and $\phi'$, which relates the two, is defined as the **friction angle**. For undrained loading, the shear strength is represented by

$$s_u = \sigma'_v S \tag{3}$$

where $s_u$ is the undrained shear strength, $\sigma'_v$ is the vertical effective overburden stress and $S$ is a sediment constant (often equal to about 0.3 for fine-grained marine sediment; Lee & Edwards, 1986). The vertical effective stress is

$$\sigma'_v = \gamma' z - u \tag{4}$$

where $\gamma'$ is the average buoyant weight of sediment, $z$ is the depth in the sediment column and $u$ is the excess pore-water pressure (in excess of hydrostatic).

Equations 2 and 3 show a simple application of the concept of **normalized shear-strength behaviour**, that is, shear strength normalized by effective stress can be related to simple expressions that involve a limited number of sediment constants.

When overburden is removed from normally consolidated sediment (by erosion, for example), it becomes **overconsolidated**. The largest stress that was ever reached is termed the maximum past stress, $\sigma'_{vm}$, and the **overconsolidation ratio** (OCR) is $\sigma'_{vm}$ divided by the present overburden stress or $\sigma'_v$. The normalized strength formulation has been determined through extensive experimental work (Ladd *et al.*, 1977; Lee & Edwards, 1986) to be

$$s_u = \sigma'_v S(\mathrm{OCR})^m \tag{5}$$

where $m$ is a sediment constant that can be determined by experiment but commonly is equal to about 0.8.

A problem with marine sediment is that classic overconsolidation such as that resulting from erosion, which is expressed by Eq. 5, is not the only mechanism by which sediment can become densified and strengthened. Other factors such as bioturbation, repeated seismic loading and cementation also can play a role. Strength that is higher than expected in a sediment that appears to have a normal-consolidation history is termed **pseudo-overconsolidation** (Silva, 1974).

#### Slope stability analysis

Most simplistically, slopes fail when the driving stresses exceed the resisting stresses. In the marine environment the **factor of safety** of a slope is often calculated by simply dividing the shear strength (e.g. obtained from Eq. 5) by the shear stress exerted on an infinite surface (Eq. 1). Sometimes an earthquake-acceleration term is included to allow for seismic loading (Morgenstern, 1967; Lee & Edwards, 1986). Other, more complex techniques that allow for the geometry of real surfaces are given in Syvitski *et al.* (this volume, pp. 459–529).

### PORE-WATER PRESSURE

As can be seen in Eq. 4, the effective stress is strongly impacted by pore-water pressure, which in turn has an impact on the shear strength through Eqs 2–4. Accordingly, much of the literature and research in marine geotechnology and marine slope stability have been directed toward estimating or measuring pore-water pressure.

Sangrey (1977) provided a review of the various mechanisms that can produce excess pore-water pressures in marine sediment. Perhaps the most common cause is rapid sedimentation. When sediment is initially loaded by **overburden**, all of the new load is carried by pressure in the pore water. This occurs because the sediment mineral framework cannot increase its load carrying capacity (**effective stress**) without compressing, and compression cannot occur instantaneously in a fully saturated medium (i.e. water must flow out for the mineral framework to compress). If the sediment has a low permeability or a high compressibility, considerable time may be required for the excess pore-water to drain away. A measure of the sediment's ability to discharge water in a short amount of time is the geotechnical engineering parameter, $c_v$, termed the **coefficient of consolidation**. Rate of drainage varies directly with $c_v$, which is the ratio of permeability to compressibility (change in thickness per unit change in vertical effective stress). If the sedimentation rate is high and $c_v$ is low, then potentially large excess pore-water pressures can form in the sediment column.

Gibson (1958) developed a theoretical relation for predicting the level of excess pore pressure that might result from rapid consolidation. High pore-water pressures, approaching **lithostatic** (the pressure exerted by the buoyant weight of the overlying sediment), can exist for the combinations of accumulation rate and $c_v$ found in many active river deltas, including the Mississippi. In fact, the large numbers of landslides on very gentle gradients found in the Mississippi Delta are generally attributed to pore pressures produced by rapid sedimentation (Coleman & Garrison, 1977).

A second source of pore-water pressure results from gas charging. **Bubble-phase gas** can develop in marine sediment through a variety of geochemical and physical processes. These include the decay of organic matter, migration from other locations and dissociation of hydrates during temperature or pressure changes (Kayen & Lee, 1991; Sultan *et al*., 2003). Whatever the cause, the expanding bubbles pressurize the water around them. Again, if this pressured water cannot flow away fast enough, the pore-water pressure builds up, the effective stress drops and the shear strength decreases (Esrig & Kirby, 1977). For a study in Norton Sound, Alaska, Hampton *et al*. (1982) found that *in situ* penetration resistance (directly related to strength) varied considerably with apparent gas charging. In areas of gas anomalies, the penetration resistance was as much as 10 times lower than that in sediment only 1 km away that did not show gas anomalies.

Investigators have attempted to determine the influence of gas charging on sediment strength behaviour in the laboratory. Recently Grozic *et al*. (2000) evaluated the ability of gassy sediment to resist dramatic strength loss (liquefaction) using cyclic triaxial tests. Standard sands were artificially charged with gas in a controlled manner. They were then tested using standard techniques to determine the **cyclic stress ratio** (ratio of applied cyclic shear stress to effective stress) necessary to cause liquefaction (termed the **cyclic resistance ratio**). The results of the laboratory experiments showed that the cyclic resistance ratio increases as sediment density and gas content increase. In other words, the higher the gas content, the less susceptible the sediment is to dramatic strength losses during cyclic loading events, including earthquakes and storms. This is likely because the gas compresses and dissolves during cyclic loading, thereby increasing the density and increasing the strength. Such a finding seems to conflict with the general understanding of marine geologists that gas-charged sediment is more susceptible to slope failure (Field & Barber, 1993). Perhaps there are trade-offs; gas-charged sediment is much weaker with respect to static loads, as illustrated by the penetration tests in Norton Sound discussed above. Then, even if the sediment does not lose strength as readily during cyclic loads, the strength is already so low because of its intitial state that failures in gas-charged sediment may be more likely.

A special type of gas charging results from gas-hydrate dissociation. In fact, gas-hydrate dissociation has been suggested as a cause of mega-landslides and has even been considered to be a 'gun' that responds to climate change (Maslin *et al*., 2004). **Gas hydrates** are solid-solution compounds in which natural gases are caged within a rigid lattice of water ice. These compounds can exist only under conditions of high pressure and low temperature, and they serve as enormous and highly concentrated reservoirs of gaseous hydrocarbons (Kayen & Lee, 1991). When they are intact, gas hydrates form strong layers in the sediment column by virtue of their ice-like structure. However, gas hydrates can disassociate when there is a change in environmental conditions: specifically an increase in temperature or a decrease in pressure. When this occurs, large quantities of free gas can be released into the sediment column. If the pressures produced by this gas release cannot dissipate, perhaps because the coefficient of consolidation, $c_v$, is too low, pore-fluid (water + gas) pressures will increase dramatically and sediment shear strength will decrease. Such changes could produce massive slope failures. Clearly, global increases in temperature or decreases in pressure (sea-level fall) have the potential for causing seafloor failures on a world-wide scale, thus the notion of a hydrate 'gun'.

A third source of elevated pore-water pressure is **groundwater flow** and artesian pressure conditions. Such pressures can easily result when the water table near the coast is above sea level and water flows out of the seafloor though coastal aquifers (Sangrey, 1977). A somewhat similar situation exists in subduction zones; high porosity sediment is subducted, and the interstitial fluids are forced upward into the accretionary complex. Again, if the fluids cannot be removed fast enough, pore-water pressures increase dramatically, possibly approaching lithostatic (Shi & Wang, 1988). Orange & Breen (1992) and Orange *et al*. (1997) showed that pore pressures which developed in subduction complexes can contribute to slope failure and the formation of headless canyons.

A fourth source of excess pore pressure is **cyclic loading** of sediment. When cyclically varying shear stresses are applied by either an earthquake or storm waves, sediment grains can become mobile. With increasing numbers of cycles, the grains can gradually move from being in contact with, and supporting, each other to being separated from each other and supported by the pore water. In extreme examples, the grains become totally supported by pore fluid (100% pore pressure response) and the shear strength can decrease to almost zero. This last situation is referred to as **liquefaction**, because the sediment begins to behave as a liquid with almost no shear strength (Seed, 1968). Sands and silts tend to be more susceptible to liquefaction; however, certain classes of fine-grained sediment known as **quick clays** also can lose their strength catastrophically (Bjerrum, 1955).

Strength loss because of cyclic loading can be evaluated either in the laboratory or in the field. In the laboratory (Fischer *et al*., 1976; Silver *et al*., 1976), samples can be conditioned under a state of stress representative of *in situ* conditions before an earthquake or storm. This is done in either a triaxial cell or simple shear device. Next, cyclically varying shear stresses are applied and both strain and pore-pressure response are monitored. For the sake of consistency and because of laboratory equipment limitations, failure is defined as either a certain strain level (e.g. 15%) or a certain pore-pressure response (e.g. 80%) (Lee & Focht, 1976). The results are then used to define strength loss during cyclic loading, and these loss terms are used to forecast the failure. Lee & Edwards (1986) developed a cyclic-loading strength-reduction factor, $A_r$, that represents the cyclic stress level (relative to the static shear strength) that causes failure in 10 cycles (representative of a moderate earthquake). This methodology is most suitable for fine-grained sediment because the sediment is less sensitive to coring disturbance.

The potential for liquefaction in sands is generally evaluated with field tests using the methods of Seed & Idriss (1971). The procedure involves an empirical curve on a plot of **cyclic stress ratio** (CSR; cyclic shear stress, $\tau_c$, divided by the overburden stress, $\sigma'_v$) versus modified blow count from a standard penetration test performed using a geotechnical drilling rig (Fig. 5). The CSR is calculated for an assumed level of earthquake shaking represented by a peak acceleration (Seed & Idriss, 1971).

## SEDIMENT MOBILIZATION AND STRENGTH LOSS

Following initial failure, some landslides mobilize into flows whereas others remain as limited deformation slides (Hampton *et al*., 1996). The mechanisms for mobilization into flows are not well understood but the initial density state of the sediment is likely to be one important factor (Poulos *et al*., 1985, Lee *et al*., 1991). If the sediment is initially less dense than an appropriate steady-state condition (**contractive sediment**) the sediment is more likely to flow than one that is denser than the steady-state condition (**dilatant sediment**) (Fig. 6). The **steady state** represents a boundary between contractive and dilatant behaviour and is described by the porosity-effective stress conditions

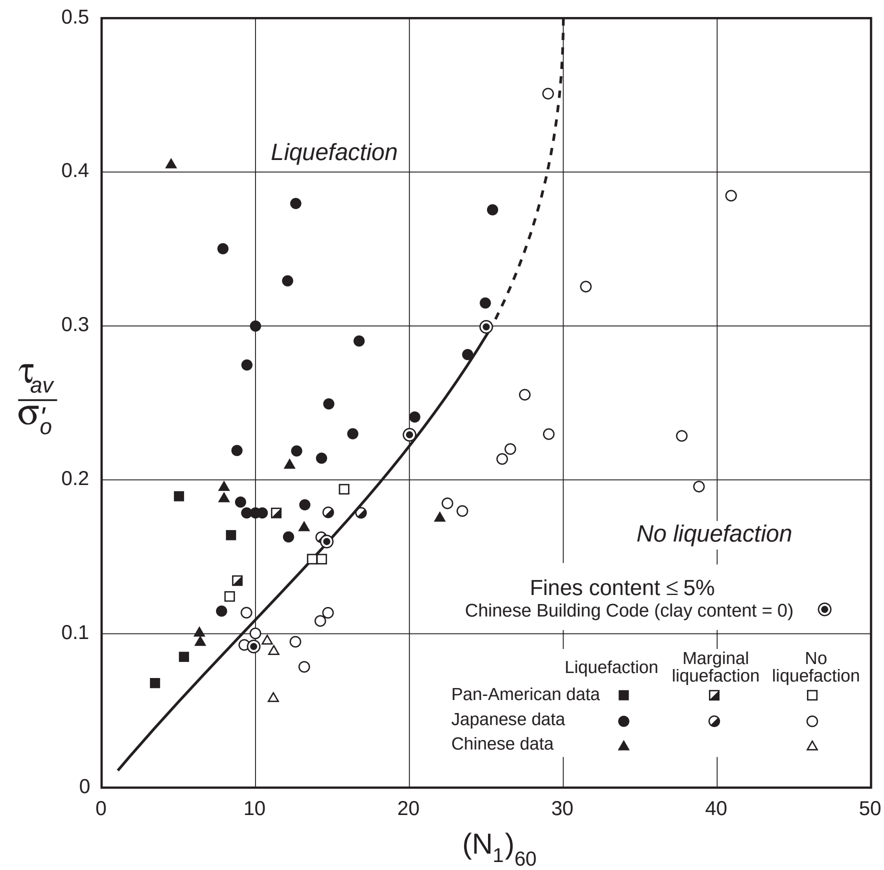


**Fig. 5** Common procedure for predicting liquefaction susceptibility: $(N_1)_{60}$ is a measure of the resistance to penetration from a standard penetration test; $\tau_{av}$ is the average shear stress anticipated from a design earthquake; $\sigma_o'$ is the overburden effective stress. The solid line defines the boundary between sediment that will liquefy and sediment that will not. (After Seed & Idriss, 1971.)

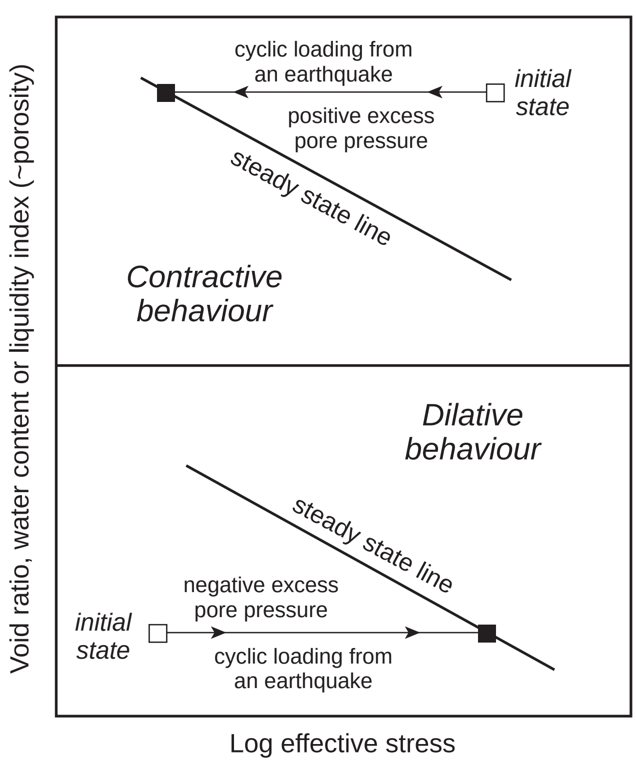


that a sediment will assume when strained by a large amount. This response is another example of pore-pressure generation; contractive sediment generates positive pore pressure during shear and these increased pore pressures reduce the strength. Contractive failure of loose sedimentary deposits can occur at constant porosity. The sediment essentially collapses upon itself and loses much of its strength in the process. Dilatant sediment generates negative pore-water pressures

**Fig. 6** (*left*) Line of steady-state deformation. If the initial sediment state lies above the steady-state line, there will be a tendency toward the generation of positive pore pressures during a failure event (e.g. an earthquake). Such pore-pressure generation will lead to a dramatic decrease in effective stress and shear strength and will increase the tendency for sediment flows. An initial sediment state below the steady-state line will produce dilatant behaviour, negative pore-pressure generation, increased effective stress and decreased tendency to flow. (After Lee *et al*., 1991.)

during shear and becomes stronger in the process. The ability to flow also may be related to the amount of energy transferred to the failing sediment during the failure event (Leroueil *et al*., 1996; Locat & Lee, 2002).

Strength loss at constant porosity cannot explain the behaviour of some far-reaching debris flows (Locat *et al*., 1996; Schwab *et al*., 1996). For example, there is evidence for debris flows reaching the distal lobes of the Mississippi Fan that must have flowed for roughly 500 km on slopes as gentle as 0.06° (Locat *et al*., 1996). If these deposits represent such flows, then an estimate for the threshold yield strength is 9 Pa. Such a value is three orders of magnitude lower than an estimated remoulded shear strength in the presumed source region (Locat *et al*., 1996), where the **remoulded shear strength** is the minimum strength value obtained by manually working a sample. Accordingly, the sediment must have taken on additional water during flow, increasing its porosity and decreasing its strength, or the flow must have hydroplaned (Parsons *et al*., this volume, pp. 275–337; Syvitski *et al*., this volume, pp. 459–529). The dilution mechanism is consistent with that suggested by Hampton (1972), who described an increase in the sediment water content caused by the jostling and deformation within the sediment during the remoulding phase of the failure event. This greatly reduces the shear strength and provides a fluid-like behaviour to the mixture. During this dilution process, however, the water content cannot become so high that the resulting flow transforms into a turbidity current. In the example of the Mississippi Fan debris-flow deposits, the presence of clasts demonstrates that the sediment flow still retained competence and was not so energetic as to cause the clasts to disintegrate.

## TRIGGERS

Submarine landslides are triggered either by an increase in the driving stresses, a decrease in strength, or a combination of the two. The following possible triggers show the interplay of these factors. Note that the relative importance of each of these triggers is not well understood. For example, in some environments one of these triggers will dominate, whereas in others a different trigger will be most significant.

### Sediment accumulation

Rapid sediment accumulation contributes to failure in several ways. First, as discussed above, when sediment accumulates rapidly, most of the weight of newly added sediment is carried by pore-water pressures. The shear strength probably increases somewhat because some water will always be squeezed out, even if the coefficient of consolidation ($c_v$) is low (i.e. relatively low permeability and/or high compressibility). However, the shear stress acting downslope increases more rapidly. As seen in Eq. 1, the shear stress increases with the weight of sediment and is not influenced by pore pressure. The shear stress also may increase because more sediment may be deposited at the head of the sloping surface than at the toe. All three of the following processes push the slope toward failure: retarded strength development, increased development of shear stress because of thickness of the sediment body, and increased development of shear stress because of increases in the slope steepness.

As discussed above, the Mississippi Delta is an ideal example of sediment failure induced by sediment accumulation. Coleman *et al*. (1993), Prior & Coleman (1978) and many other publications document a large variety of sediment failures on the Mississippi prodelta (Fig. 7). Coleman (1988) showed that virtually the entire seafloor surface of the delta front was covered with failure features.

### Erosion

Localized erosion by moving water or sediment flows is common in deep-sea channels, submarine canyons and other active sediment-transport systems. When seabed surfaces are undercut, this can decrease the stability by increasing shear stress and in some cases decreasing the shear strength. Monterey Canyon, located off central California, shows many examples of erosion-induced slope failures (Fig. 8). Often these failures dam the canyon so that subsequent turbidity-current flows are diverted, leading to further erosion and second-generation landslides (Greene *et al*., 2002).

### Earthquakes

Earthquakes are called upon as a cause for many unexplained submarine landslide features (Lee &

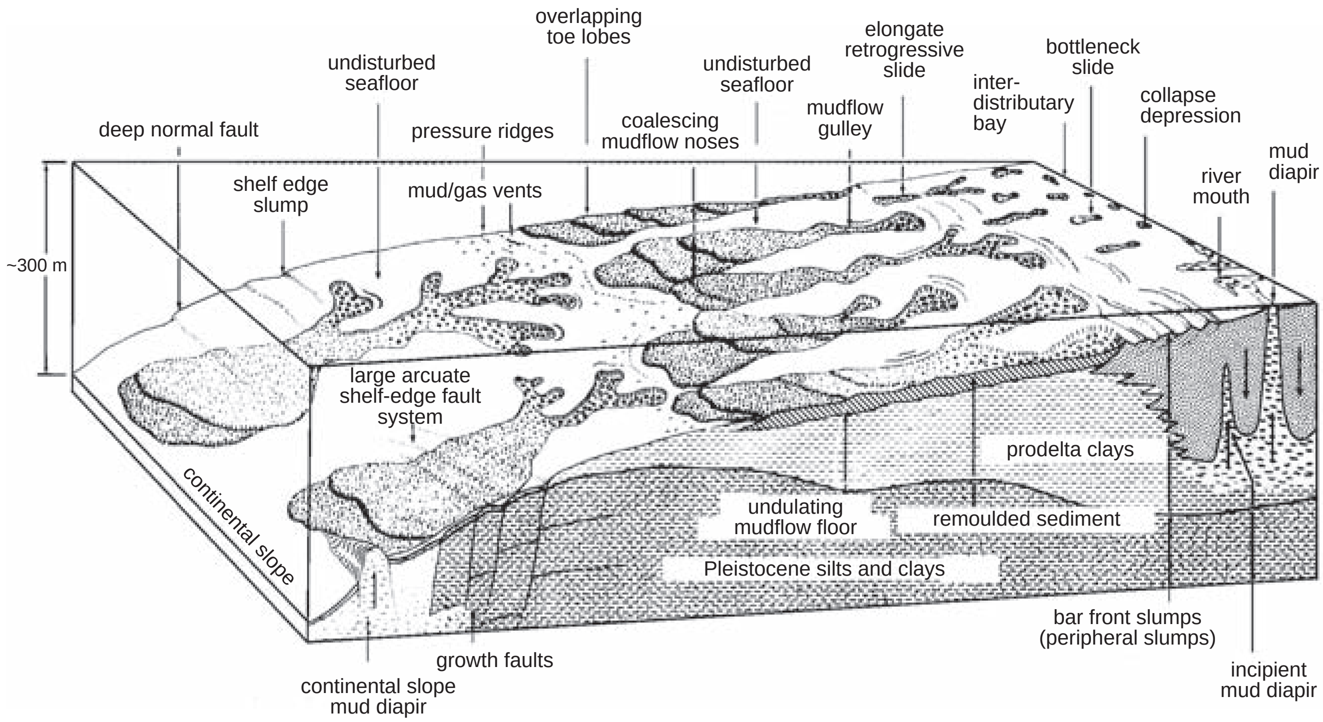


**Fig. 7** Schematic block diagram showing the relationship of the various types of submarine sediment instabilities for the Mississippi Delta. (From Coleman *et al*., 1993.)

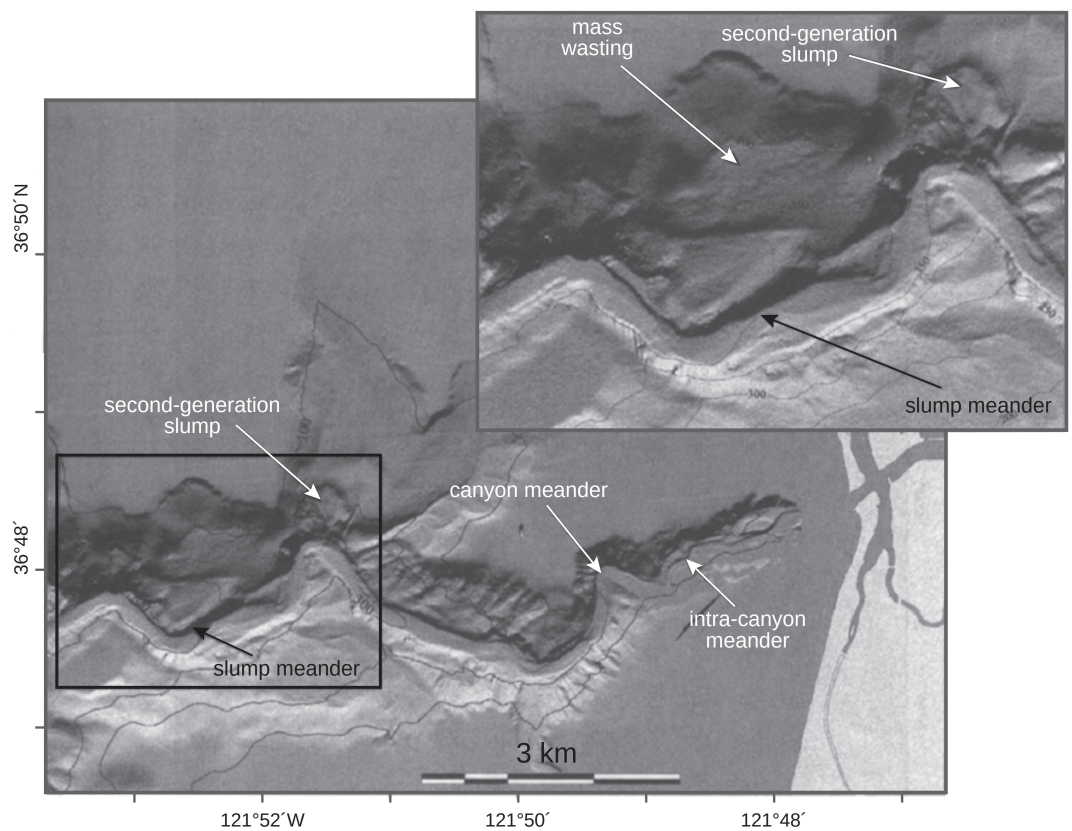


**Fig. 8** Multibeam image of the headward part of Monterey Canyon showing canyon and intracanyon meanders, slump-produced meanders, and mass-wasting associated with undercutting along the sides of the canyon axis. Expanded view shows a slump meander and a well-defined second-generation slump resulting from erosion at the apex of a meander. (From Greene *et al*., 2002.)

Edwards, 1986; Hampton *et al.*, 1996). One reason is that, under water, earthquake-induced shear stresses are quite large relative to shear strength. The seismic shear stress is high because the earthquake must accelerate all of the sediment column including the interstitial water. The shear strength is relatively low because it builds up in proportion to the submerged unit weight of the sediment (Eqs 3 & 4) and may be even lower if there are excess pore pressures (Eq. 4). The ratio of driving stress to resisting strength is high relative to what is usually found on land for the same earthquake. This is because, on land, the water table is seldom at the surface continuously so the strength builds up with the total weight of sediment above the water table. Earthquakes also generate excess pore pressures through cyclic loading as discussed above, which can lower the strength more and possibly induce a state of liquefaction.

Examples of earthquake-induced submarine failures are numerous and include the 1929 Grand Banks event (Piper *et al.*, 1999), multiple failures in Alaskan fjords during the 1964 earthquake (Coulter & Miliaccio, 1966; Fig. 9) and the 1998 Papua New Guinea earthquake and tsunami (Tappin *et al.*, 2003). Earthquake-induced landslides, the resulting turbidity currents, and the turbidites they produce have been used to date major subduction-zone earthquakes in Cascadia (Goldfinger *et al.*, 2003).

**Fig. 9** Submarine landslide area at Valdez, Alaska, following the 1964 earthquake. The dashed lines indicate the dock area destroyed by the landslide. (After Coulter & Miliaccio, 1966.)

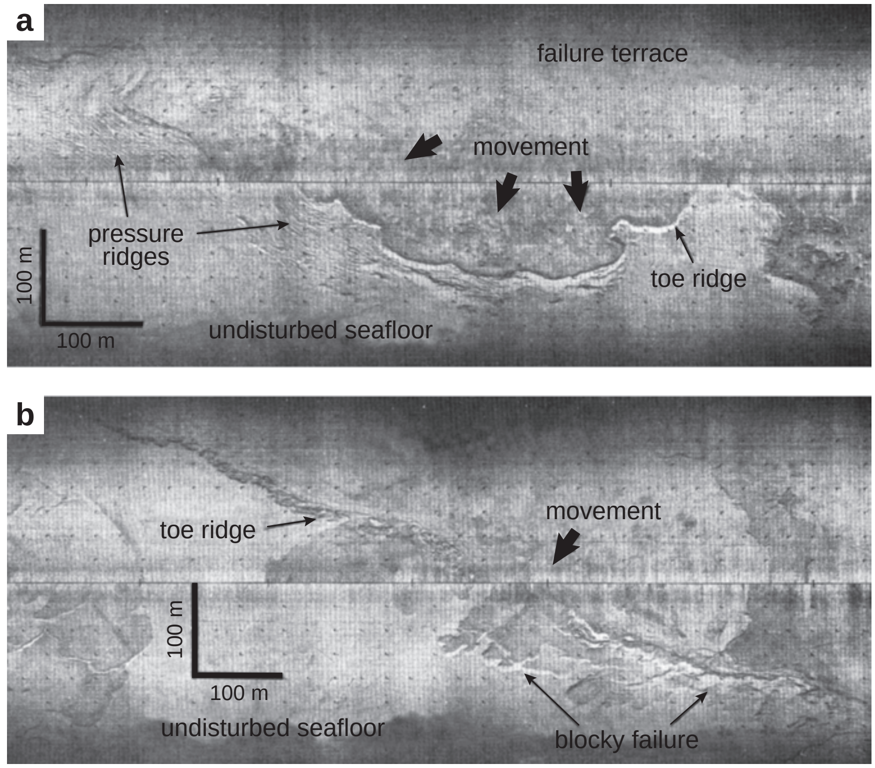


**Fig. 10** Sidescan-sonar images of the seafloor off the Klamath River mouth following the 1980 earthquake. (a) The failure terrace has a mottled appearance that is distinctly different from that of the unfailed area. Note the well-defined toe ridge that marks the seaward edge of the landslide and the parallel pressure ridges within the landslide deposit. (b) More complexity occurs near the terminus. The boundary between the landslide zone and the undisturbed seafloor is marked by a series of discrete blocks measuring 10–50 m on each side. (From Field, 1993.)

Another example of earthquake-induced failure is the magnitude 7.0 earthquake that struck the northern California coast in 1980 in an area that had been surveyed previously using sub-bottom profiling equipment. Following the earthquake, local commercial fishermen, who frequently travel the coastal waters, reported the presence of one or more north-west-trending scarps seaward of the Klamath River mouth. The previous surveys had shown the area to be a smooth, featureless depositional environment, and the sudden appearance of scarps suggested a causal relation to the earthquake. Surveys of the area were conducted 2, 7 and 12 months after the earthquake using cameras, sidescan sonar and high-resolution sub-bottom profiling equipment (Field, 1993). The surveys showed a series of features indicative of sediment liquefaction, lateral spreading and flows, all on a gradient of only 0.25°. Pressure ridges and a toe ridge occurred near the seaward boundary of the failed area, which approximated the sand–mud depositional boundary (Fig. 10). The failed area was about 2 km wide and 20 km long. This survey was one of the first to show that continental shelf sands can liquefy readily during earthquakes and that the northern California margin is susceptible to earthquake-induced failures.

### Volcanoes

The existence of giant submarine landslides on the flanks of the Hawaiian Islands has been the subject of debate for at least 50 yr (Normark *et al*., 1993). Using limited bathymetry data, Moore (1964) interpreted irregular blocky ridges extending downslope from giant amphitheatre-shaped scars on the submarine north flanks of Molokai and Oahu as representing giant landslides. The origin of these deposits was confirmed when complete GLORIA sidescan-sonar data were acquired in the 1980s (Moore *et al*., 1989). In fact, the GLORIA surveys showed that the Hawaiian Islands were surrounded by many giant submarine landslides (Fig. 11). Further work (Holcombe & Searle, 1991) has shown that the Hawaiian Islands are not alone, and that many, if not most, oceanic volcanoes fail catastrophically during part of their existence.

Some component of oceanic volcanism is clearly a trigger for submarine landslides, but the nature

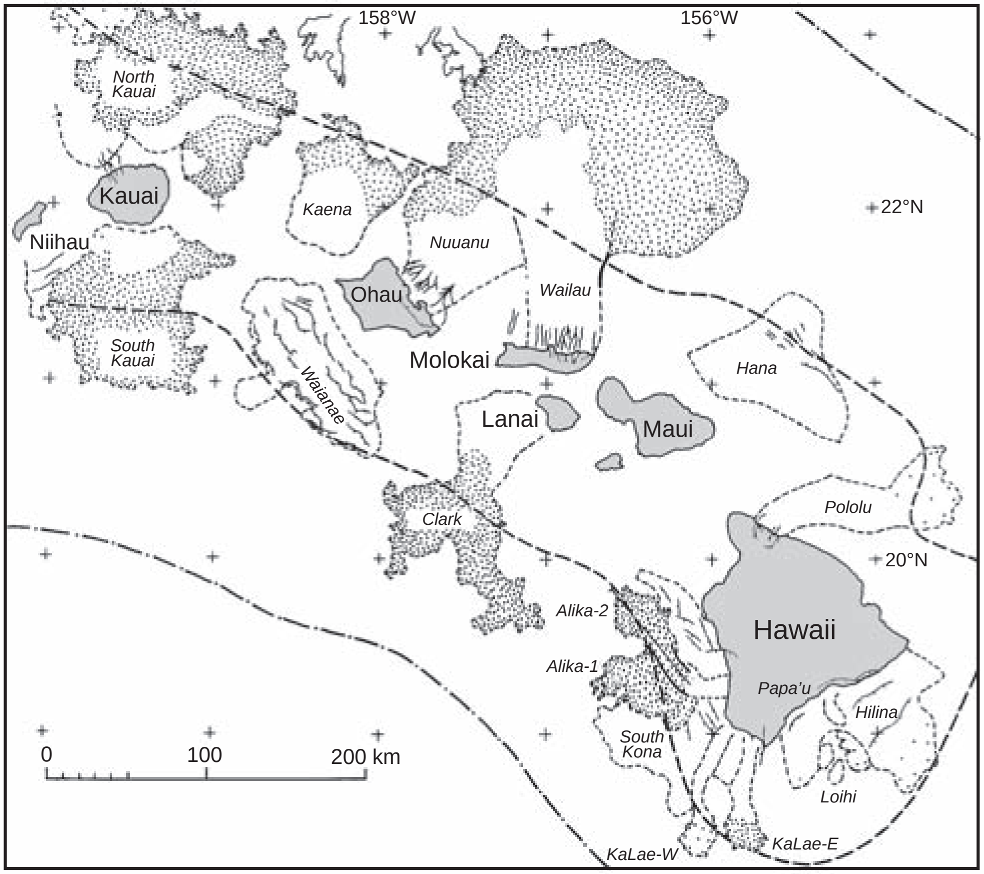


**Fig. 11** South-eastern Hawaiian Ridge showing the outline of major landslides identified by name. Dotted pattern indicates hummocky deposits observed on seismic-reflection profiles and GLORIA images; more widely spaced dot pattern indicates subdued relief. Ticked lines indicate major fault scarps. Thin, downslope-directed, irregular lines indicate submarine canyons and their subaerial extensions. Heavy dashed line is the axis of the Hawaiian Trough, and the dashed–dotted line is the crest of the Hawaiian Arch. (Modified from Normark *et al*., 1993.)

of that component has not been determined. Most of the larger, older landslides seem to have occurred late in the shield-building phase of the host volcano (Moore *et al*., 1989). At this point, the volcano is still producing significant magma and stands at its highest elevation above sea level. Many factors are present at this point and may combine to produce a trigger. Clearly there are earthquakes and significant gravitational downslope stresses resulting from the great topographic relief of the islands. Such factors are also present on most active continental margins, but giant landslides are infrequent in these locations (McAdoo *et al*., 2000). Many volcanic islands, including the Hawaiian Islands, are built upon pre-existing pelagic sediment bodies, commonly clay. This could produce a weak basal layer (Dietrich, 1988) that might contain excess pore-water pressures, even though the island basalts are fairly permeable and were built over millions of years. Magma pressure in the rift zones is too small to trigger landslides wider than a few kilometres (Iverson, 1995). Groundwater forces provide another possible trigger, but are probably not important except under special circumstances (Iverson, 1995). Another intriguing but speculative possibility is that magma fractionates near erupting volcanoes producing a body of olivine cumulates, which has a rheology similar to ice and should flow down from the summit of the volcano, causing a massive submarine landslide (Clague & Denlinger, 1994). The ultimate trigger for the giant submarine landslides cannot be identified at present and probably includes a combination of several of the above factors.

#### Waves

Storm waves can trigger slope failure, as illustrated by damage to offshore drilling rigs during Hurricane Camille in 1969 (Bea *et al*., 1983). Storm-wave-induced failure actually involves several elements. As was demonstrated by Henkel (1970), the passage of a wave train subjects the seafloor to alternating water pressure as the crests and troughs pass. This non-uniform pressure field induces the greatest shear stresses between crest and trough. Henkel (1970) considered the situation to be one of a simple moment resulting from alternating zones of positive and negative pressure. Seed & Rahman (1978) improved upon Henkel's approach and developed the following equation for the induced shear stresses

$$\tau_c/\sigma'_v = f_z f_d 2\pi(\gamma_w/\gamma')H/L \tag{6}$$

where $\tau_c$ is the induced peak cyclic shear stress, $\sigma'_v$ is the vertical effective stress, $f_z = \exp(-2\pi z/L)$, $f_d = 0.5[1/\cosh(2\pi d/L)]$, $\gamma_w$ is the unit weight of water, $\gamma'$ is the buoyant unit weight of sediment, $H$ is wave height, $z$ is depth below the seabed, $L$ is wave length and $d$ is water depth.

Equation 6 demonstrates that induced shear stresses vary with the characteristics of the waves, the water depth and the depth below the seafloor. These shear stresses are much like earthquake loads in that they add to pre-existing downslope gravitational stresses and they are cyclic in nature, so that they gradually induce increasing pore-water pressures in the sediment. The sediment can fail after the passage of a wave train, or it can liquefy and flow if the pore pressures reach a high enough value (Van Kessel & Kranenburg, 1998).

Lee & Edwards (1986) showed that there can be a transition in the importance of triggers in environments that are both subjected to large storms and are seismically active. In shallow water, the largest shear stresses may be induced by storm waves, and these would control seabed stability. Seismic loading would be more important in deeper water. For example, in the north-east Gulf of Alaska, storm waves appear to be the dominant trigger in water depths < 80 m, and earthquake loads are more important in greater water depths.

Clukey *et al*. (1985) considered another implication of wave-loading effects. As the storm-wave-induced pore-water pressures build up, the effective stress decreases and the sediment approaches a state of liquefaction. As a result, the current velocity necessary to initiate sediment transport decreases. Accordingly, wave loading, cyclic-shear-stress development and pore-pressure generation lead to slope failure and also to enhanced bottom-current-induced sediment transport.

#### Gas and gas hydrates

Gas charging of sediment is not so much a trigger as a means by which shear strength may be altered. Gas charging can affect sediment strength either by decreasing it through the development of excess pore pressures, or potentially increasing it by reducing the impact of cyclic loads. In cases where gas charging reduces strength, the actual trigger causing failure is likely to be some other factor such as an earthquake.

Dissociation of gas hydrates can be considered a trigger because it results from environmental changes. Sea-level fall has often been invoked as a means of triggering landslides through destabilization at the base of the gas-hydrate zone, the part of the sediment column closest to gas-hydrate equilibrium. Kayen & Lee (1991) modelled pore-pressure generation on the continental slope of the Beaufort Sea during the last eustatic fall in sea-level. They determined that fluid-diffusion properties dominate the process. Following sea-level fall, pressures develop within the pore space of sediment at the base of the hydrate in response to the liberation of gas. They concluded that excess pressure generated at the base of the gas hydrate zone during Pleistocene falls in sea level was probably sufficient to initiate seafloor landsliding in the unlithified sediment that underlies the continental slope in the Beaufort Sea. This process probably operated at many other locations in the world's oceans at the same time.

Sultan *et al*. (2003) modelled the impact of sea-level rise and warming of the North Atlantic on the stability of the Norwegian continental slope where the giant Storegga Slide occurred about 8200 yr ago (Bryn *et al*., 2003). Sultan *et al*. (2003) suggested a mechanism by which increases in pressure and temperature associated with the end of the last glacial period could have increased the solubility of methane and induced a dissociation of methane hydrate at the top of the hydrate layer. The resulting excess pore-water pressures could have led to massive slope failure. Such a mechanism for producing the Storegga slide is still being debated. Another mechanism for triggering the slide is rapid sediment accumulation during peak glaciation, followed by earthquake loading due to post-glacial isostatic rebound (Bryn *et al*., 2003).

#### Groundwater seepage

Sangrey (1977) speculated, based on experience and proprietary information, that underconsolidation and excess pore pressures resulting from artesian reservoir sources are 'very common offshore and may be the most significant mechanism' for causing slope failure. Orange & Breen (1992) suggested that pore fluids percolating up from subducted sediment could induce slope failure and lead to the development of **headless canyons**, i.e. submarine canyons that are not linked to incised valleys on the shelf. Many others (Saffer & Bekins, 1999) have developed models for the ways in which subducted fluids and the resulting excess pore pressures influence the mechanics of subduction zones.

Groundwater seepage from coastal aquifers also could serve as a trigger for landslides. Based on an examination of morphology, Robb (1984) suggested that spring sapping (i.e. erosion of sediment and rock by underwater springs) may have occurred on the lower continental slope off New Jersey during periods of lowered sea level. In support of this suggestion, it was observed that nearly fresh interstitial water is found beneath the continental shelf ~100 km off the New Jersey coast. Hot fluid seeps also are known to occur (Hampton *et al*., 2002) on the Palos Verdes continental shelf (southern California) near the head of a very large submarine landslide (Bohannon & Gardner, 2004).

Failures often occur in fjords and other coastal locations during periods of low tides (Prior *et al*., 1982a,b). These failures occur because of a phenomenon that engineers term **rapid drawdown** (Lambe & Whitman, 1969, p. 477). When water levels fall rapidly, pore pressures within coastal slopes often cannot adjust quickly enough. This results in an elevated water table directly adjacent to the coast and in accelerated seepage of groundwater. This situation can be modelled as **seepage forces**, which effectively add downslope driving stress, or as excess pore pressures reducing the effective stress and the corresponding sediment shear strength. Regardless of the specific mechanism, the slope becomes less stable and failures can occur. Atigh & Byrne (2004) modelled liquefaction in the Fraser delta resulting from tidal variations, which cause unequal pore-pressure generation.

#### Diapirism

Any tectonic or diapiric deformation that results in steepened seabed surfaces will lead to a reduction in the factor of safety and increased likelihood of slope failure. This element becomes one of a number of factors that ultimately determine whether or not a slope will fail. The northern Gulf of Mexico is an area in which diapiric deformation is one of the major causes of failure on the continental slope. Martin & Bouma (1982) noted that large diapiric and non-diapiric masses of Jurassic salt and Tertiary shale underlie the northern Gulf of Mexico continental slope and adjacent outer continental shelf. The masses show evidence of being structurally active at present and in the very recent geological past. The vertical growth of these structures causes local steepening of the seafloor and causes many knolls and ridges interspersed by topographic depressions and canyon systems. Large overburden pressures created by sediment accumulation from the late Jurassic to the present have caused the underlying salt sheet to flow and sometimes extrude toward the surface. The movement of the salt sheet, or **halokenesis**, is largely responsible for the surface morphology (Silva *et al*., 2004).

#### Human activity

Human-constructed facilities, either along the coastline or on the seafloor, have the potential for causing submarine slope failures. Typically, these facilities increase the downslope stresses. Human influence in causing landslides is hotly debated because fault must be assigned to damages, injuries and even death. The question debated is commonly whether a natural slope failure affected the human development or whether the human development caused the slope to fail.

The role of human activity is clear in the case of the quick-clay failure in Rissa, Norway, during 1978. The landslide was initiated when 700 $m^3$ of earth fill was placed by the shore of Lake Bottnen to expand the area of a farm. The movement of fill had just been finished when 90 m of shore slid into the lake. The slide then developed retrogressively with each new slide fully liquefying and flowing into the lake. After about 40 min, a very large slide removed an area of about 150 m × 200 m. The sliding took only about 5 min. A house was seen moving down the 'quick clay river' at 30–40 km $h^{-1}$ (Gregersen, 1981).

Two cases that involved coastal failures and tsunamis have been debated as to whether they were human-induced or natural. The first occurred at Nice, France, in 1979, and involved the failure of fill that had been placed near a delta to construct a new airport (Seed *et al*., 1988). The slide contained ~$10^7$ $m^3$ of fill and native material, and occurred over a period of about 4 min. The debris moved down the sloping face of the delta deposit, into a submarine canyon, and onto an abyssal plain, eventually rupturing two sets of cables as far as 120 km offshore. A tsunami struck the coastline with a maximum amplitude of 3 m. Several lives were lost and considerable damage was done to local communities and harbours.

Two hypotheses were advanced to explain the failure at Nice.

**1** The construction area failed first, perhaps because of the construction activity. The sliding material moved downslope, undercut the canyon walls and caused continued failure of considerably more natural material.

**2** There was a large natural underwater landslide that caused a tsunami. The tsunami caused a 'rapid drawdown' condition that produced a failure in the newly constructed fill (Seed *et al*., 1988).

Considerable debate has followed both in the scientific literature and in court over the true cause of the disaster.

A similar case occurred in Skagway Alaska, in 1994, when a dock that was under construction slid into a fjord. A particularly low tide was accompanied by a series of tsunami waves estimated to be as high as 11 m. Subsequent surveys showed that a submarine landslide had occurred. Again, the debate focused on whether the dock construction caused the landslide or a large natural landslide caused the dock to fail. Rabinovich *et al*. (1999) developed a model that showed that the tsunami was caused by the dock failure and not by an external submarine landslide. However, others have argued to the contrary (Mader, 1997).

A final example of a human-induced submarine landslide occurred in 1985 near Duwamish Head in Seattle, Washington (Kraft *et al*., 1992). Dredging operations were undertaken to extend sewage effluent pipes about 3 km into Puget Sound (Fig. 12). The slide occurred during low tide, involved 400,000 $m^3$ of sediment, and resulted from liquefaction. The landslide was clearly triggered by the low tide, but the dredging operation was an underlying cause.

## CONTRIBUTIONS TO SUBMARINE LANDSLIDE RESEARCH FROM THE STRATAFORM PROJECT

The Eel margin study area of the STRATAFORM programme is an excellent place to study submarine mass-movement processes. The study area includes a sediment-laden river entering the sea, a major submarine canyon (Eel Canyon), and the area is extremely active seismically. The repeated seismic events could induce landslides. Perhaps most importantly for landslide research, previous maps had shown a submarine landslide deposit, the 'Humboldt Slide', situated within the study area (Field *et al*., 1980; Lee *et al*., 1981).

The New Jersey study area also showed evidence of mass movements. Locat *et al*. (2003) conducted a geotechnical analysis of a failure on the Hudson Apron slope using results of testing on ODP cores (Austin *et al*., 1998; Dugan *et al*., 2002) and long Calypso piston cores. The analysis showed that high excess pore pressures were required to cause the failure and that they probably acted in the context of a layered system with groundwater seepage.

In addition to the possibility of investigating landslide features, the STRATAFORM programme (in particular the Eel margin study area) provided an abundance of closely spaced and dated sediment cores that could be analysed for physical and geotechnical properties. These analyses led to a better understanding about the variability of sediment physical properties (Goff *et al*., 2002) and how marine sediment acquires shear strength as a function of increasing burial (Locat *et al*., 2002). The closely spaced cores also provided a basis for

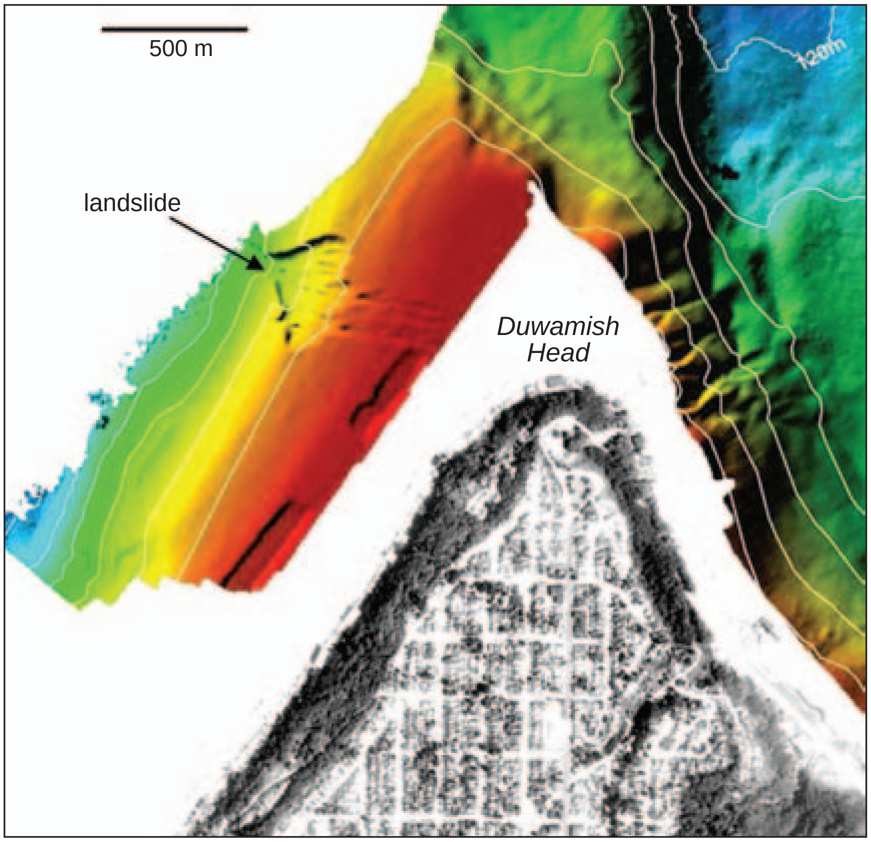


**Fig. 12** Multibeam image and aerial photography in the vicinity of Duwamish Head, Seattle, Washington. The landslide feature to the north-west of Duwamish Head occurred in 1985 during dredging operations associated with construction of two sewage effluent pipes (parallel depressions extending east from the slope failure). Two shore-parallel pits are also shown, which were produced independently by removing sediment for beach nourishment. (US Geological Survey and NOAA data.)

regional mapping of sediment properties and the development of GIS-based landslide-susceptibility predictions (Lee *et al*., 1999, 2000).

The sections below report on application of the findings to submarine landslide research, beginning with a discussion of the 'Humboldt Slide' and the controversy that has developed as to whether or not it actually represents a continental-slope failure. Next considered are failures in Eel Canyon and the factors that caused them. The following sections on gas charging and pore pressures, and the development of shear strength and rheology in marine sediment, discuss the elements that determine shear strength, which is often the most important factor in predicting instability. In fact, determining how shear strength develops in marine sediment as a result of sedimentation, stress history, biological activity and geochemical changes has been one of the most important topics investigated by marine geotechnical engineers over the past 40 yr, and has relevance to seafloor engineering as well as slope stability. The final sections discuss submarine landslide occurrence and prediction over medium to large regional scales.

## 'Humboldt Slide' controversy

### *Background*

Hummocky terrain extending over at least 90 km$^2$ was discovered on the Eel margin during offshore hazards studies conducted in the late 1970s (Field *et al*., 1980). This terrain was interpreted to be a giant submarine landslide and was subsequently named the 'Humboldt Slide'. The occurrence of giant landslides in this area is reasonable, given the many potential triggers: the rate of sediment accumulation is high owing to the proximity of the Eel River; numerous areas of gas charging and pockmarks are present (Field & Barber, 1993; Yun *et al*., 1999); and the rate of seismicity is one of the highest in the USA (Clarke, 1992). In addition, massive liquefaction failures were recorded in the nearby Klamath Delta during the 1980 earthquake.

A series of papers described the details of the 'Humboldt Slide' and attempted to analyse its cause quantitatively (Lee *et al*., 1981, 1991; Lee & Edwards, 1986; Field & Barber, 1993). Given the results of strength tests on sediment cores taken in the deposit during 1979, geotechnical analyses showed that a lateral pseudostatic earthquake acceleration of 0.12 g could have produced the failure (Lee & Edwards, 1986). Such accelerations are expected to occur frequently on the Eel margin (Frankel *et al*., 1996; Lee *et al*., 1999) as a result of the high level of seismicity known to exist near the Mendocino triple junction. Lee *et al*. (1991) performed an analysis of sediment mobility and determined that the density state (Fig. 6) was too dense to allow an initial landslide to convert into a debris flow. Rather, the sediment would fail during an earthquake, produce limited deformation along shear planes, and then maintain its stability after the earthquake shaking had stopped. This would lead to a limited deformation slide, with blocks that would not evacuate the source region. This appeared to be the morphology observed in the 'Humboldt Slide'.

Multibeam (Goff *et al*., 1999) and high-resolution sub-bottom profiles (Huntec Deep Tow System (DTS); Gardner *et al*., 1999) were obtained early in the STRATAFORM Project and provided far superior information on the 'Humboldt Slide' feature than had been available previously. Multibeam data (Fig. 13) show a crenulated surface contained within a bowl-like depression, which has been identified as an amphitheatre. The amphitheatre has a steep eastern face that is highly gullied and is separated from the crenulated surface by a smooth sloping surface. In profile (Fig. 14), the crenulated surface consists of a series of identifiable units containing reflectors that dip shoreward. The zones separating units of shoreward-dipping reflectors (Fig. 15) show that there is rough connection of reflectors between units. The zones both above and below the crenulated surface contain slope-parallel beds. There is no headwall at the boundary separating crenulated beds from slope-parallel beds.

Discussions following the acquisition of these data led to a division among participants in the project that has not yet been settled. Some participants feel that the data confirm the earlier interpretations of the feature as a giant submarine landslide (Gardner *et al*., 1999). Other participants feel that the data are more suggestive of migrating sediment waves; that is, a depositional feature formed slowly under the influence of bottom water or turbidity currents (Lee *et al*., 2002). The details of each argument follow.

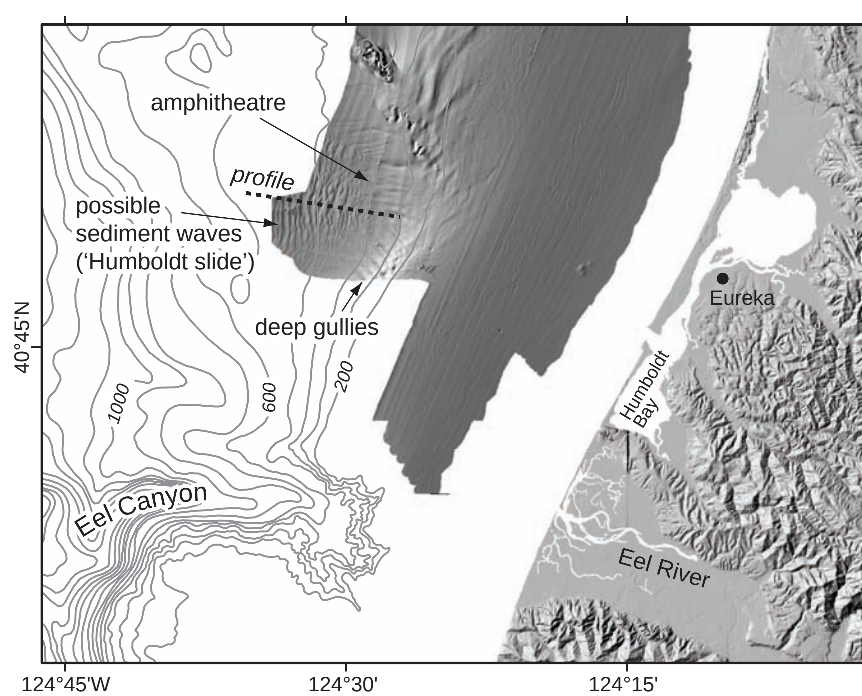


**Fig. 13** Overview of Eel River STRATAFORM area (after Field *et al*., 1999) and the 'Humboldt Slide'. Data include US Geological Survey on-shore digital elevation model, as well as shaded relief bathymetry from Simrad EM-1000 (Goff *et al*., 1999). Location of track line shown in Fig. 14 is identified.

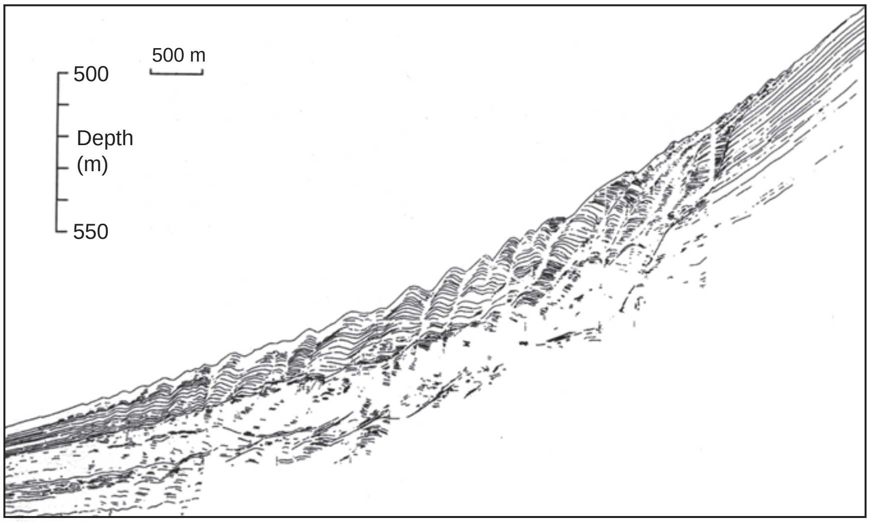


**Fig. 14** Simplified line representation of acoustic stratigraphy for the 'Humboldt Slide', obtained using a Huntec deep-tow, seismic-reflection system operating at a narrow peak frequency of about 3.5 kHz. (After Gardner *et al*., 1999.)

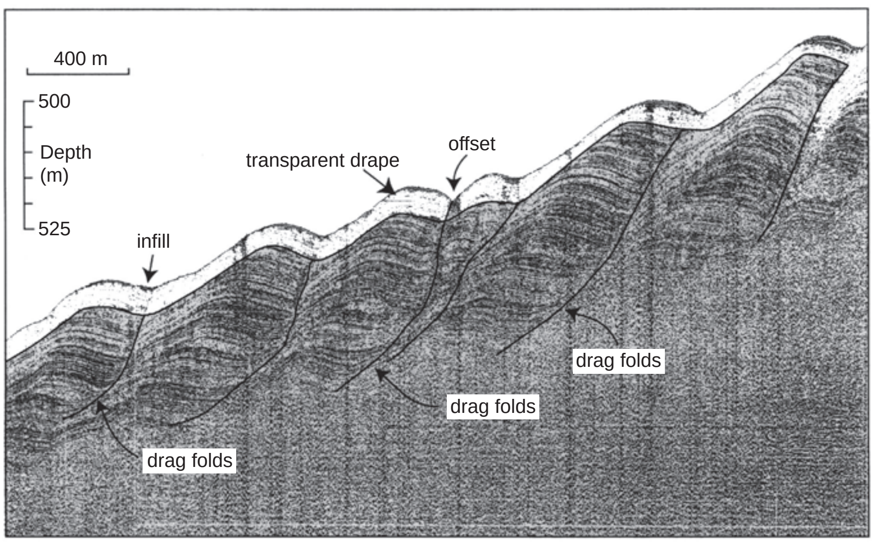


**Fig. 15** Portion of a high-resolution (Huntec) sub-bottom profile showing the main body of the 'Humboldt Slide'. Interpretations of folded and back-rotated slide blocks are supportive of a slope-failure origin (from Gardner *et al*., 1999). Interpreted shear surfaces are traced with black lines. Vertical exaggeration 20×.

*The slope-failure interpretation*

Gardner *et al*. (1999), interpreting the results of multibeam mapping (Goff *et al*., 1999), observed that the 'Humboldt Slide' lies within a shallow amphitheatre-shaped depression (Fig. 13). The depression is bounded by the shelf break to the east, by the Little Salmon Fault and an associated plunging anticline on the north, and by a bathymetric high on the south. The east (upslope) side of the depression is located at the 220-m isobath and the downslope limit of crenulation is at the 650-m isobath. The main body of 'Humboldt Slide' is elongate with a length (10 km) and thickness (60 m) that places the feature in the middle of the population of reported slides documented by Woodcock (1979). The overall feature has a thickness/length ratio (expressed as a percentage; following Skempton, 1953) of 0.6%, although the upslope portion of the feature is more elongate with a ratio of 0.2%. These relationships are consistent with those from reported submarine slides (Prior & Coleman, 1979). The eastern boundary of the depression is distinctly steeper (3°–6°) than farther down (1°–2°) in the zone of crenulations. Gullies occur along the steeper eastern side of the depression between water depths of 230 m and 380 m. They have < 20 m of relief and occur within a zone of erosion correlated with high backscatter on the multibeam image.

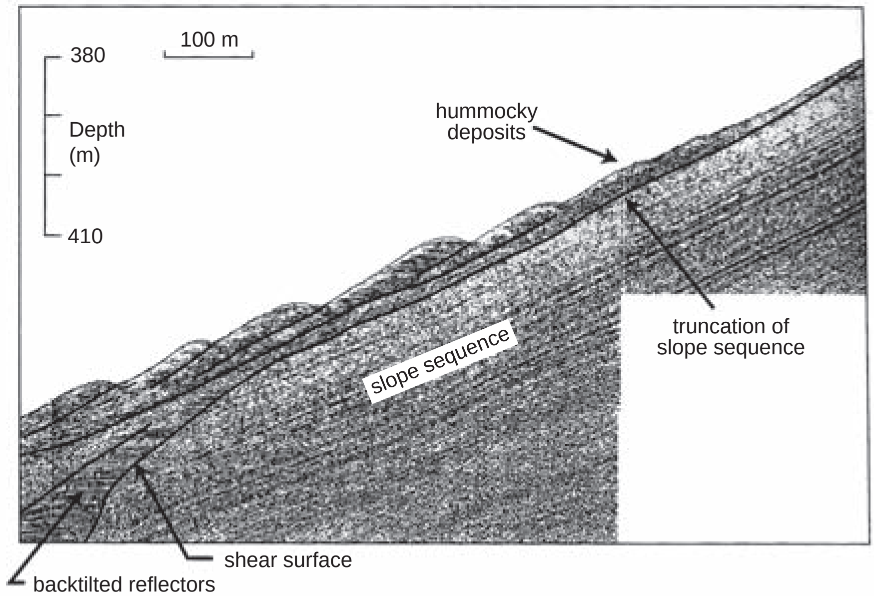


**Fig. 16** Part of a high-resolution (Huntec) sub-bottom profile showing a portion of the 'Humboldt Slide'. Interpretations shown are supportive of a slope-failure origin. (From Gardner *et al*., 1999.)

Below the base of the gullied slope, hummocky deposits of sediment occur with fingers onlapping upslope (Fig. 16). These deposits bury the lower portions of the eroded slope between the 380-m and 430-m isobaths. Farther downslope the seafloor is dominated by distinctive ridges and swales (Fig. 15) that resemble subaerial retrogressive landslides described by Mitchell (1978). The bathymetry reveals an intricate pattern of branching and truncated ridges. The ridge cross-section profiles appear as asymmetric steps with inclined risers of < 8 m relief and back-dipping treads generally 100–300 m wide. In plan view, the ridges appear relatively short and irregular around the lower flanks of the zone where slope erosion occurs (380–430 m). They are longer and more regular toward the centre and downslope portions of the 'slide' zone (Fig. 13). The treads of the ridge crests strike directly across the depression and do not parallel the curvature of the bathymetric contours. The seismic profiles between 560-m and 590-m water depths show that the ridges evolve into rhythmic, undulating forms interpreted as folds, that die out at a water depth of about 650 m (Fig. 17).

Sidescan-sonar images reveal numerous pockmarks on the seafloor throughout the region. The pockmarks on the 'Humboldt Slide' are small depressions with a random and dense distribution. Compared with the adjacent continental slope to the north, the 'Humboldt Slide' zone has a higher concentration of pockmarks (Yun *et al*., 1999), possibly indicating a greater tendency toward gas charging and strength reduction.

The erosion and gully zone (Fig. 18) extends between the 230-m and 380-m istobaths where Huntec seismic profiles show truncations of shelf reflectors with an estimated 5–15 m of sediment missing. Geotechnical tests (Lee *et al*., 1981) from cores collected in the zone show that the sediment is overconsolidated, consistent with the loss of 15 m of sediment by erosion or slope failure. Huntec seismic data show local hummocky deposits (< 5 m thick) that unconformably overlie the slope below the gullies (Fig. 16). A surface defining the upslope limit of crenulations cuts the slope sequence and crops out at the 380-m isobath (Fig. 16). This exposed basal surface separates the sequence of slope-parallel-bedded, seaward-dipping reflectors that lie upslope from crenulated, back-tilted reflectors of what is interpreted to be the main slide mass. The basal surface is locally buried < 5 m near its upslope limit by disrupted reflectors, and dips 3°–4° seaward, parallel to the slope reflectors. Farther downslope, the basal surface dips ~8° and cuts deeply into the slope section (Fig. 16).

According to Gardner *et al*. (1999), the main body of the landslide is composed of a zone of back-tilted and gently folded blocks (Fig. 15). The landward side of each back-tilted block is bounded by a gently warped surface defined by the termination of reflectors. The defining surfaces of each block generally dip seaward ~8° near the seafloor and

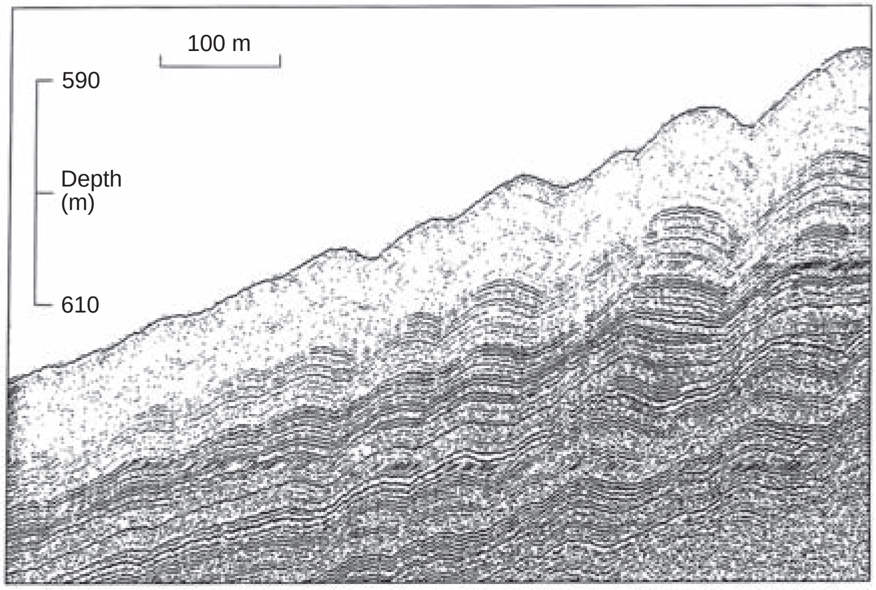


**Fig. 17** Portion of a high-resolution (Huntec) sub-bottom profile showing the toe of the 'Humboldt Slide'. According to the slope-failure hypothesis, this figure shows the transition from back-rotated blocks to gently folded to almost undeformed sequences. (From Gardner *et al*., 1999.)

gently flatten and merge with underlying reflectors having dips < 0.5° at about 65 m below the seafloor. Each tilted block is composed of anticlinally folded reflectors that dip landward 2°–4° and seaward 4°–6°. Landward-dipping reflectors within the blocks have drag folds along the separating surfaces which clearly show growth features (Fig. 15). Gardner *et al*. (1999) interpreted seaward-dipping

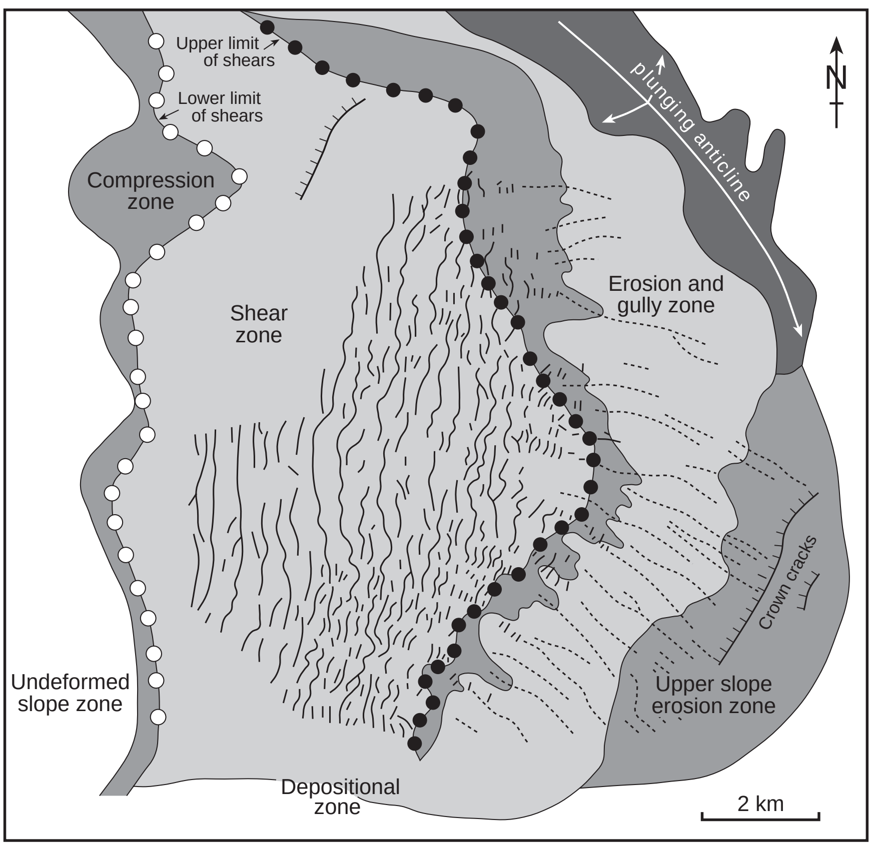


**Fig. 18** Map of the surface features of 'Humboldt Slide' derived from multibeam images and Huntec seismic profiles. Assuming a slope-failure origin, shear planes occur between the two lines of circles. Ridge crests are mapped as solid black lines within the shear zone. Gullies are mapped as dashed lines. (From Gardner *et al*., 1999.)

portions of the folds to be diffraction features from the abrupt edge of rotated blocks. If so, some of the reflectors must be broken, rather than folded, at their anticlinal axes. The diffraction features appear as seaward-dipping reflections, but they also converge and match a model of expected diffraction patterns (Gardner *et al.*, 1999). The main body of the 'slide' has been draped uniformly with a ~10-m-thick surficial unit. The drape unit is almost acoustically transparent, compared with the section it covers. Huntec profiles provide only limited information more than ~65 m below the seabed. Indications of older 'failures' beneath the 'Humboldt Slide' are suggested also by sparker profiles (Field *et al.*, 1980) and recently acquired, high-resolution multichannel seismic-reflection profiles (Fulthorpe *et al.*, 1996) confirm at least four older features with geometries similar to 'Humboldt Slide'.

The downslope transition from the main body of the 'slide' to undisturbed slope sediment occurs over a distance of ~2 km. The downslope portion of the 'slide' is characterized by gentle folds with seafloor relief less than 2 m (Fig. 17). The fold axes generally are 75–150 m apart (Fig. 17) and fold amplitudes tend to increase up-section. The undisturbed sequence beyond the distal toe of the 'slide' can be traced upslope into the increasingly deformed main body of the 'slide'. There is no evidence in the seismic data of a basal surface cropping out in the toe of the 'slide'.

Gardner *et al.* (1999) interpreted the data to show that the 'Humboldt Slide' began with basin subsidence that initiated extension-related shearing of the slope sequence to sub-bottom depths of ~65 m (Fig. 17), followed by rotation and folding of shear-bounded blocks (Fig. 19). Failure began in the middle of the 'slide' and simultaneously progressed upslope (retrogressive) and downslope (progressive). This interpretation is based on the observation that the largest apparent displacements of blocks (both horizontally and vertically) appear in the middle of the feature.

According to the landslide interpretation, the main body of the 'slide' was deformed by a combination of limited downslope translational and shallow rotational movements. The shear-bounded blocks moved short distances downslope over long, shallow, shear surfaces. The shear-surface geometry created more downslope extensional movement than rotational subsidence. The overall displacement was limited, consistent with the relatively intact

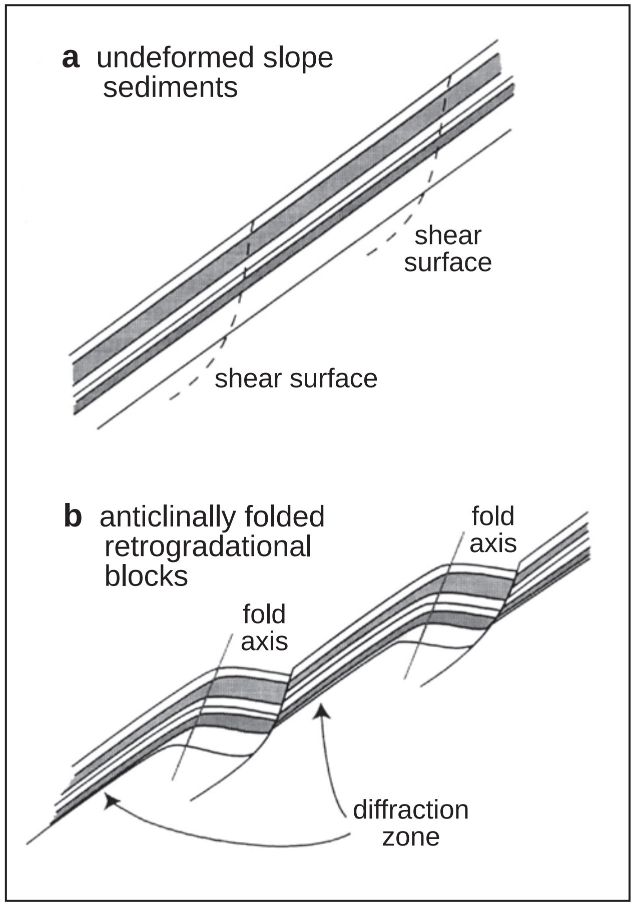


**Fig. 19** Conceptual cartoon of deformation (according to the slope-failure interpretation) within the main body of the 'Humboldt Slide'. (From Gardner *et al.*, 1999.)

character of individual shear surfaces. The toe of the slide did not fail and shows only compressional displacement because the slide movements were shear-dominated with relatively small net downslope movement.

#### *The sediment-wave interpretation*

Lee *et al.* (2002) compared the morphology of the 'Humboldt Slide' with documented observations of sediment-wave fields in a variety of environments. For example, the sediment wave field off the Selvage Islands, near the west coast of Africa, has recently been described by Wynn *et al.* (2000). As shown in Figs 20 & 21, the sediment-wave field extends over ~15 km and is present between two zones of parallel-stratified sediment consisting of interbedded turbidites and pelagic sediment. The beds within the sediment-wave field appear to

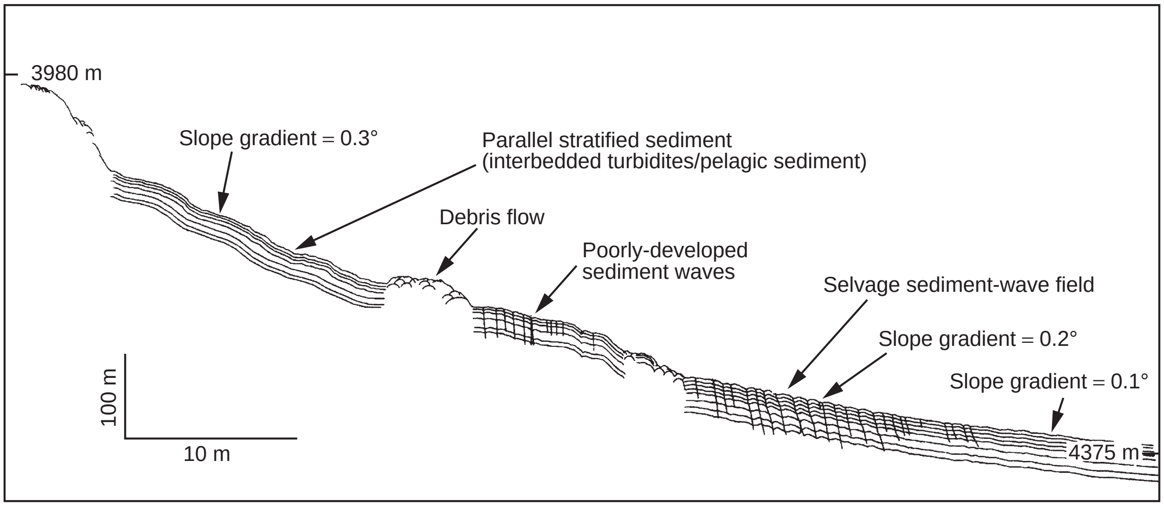


**Fig. 20** An interpretative line drawing of high-resolution (TOPAS) acoustic profiles taken across the continental rise north of the Selvage Islands. The profile shows that sediment waves occur only over a narrow range of slope angles (0.1°–0.3°) and that the sediment-wave field has expanded with time (as indicated by sediment-wave deposits near the seabed overlying slope-parallel beds at depth). (After Wynn *et al*., 2000.)

be continuous with parallel-stratified beds in the zone downslope from the wave field. The upslope transition is less clear because of rock outcrops and debris-flow deposits. However, the trend appears to be one in which individual turbidity currents (corresponding to individual turbidite beds) can contribute to both parallel-stratified bedding and sediment waves during a flow event. Significantly, the general form of the seafloor is concave upward with the sediment waves existing only within a particular range of slope gradients (0.1°–0.3°). Figure 20 shows that the wave field was less extensive in the past and that sediment waves are expanding both upslope and downslope with time. Based on a study of a number of turbidity-current sediment-wave fields, Wynn *et al*. (2000) concluded that both the wavelength and wave height typically decrease downslope.

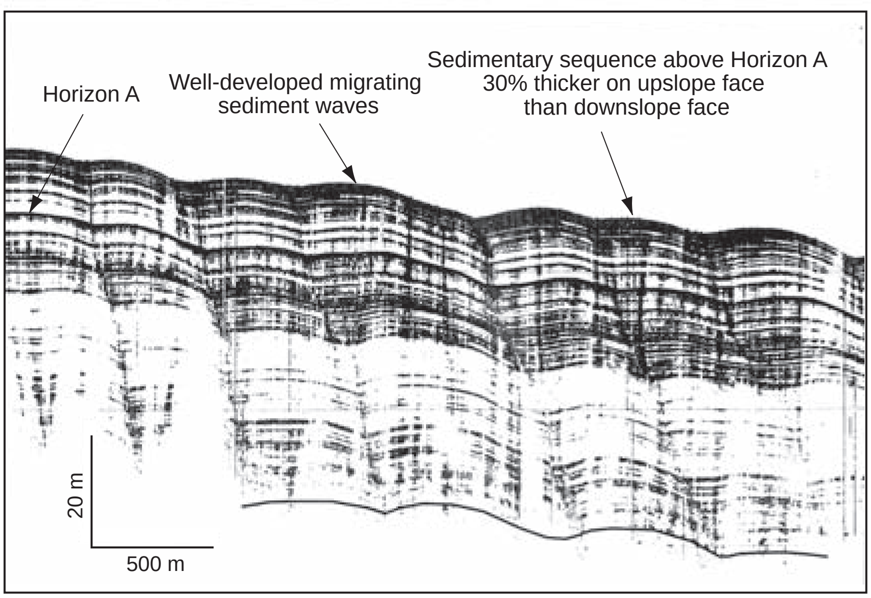


**Fig. 21** High resolution (TOPAS) acoustic profile of well-developed sediment waves in the Selvage sediment-wave field. (After Wynn *et al*., 2000.)

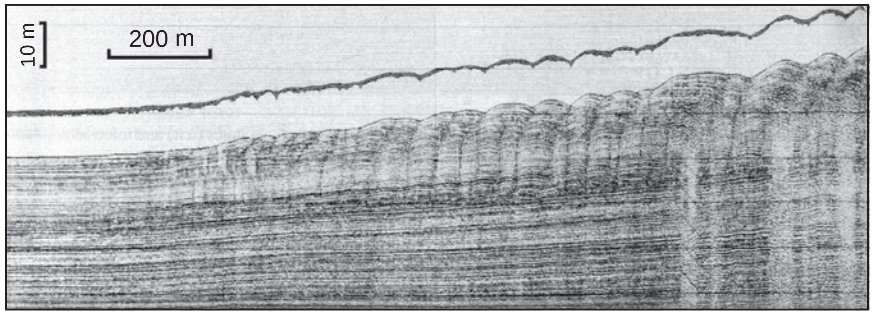


**Fig. 22** Features on the Noeick Delta interpreted as sediment waves by Bornhold & Prior (1990).

An enlargement of the central part of the Selvage sediment-wave field (Fig. 21) shows other characteristics. First, based on measurements by Wynn *et al*. (2000), the sedimentary sequence above a defined reflector is 30% thicker on the upslope face of the sediment waves than on the downslope face. This preferential accumulation pattern causes the crests of the sediment waves to migrate upslope. In addition, inflection points of reflections passing from one wave to the next line up in such a way as to mimic bounding surfaces between blocks. Close observation shows that the reflections are continuous across these 'surfaces', which are visual artefacts that provide a false impression of 'blocks' that have moved along shear planes relative to each other. These apparent surfaces can be either concave upward, concave downward or linear, depending upon the details of deposition within the sediment-wave field. The waves in Fig. 21 show all three of these shapes, occasionally within a single bounding 'surface'. The overall appearance of the sediment-wave field is one of regular, rhythmic waves.

Another feature interpreted as a migrating sediment-wave field has been reported for the Noeick River prodelta (Fig. 22, Bornhold & Prior, 1990), in British Columbia, Canada. This field is similar to, but smaller than, the Selvage sediment-wave field. The gradient of the slope is ~0.1°–1.4°, wavelengths are 50–100 m and wave heights are 2–5 m. The wave field has a general concave-upward shape in cross-section and the wavelength decreases with distance from the source. Apparent boundaries between separate waves have a generally convex-upward shape. Sub-bottom reflectors show that the wave field was less extensive in the past and that it is building out from its source. Downslope from the sediment-wave field, reflectors appear similar to or continuous with reflectors in the waves, indicating that turbidity currents in the fjord can produce either slope-parallel bedding or sediment waves. After the slope steepens beyond a certain point (a slope gradient of about 0.1°), waves begin to form; on more gentle slopes, the turbidity currents produce parallel beds.

Based on these and other examples of documented sediment-wave fields, Lee *et al*. (2002) developed the following list of criteria for recognizing sediment waves.

**1** Differential accumulation rates. The upstream flanks accumulate sediment more rapidly than the downstream flanks. This effect causes the sediment waves to migrate upslope.

**2** Continuous acoustic reflections through the features. Although spacing between reflections may vary as a result of **1**, the reflections are typically continuous throughout the sediment-wave field.

**3** In cross-section, the apparent boundaries between sediment waves may be linear, convex upwards or concave upwards. **Listric faulting**, characteristic of rotational slumps, would produce concave-upward boundaries almost exclusively.

**4** In cross-section, the overall sediment-wave field commonly has a concave-upward surface.

**5** If there is a trend, the wavelength and wave height of the sediment waves appear to decrease with distance from the source of sediment (Wynn *et al*., 2000). This may be related to a slowing of the turbidity current as it passes onto progressively more gentle gradients (Normark *et al*., 1980).

**6** Beds can be traced through sediment-wave fields into areas of parallel reflectors. This suggests that the same sequence of turbidites can produce or not produce sediment waves depending upon changes in environmental conditions (e.g. slope gradient). This effect may be related to the range of Froude numbers over which sediment-wave formation can occur (Wynn *et al*., 2000).

**7** Within many sediment-wave fields, the structure of internal reflectors appears similar from one wave to the next, that is, the waves display regularity. For example, beds within the upstream flanks tend to have generally the same dip throughout the sediment-wave field.
**8** Migrating sediment-wave fields do not require a headwall scarp or a zone of evacuation, such as is usually found in a landslide.
**9** Sediment-wave fields are constructed over a long time period and involve deposits from many turbidity currents (e.g. the Amazon fan, Shipboard Scientific Party, 1995). Accordingly, profiles through the deposits often show rhythmic bedding extending all the way to the sediment surface.

Within the 'Humboldt Slide' there are alternating bathymetric highs and lows that create block-like units (or 'sediment waves') with a wavelength of 400–1000 m, and a wave height of 2–10 m. Individual 'wave' crests can be traced for up to 4.5 km along isobaths (Fig. 13). Within the main body of the feature, internal reflections can be traced across the crests and troughs of each wave (Figs 23, 24a & 25). The downslope flank of one wave meets the upslope flank of the next lower wave within a zone that can vary from sharp and acoustically incoherent to broad and traceable across the features (Fig. 23). In some cases, these zones become broader up-section, whereas in other cases they become broader down-section. The latter observation provides a critical constraint on the origin of these features. If the block-like units were in fact slide blocks, then there would be a discontinuity (fault) between the units. Growth faults, which would be active at the time the sediment is being deposited, should decrease in slip up-section. Faults rarely decrease in slip down-section. In Fig. 24a, apparent displacement between units decreases down-section, so strain would have to be accommodated down-section some other way, for example, through a low-angle **décollement**. No such décollements are apparent. Given these observations, the suggestion can be made that in many of the block-like units ('waves') sediment beds are continuous, favouring a sediment-wave origin for the feature. Note that the scale of the wavelengths and wave heights is comparable to that observed in recognized sediment-wave fields, and that wave length and wave height decrease with distance seaward (Fig. 14), in accordance with the usual trend observed in sediment-wave fields elsewhere (Wynn *et al*., 2000).

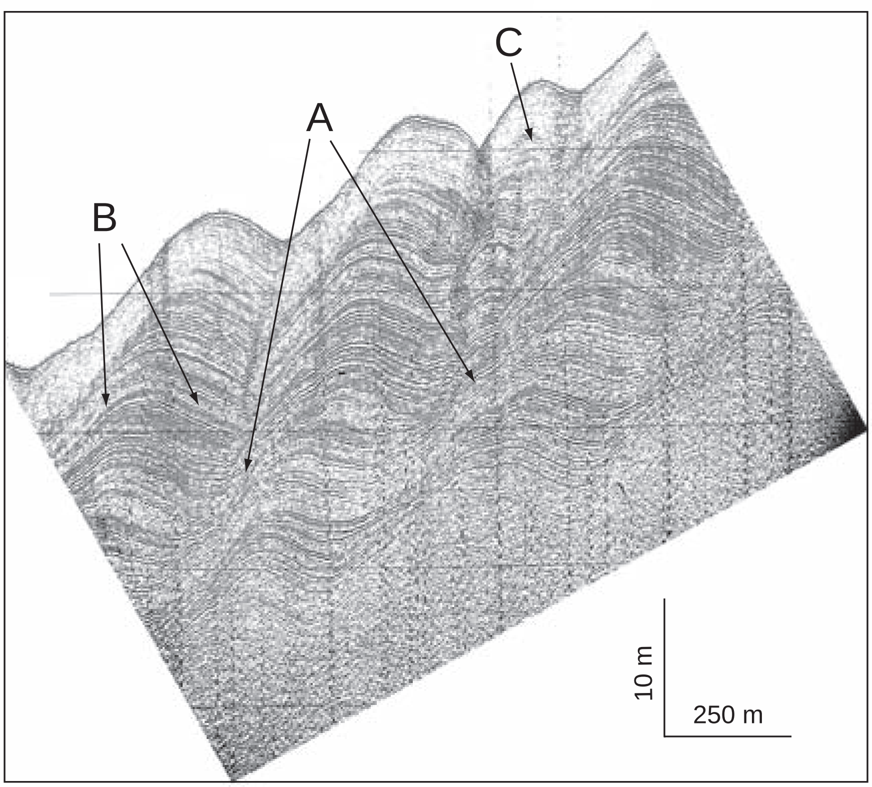


**Fig. 23** Huntec sub-bottom image from the main body of the 'Humboldt Slide', showing: A, internal reflections that can be traced from one wave to another; B, layers in the downslope flanks that are thinner than the same layers in the upslope flanks; C, a wave that merges down-section with the upslope wave. (From Lee *et al*., 2002.)

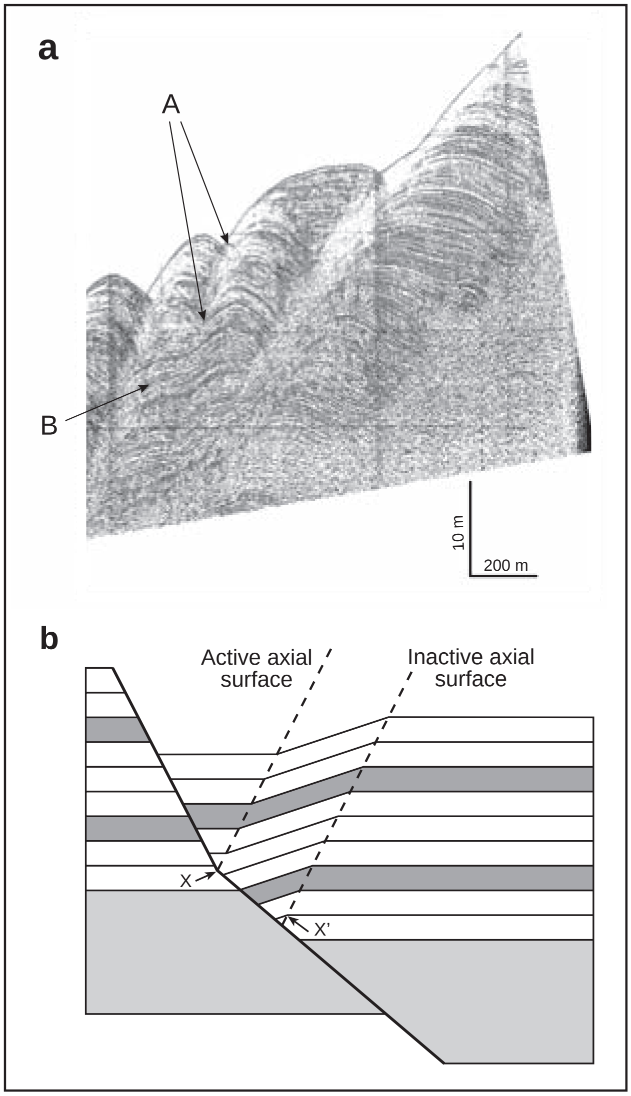


**Fig. 24** (a) Huntec sub-bottom image of waves within the main body of the 'Humboldt Slide', showing: A, a zone that separates two waves decreases in offset down-section, counter to most structural faults; B, at depth, internal reflectors can be traced across the two units, whereas up-section at A the continuity cannot be traced through the hyperbola. If a fault is present up-section, the displacement must be transferred parallel to bedding and over the 'folded' strata above B. (From Lee *et al*., 2002.) (b) Diagram illustrating the deformation that would develop for a block sliding from X to X' along a listric fault. (From Xiao & Suppe, 1992.) The active and inactive axial planes of the block dip seaward, in contrast with the axes of the wave-like features in the 'Humboldt Slide', which dip landward.

In contrast, the slope gradient is steeper for the 'Humboldt Slide' than for deep-water sediment waves, and the overall environment is different (continental slope versus deep-sea fans).

Individual 'waves' off the Eel River have upslope flanks that display thicker beds than the downslope flanks. This results in a landward (upslope) migration of the 'wave' crest. If the landward-migrating packages were in fact slide blocks, a concave-upward basal shear surface (slip plane) would produce a landward-dipping axial plane and an apparent seaward migration of the block's crest (Xiao & Suppe, 1992; Fig. 24b). Such geometry is, in fact, the opposite of what is observed in the 'Humboldt Slide', where the boundaries between block-like units commonly appear to be convex upward or linear (Fig. 24a). If the linear boundaries between blocks were slip planes, then the intersection of these internal slip planes and the basal surface would be concave upward (and the axial surface of the fold would dip landward). The surface that joins the crest of the 'waves' dips seaward, however, contrary to geometry of an axial plane that would form in a fold above a slip plane. The geometry of the internal structure for the 'Humboldt Slide' is not compatible with the kinematics for a series of moving blocks.

Figure 25 shows neither a headwall scarp nor zone of evacuation at the landward margin of the 'Humboldt Slide'. In fact, this figure allows the tracing of individual reflections from the slope-parallel region above the feature to the undulating block-like units observed within the feature. Such an interpretation implies a depositional origin for the feature rather than shear deformation and faulting at the landward margin. Near the downslope edge of the feature, undulating reflections pass into a zone of slope-parallel reflections without interruption.

On the basis of the above arguments, Lee *et al*. (2002) concluded that the 'Humboldt Slide' is not a landslide deposit, but rather is a field of migrating sediment waves. Lee *et al*. (2002) suggested that a plausible explanation for the formation of this field is that turbidity currents form at or near the mouth of the Eel River (perhaps related to hyperpycnal flows from the river) and flow through a series of deep gullies into the bowl-shaped depression (amphitheatre) that contains the 'sediment wave field' (Fig. 13). In the steeper area of the exposed gullies, on the upper part of the continental slope,

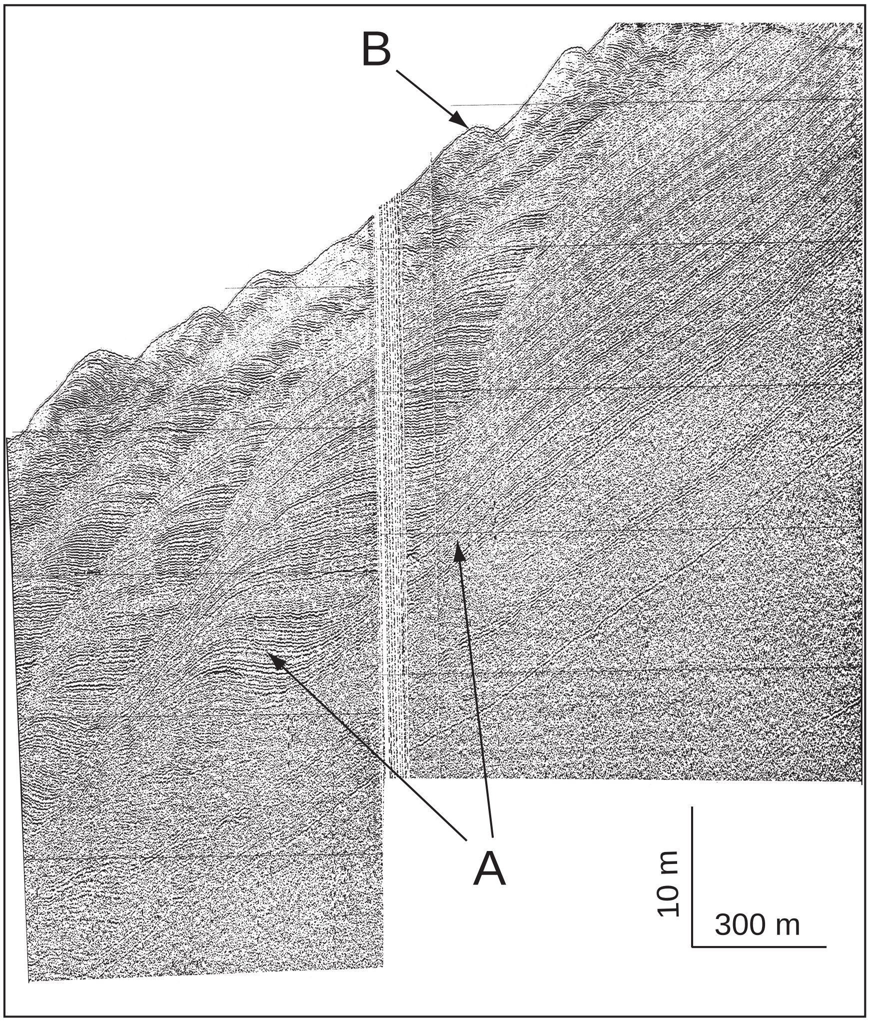


**Fig. 25** Huntec sub-bottom image of the upper portion of the 'Humboldt Slide' (Fig. 16). Note that strata A can be traced across the 'shear surface' interpreted by Gardner *et al*. (1999; Figs 16 & 19). The uppermost 'wave' field B represents the most recent period of 'sediment wave' accumulation. (From Lee *et al*., 2002.)

the sediment is overconsolidated (Lee *et al*., 1999). This may indicate bypassing or erosion by traversing turbidity currents. In greater water depths than this overconsolidated zone, turbidity currents would accumulate slope-parallel beds over a short (~1 km) distance (Fig. 14). The turbidity currents could then begin to deposit their load as sediment waves (Fig. 25). Sediment-wave accumulation continues for 6 km downslope, with distal sediment waves having lower wave height and wave length than the proximal waves (Fig. 14). To the west of the wave field, the turbidity currents again deposit slope-parallel beds.

Recent studies have provided further information on the formation of the 'Humboldt Slide'. Schwehr & Tauxe (2003) developed a technique that measures the **anisotropy of magnetic susceptibility** (AMS) of sediment as an indicator of deformation. The technique has been applied to known slump deposits on land and adjacent undeformed sediment, and has shown that the AMS records are clearly different and that deformed sediment presents a clear AMS signal. The same technique has been applied to core samples from the 'Humboldt Slide'. Based on examining cores from the centre and top of the 'Humboldt Slide' structure, Schwehr *et al*. (2003) found no evidence for deformation. The cores are from areas that are clearly free from drape, and thus the authors were sure that they were sampling the structure seen in high-resolution sub-bottom profiles.

*A similar controversy in the Adriatic Sea*

Crenulated features similar to the 'Humboldt Slide' have also been identified in the Adriatic Sea and described by Correggiari *et al*. (2001), who interpreted the features as examples of failures in a late Holocene highstand prodelta wedge. Lee *et al*. (2002) noted the resemblance to sediment waves and questioned the landslide origin proposed by Correggiari *et al*. (2001). Lee *et al*. (2002) applied the criteria for recognizing sediment waves listed above, and concluded that the features probably are sediment waves. Subsequently, Cattaneo *et al*. (2004) revisited the subject and asserted that there are differences between the crenulated features in the Adriatic and the deep-water sediment waves that Lee *et al*. (2002) reviewed in developing the list of criteria. The differences listed by Cattaneo *et al*. (2004) include:

**1** the Adriatic features occur in shallow water (30–70 m water depth);
**2** they are several orders of magnitude smaller than the deep-water waves and the sediment accumulation rates are as much as three orders of magnitude higher;
**3** they do not develop upslope-dipping limbs;
**4** they do not show any consistent trend in downslope variation of undulation parameters;
**5** they show a great morphological variability with minor changes in water depth away from the offlap break.

The differences discussed by Cattaneo *et al*. (2004) are important, but they do not disprove a sediment wave origin for the features. Rather, they may imply that turbidity-current sediment waves can occur in a variety of environments, including shallow water, and that the resulting morphologies may be somewhat different. The Adriatic crenulations do not show clear shear planes or a headwall scarp that would confirm a landslide origin. They do, however, show some evidence of deformation at the base of their section and also possible fluid-escape deformations within the crenulated sediment body. Accordingly, the situation in the Adriatic (and possibly at 'Humboldt Slide' as well) may not be one of pure landslide or sediment-wave origin, but rather a hybrid containing elements of each (similar to features described by Faugères *et al*. (2002) in the Bay of Biscay). Another factor affecting the growth of crenulations in the Adriatic may be bottom sediment transport, possibly influenced by internal waves (Puig *et al*., in press).

The controversy in the Adriatic Sea may be resolved at least partially by careful examination of deep cores that were drilled through the crenulations in the summer of 2004 by the PROMESS Project. Similar cores in the 'Humboldt Slide' could also contribute to a resolution. Finally, a kinematic model of the 'landslide' blocks would be useful to determine if the resulting deposits are geometrically possible.

#### Liquefaction failures in Eel Canyon

Studies of sediment input to Eel Canyon demonstrate that considerable amounts of sediment are being supplied on annual and century timescales (Mullenbach & Nittrouer, 2000; Mullenbach *et al*., 2004). During the winter of 1999–2000, an instrumented mooring and a benthic tripod were installed in the northern thalweg of the canyon, and a tripod was installed on the shelf (Puig *et al*., 2003). The instruments showed that Eel Canyon acts as a preferential conduit of sediment to the deep sea. Sediment fluxes within the canyon were not directly related to the Eel River discharge, but they were linked to the occurrence of major storms that generated down-canyon density-driven flows, carrying large amounts of sediment toward deeper parts of the margin (Puig *et al*., 2003).

The mechanism for mobilizing flows down-canyon probably involves components of mass movement, where recently deposited sediment fails or liquefies during storms and the failed sediment is easily eroded, entrained into the water column and transported down-canyon as a sediment gravity flow (Puig *et al*., 2004). Another possibility might be the migration of fluid muds off the shelf and into the canyon, but measurements from one of these events demonstrated that it would take 12 h for fluid mud to move from 60 to 65 m water depth. Such a flow would arrive at the outer shelf many hours after being generated by wave action in shallower locations. Tripod data showed that the sediment gravity flows occurred almost simultaneously with an increase in orbital velocity at the bed of the canyon head. The flows did not coincide with a major flood event, and fluid muds were not observed on the shelf when sediment gravity flows were observed in the canyon head (Puig *et al*., 2003). The rapid formation of sediment gravity flows, immediately after the increase of wave-orbital velocity, suggests that such flows could not be initiated from wave-current resuspension alone. Entrainment of sediment into suspension requires a period of time (hours) to fill the boundary layer with enough particles to generate fluid-mud and develop a gravity flow (Traykovski *et al*., 2000).

The more likely mechanism for mobilization is wave-load-induced **liquefaction** (Clukey *et al*., 1985; Puig *et al*., 2004). During a given storm, infiltration pressures oscillate with wave pulses, while cyclic-shear-stress-induced excess pore pressures increase progressively. When the bed structure is degraded and the effective stress is lowered, the critical shear stress for sediment erosion decreases significantly and the volume of transportable sediment under large wave stresses can increase considerably. Additional gravity shear stresses imposed by the gradients at the canyon head can help initiate transport of wave-fluidized sediment and generate sediment gravity flows. The thickest deposits were consistently observed in the upper channel thalwegs (< 500-m water depth) and not deeper (Mullenbach *et al*., 2004), suggesting that most of the sediment transported down-canyon settles to the seabed at depths just below where wave energy is sufficient to maintain the sediment gravity flow.

#### Gas charging and pore pressures

Investigations made during the STRATAFORM programme showed that the Eel margin displays plentiful examples of gas-charged sediment. Seismic reflection data (Yun *et al*., 1999) and ROV dive observations (Orange *et al*., 2002) show evidence of spatially variable subsurface gas in many areas. Gas distribution is subparallel to isobaths (Fig. 26) and occurs in both near-surface and deep sub-bottom

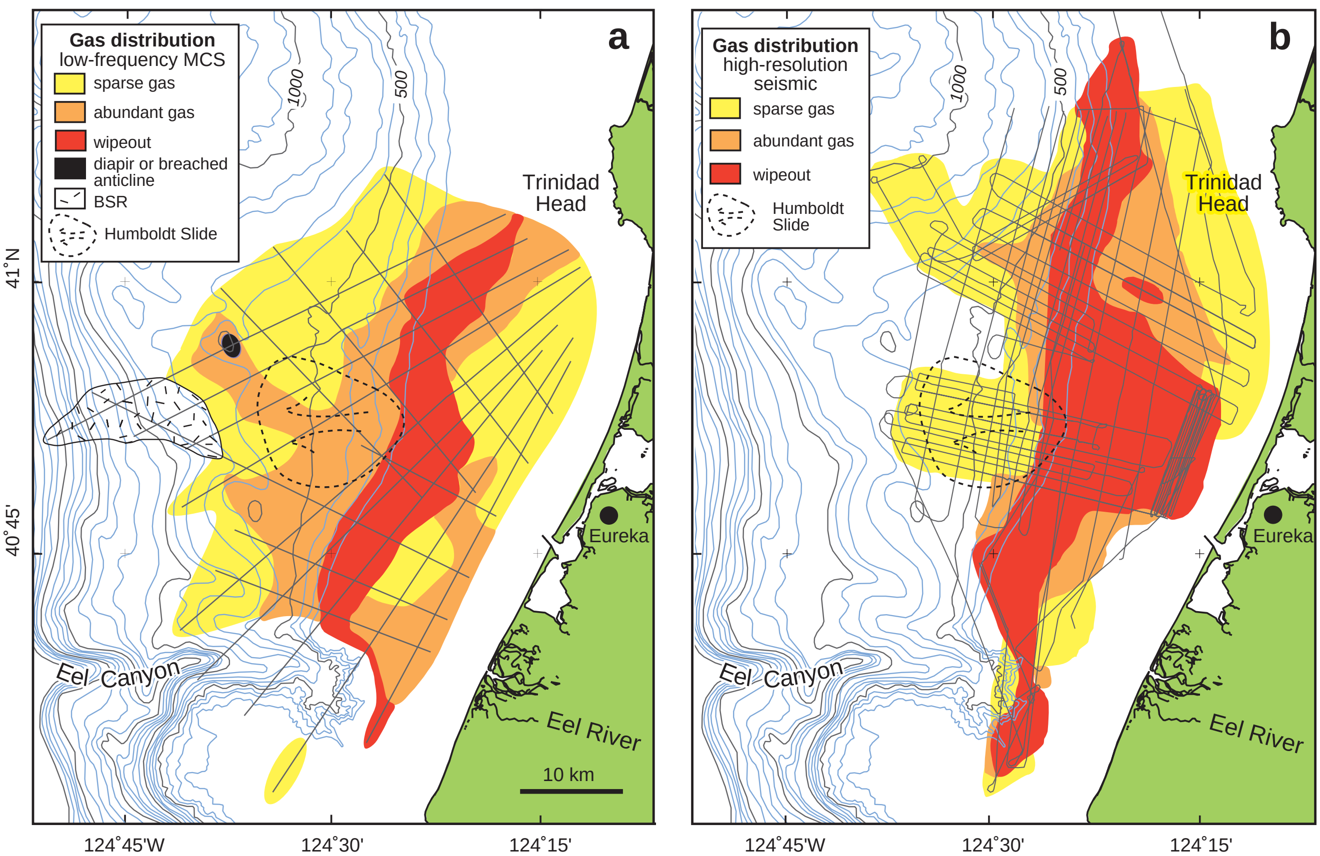


**Fig. 26** Gas distribution on the Eel margin. (a) Map based on multichannel-seismic reflection data. The area mapped as BSR is underlain by a bottom-simulating reflector, a possible indicator of gas hydrates. Note that gas-abundance trends are subparallel to isobaths, with a zone of abundant gas in the 'Humboldt Slide'. (b) Gas distribution in upper seabed determined from Huntec high-resolution seismic reflection data. Regions of most abundant gas occur landward of the 400-m isobath. The body of the 'Humboldt Slide' appears nearly free of gas in these data in contrast to (a). (Modified from Yun *et al*., 1999.)

sediment. An area of acoustic wipeouts and pockmarks is found near the head of the amphitheatre containing the 'Humboldt Slide' and suggests that gas migration is related to the feature, either as a cause or an effect. Field & Barber (1993) suggested that gas migration has played a role in forming the 'Humboldt Slide'.

Yun *et al*. (1999) concluded that gas expulsion through pockmarks is a significant force for redistributing sediment and increasing bed roughness in water depths less than 400 m, where most pockmarks are found. Using an average diameter of a detectable pockmark as 15 m and an excavation depth of 3 m, Yun *et al*. (1999) found that over $6.6 \times 10^5$ m$^3$ of sediment in an area ~2100 km$^2$ has been excavated and redistributed by gas expulsion. Some pockmarks occur in linear gullies (Fig. 27) suggesting a causative relationship between fluid expulsion in geomorphological lows and gully excavation (Orange *et al*., 2002). However, an ROV dive that focused on this region showed no evidence for fluid seepage.

*In situ* pore pressures were measured at five stations on the Eel margin using the Excaliber probe (Christian, 1993, 1998), which reached a maximum penetration depth of 4.6 m. Only small *in situ* pore pressures were measured, with the largest value of 0.5 kPa measured at a sub-bottom depth of 3 m. Such a value represents about 3% of lithostatic pressure and could result in a shear-strength reduction of about that amount. Such a level of pore pressure is probably not a significant factor in affecting the stability of the Eel margin. However, higher excess pore pressures deeper in the seabed or at other sites could exist and could be important.

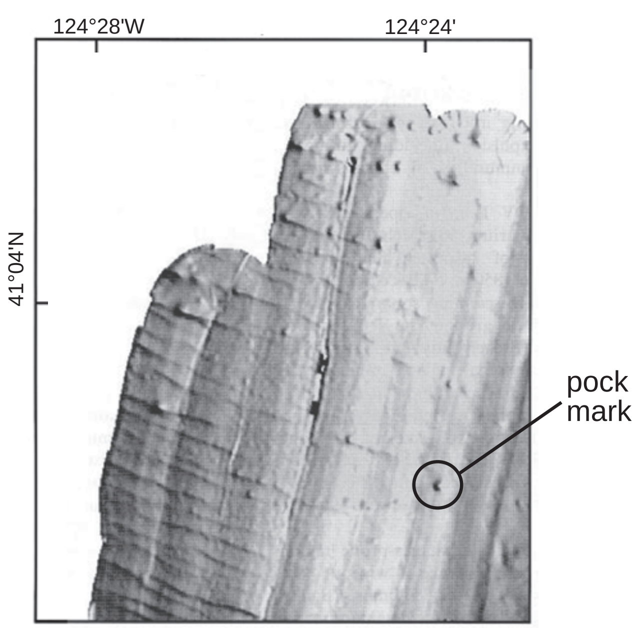


**Fig. 27** Shaded relief multibeam bathymetry of the Eel continental slope, showing the occurrence of pockmarks along the axes of gullies. (From Orange *et al*., 2002.)

In general, the results of work on gas charging and pore pressures in the Eel margin are ambiguous. There are reasons (e.g. seismic wipeouts, pockmarks, high accumulation rates) to expect both, but direct proof has been elusive and evidence of slope failure is limited.

### Development of shear strength and rheology in marine sediment

The STRATAFORM programme presented an opportunity to develop an improved understanding of how marine sediment acquires shear strength, because the northern California site demonstrated an interesting paradox. The area clearly has many of the triggers needed to cause slope failure, but broad regions of the open slope show no evidence of landslide features (even if the 'Humboldt Slide' is considered to be a failure). Either the driving stresses are lower than expected, or the strength is higher. Accordingly, factors that might lead to higher than expected shear strength were evaluated as a means of explaining the extensive slope regions without landslides.

#### *Physical properties of reconstituted sediment*

To understand the development of shear strength, a normally consolidated sediment can be reconstituted in the laboratory and compared with natural samples to determine the effects of various factors on the development of geotechnical properties. Two samples (designated S80 and Y450), corresponding to the maximum range in grain size found on the Eel continental margin, were reconstituted in a large cell that reproduced both the SEDimentation and CONsolidation phases of a sediment (SEDCON test; Locat, 1982; Perret, 1995; Locat *et al*., 1996). The **liquidity index**, $I_L$, is an important measure for the **degree of openness** (relative proportion of space filled with fluid, analogous to porosity or void ratio but normalized to account for variations in plasticity) in a sedimentary deposit

$$I_L = (w - w_p)/I_p \tag{7}$$

where $w$ is the water content (% dry weight), $w_p$ is the plastic limit and $I_p$ is the plasticity index (liquid limit minus plastic limit). The liquidity index shows how the water content of the sediment compares with the common geotechnical properties, the **Atterberg limits** (liquid, plastic limits, plasticity index). The **plastic** and **liquid limits** (determined by standard tests) correspond to the water contents at which a remoulded sediment begins to behave as a plastic or liquid. The plasticity index is the difference between the liquid and plastic limits. The liquidity index reflects the sediment's stress history much better than the water content (or porosity or density). That is, sediments with different mineralogies and grain sizes but the same stress histories will have the same liquidity index, although water contents and porosities may differ. Note that a sediment with a water content greater than or equal to the liquid limit does not necessarily behave as a liquid, if it is undisturbed. It will behave as a liquid after remoulding.

In Fig. 28, SEDCON test results for Eel margin sediment (S80 and Y450) are compared with test results for Québec clays from Saguenay Fjord (SF, Perret, 1995). The similarity of all of these SEDCON curves on a broad variety of sediments is due to the normalizing effect obtained from using the liquidity index. For a vertical effective stress ($\sigma'_v$) greater than 1 kPa, SEDCON curves for most sediment can be described as a power-law function of the following form:

$$I_L = a(\sigma'_v)^{-b} \tag{8}$$

The values of the coefficients $a$ and $b$ are given in Table 1. The range of SEDCON test results provides a good estimate for the degree of openness for normally consolidated sediment. Using the liquidity index allows a broad range of sediment types to be represented with one compression curve. Any other measure of the degree of openness of the sediment (e.g. water content, porosity) would require multiple curves.

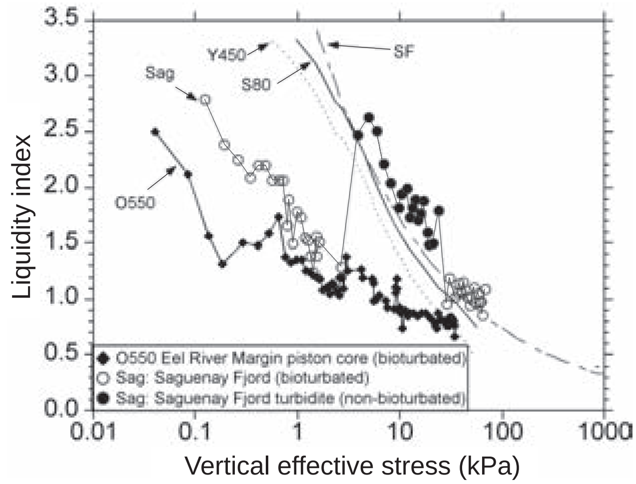


**Fig. 28** Relationship between the liquidity index and burial effective stress to show the impact of bioturbation on the consolidation properties of a sediment. Sediments from the Eel River Margin (O550) and Saguenay Fjord (Sag) are compared with respect to their reference curve obtained by SEDCON tests. Curves identified as S80 and Y450 are for two reconstituted samples of the Eel continental margin, whereas the SF curve is for a reconstituted sample from the Saguenay Fjord (Québec). All the SEDCON curves (S80, Y450 and SF) are similar. The Saguenay Fjord sediment contains a 5-m-thick turbidite (black dots), which follows more or less the SEDCON curve. The other portions (open circles), particularly above the turbidite, are at a liquidity index that is clearly below that of the SEDCON curve. The Eel margin sediment (O550) has a trend similar to the bioturbated part of the Saguenay Fjord curve which is well below the SEDCON curve. Accordingly, for these sediments, bioturbation probably reduces the liquidity index (or porosity) at least in the upper part of the sediment column. (After Locat *et al.*, 2002.)

**Table 1** Empirical evaluation of coefficients for Eq. 8 developed for three sites (see Fig. 28)

| Site | S80 | Y450 | SF |
|---|---|---|---|
| Coefficient *a* | 3.70 | 3.25 | 3.99 |
| Coefficient *b* | 0.38 | 0.40 | 0.37 |

*Sediment densification and strengthening from bioturbation*

The SEDCON curves (Fig. 28) represent sediments that are normally consolidated and have **sensitivities** (ratio of undisturbed to remoulded shear strength) varying from 5 to 10 (Locat & Lefebvre, 1986). These curves can be used to assess properties of sediments that differ in stress history (e.g. overconsolidation). The profile at O550 illustrates a typical marine sediment that has been subjected to bioturbation, whereas the 'Sag' site (Perret *et al*., 1995) contains a rapidly deposited layer that was not bioturbated. The liquidity indices for O550 lie well below those obtained using the SEDCON tests, and this is possibly due to sediment deposition rate (time) and bioturbation.

The SEDCON test procedures simulate a sediment deposition rate more rapid than that occurring in nature with the exception of catastrophic events such as debris flows or turbidity currents. These are comparable to, or even faster than, the rate imposed by the SEDCON test, i.e. centimetres of sediment emplaced in minutes to a few hours. This is shown by the 'Sag' profile, which contains a 5-m-thick turbidite (Fig. 28, filled circles). The turbidite is situated between units of bioturbated sediment, with liquidity indices (open circles) that are low relative to the SEDCON curve of Perret (1995; Fig. 28, curve marked SF). The liquidity-index values for the turbidite (effective stress levels of about 3–15 kPa) are very close to those expected from the SEDCON curve. Within the turbidite, consolidation processes are similar to the simple compaction present in the SEDCON test. The more slowly deposited and bioturbated sediment above and below the turbidite is significantly more dense (lower liquidity index).

Under its own weight, a normal sediment deposit rapidly reaches a liquidity index between 2 and 3 near the water–sediment interface. The depth and intensity of bioturbation depend on the ambient fauna, but the net impact of the community can be to aggregate particles through particle repackaging (e.g. faecal-pellet production; Wheatcroft *et al*., this volume, pp. 101–155). This will increase the bulk density of the sediment while the effective stresses are still low (< 0.5 kPa), so that the liquidity-index effective stress curve is depressed well below the SEDCON curve. At locations where rapid sedimentation occurs, the deposit may not be bioturbated, and would retain a signature characterized by an abnormally high liquidity index and more uniform changes in shear strength (Mucci & Edenborn, 1992; Perret *et al*., 1995; Maurice *et al*., 2000).

Other investigators (Bokuniewicz *et al*., 1975; Richardson *et al*., 1983; de Deckere, *et al*., 2001), working mainly with shallow coastal sediments, have not observed densification or strengthening associated with bioturbation. Typically, these investigators found that biological activity has destabilized the seabed surface, resulting in highly remoulded, high-porosity sediment in the upper 10 cm. Bioturbation also increases random variability of physical properties on the scale of a few centimetres. Investigators have also indicated that the response of sediment to bioturbation is related to the composition of the benthic community.

#### *Sediment densification and strengthening from repeated seismic loading*

Seismic loading and oversteepening were considered in the early work of Morgenstern (1967), and many procedures for prediction of submarine landslide initiation have since focused on these triggers (Lee *et al*., 2000). However, recent work on Eel margin sediment (Boulanger *et al*., 1998; Boulanger, 2000) has shown that repeated, non-failure, seismic events can actually strengthen the sediment column through development of excess pore-water pressures during earthquakes and subsequent drainage, resulting in densification during intervening periods. This effect was observed during a series of cyclic-loading and drainage tests on normally consolidated fine-grained sediment. An example of the test results is given in Fig. 29 for a reconstituted sample that was initially normally consolidated. Here, the sediment begins to exhibit overconsolidation and a significant reduction in void ratio (directly related to porosity and liquidity index) if a period of drainage (~days) is allowed between repeated earthquake simulations. By relating the amount of densification to an equivalent degree of overconsolidation in these samples, the increase of strength that would result from this process could be estimated in response to four significant (simulated) earthquakes. During each earthquake, pore-water pressures increased in the sediment, and then dissipated with time after the earthquake. The sediment slowly densified, and the shear strength increased by about 65%. This seismic strengthening possibly explains, at least in part, the paucity of shallow submarine landslides on the Eel margin, an area that has much seismic activity.

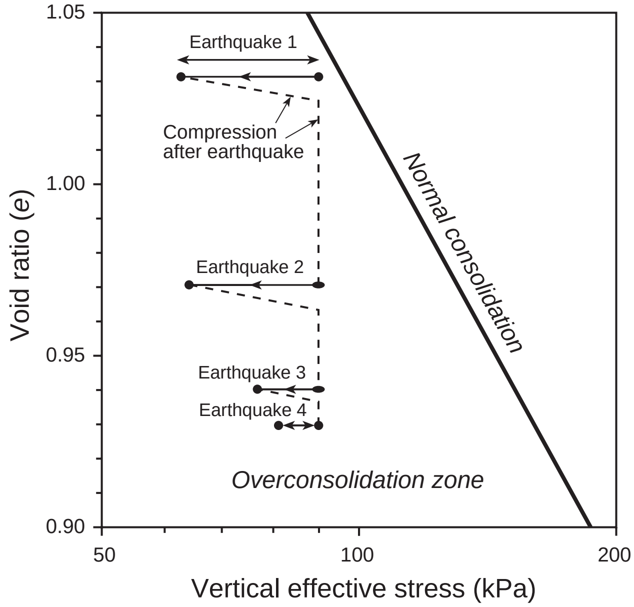


**Fig. 29** Effects on void ratio of a few alternating episodes of cyclic loading and drainage (Boulanger *et al.*, 1998; Boulanger, 2000).

*Changes in liquidity index, density and strength due to burial*

An important component of the STRATAFORM programme was to bridge the gap between early burial (few metres) and deep burial (few hundred metres). In many cases, shear strength data are available only for depths of < 15 m in the sediment column. The SEDCON curves, which simulate the process of increasing stress from sediment accumulation, allow the extrapolation of experimental data to greater depths in a manner similar to standard consolidation tests (Richards, 1976). The SEDCON curves can be expressed in terms of density, water content, or liquidity index versus depth (Locat *et al.*, 2002). Regressions of SEDCON curves S80 and Y450 were used to evaluate the effect of burial at site O550 (Fig. 30).

The liquidity index of a sediment at its natural water content correlates well with the remoulded shear strength, $s_{ur}$, which can be approximated (Locat & Demers, 1988) by the following relationship

$$s_{ur} = \frac{\delta}{(I_L)^{\varepsilon}} \tag{9}$$

where $\delta = 1.167$ kPa and $\varepsilon = 2.44$. Leroueil *et al.* (1983) conducted a similar analysis and obtained values of 1.615 kPa and 2.27 for the empirical terms, $\delta$ and $\varepsilon$, respectively. Then, by assuming a value for the sensitivity ($S_t$ ~ 2–10 typical of normally consolidated marine sediment; Richards, 1976;

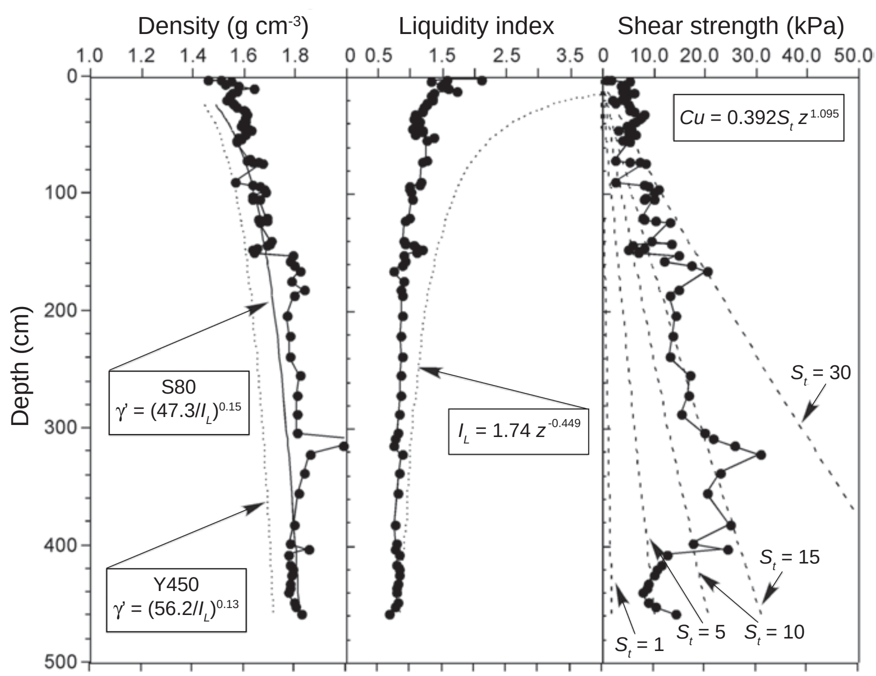


**Fig. 30** Development of sedimentation-consolidation predictive models based on SEDCON test results applied to short sample core O550 from the Eel margin. The models were developed using SEDCON curves S80 and Y450 as shown in the panels of density and liquidity index versus depth. The right panel illustrates the development of shear strength as a function of depth ($z$) based on the equation relating $Cu$ (note $Cu = S_u$) and sensitivity ($S_t$). (From Locat *et al.*, 2002.)

Locat & Lefebvre, 1986), it is possible to calculate the intact undrained shear strength ($s_u$) using:

$$s_u = S_t \lambda z^{1.095} \quad (10)$$

where $\lambda = 0.392$ kPa (a coefficient derived from Eqs 8 & 9) and $z$ is the depth below the seabed. The value of sensitivity introduces a large uncertainty for these calculations, but Eqs 3 & 10 provide two different approaches for estimating shear-strength profiles in normally consolidated sediment.

The smooth lines shown in Fig. 30 are predicted values calculated from SEDCON tests (Eqs 8 & 10). For shear strength, the predicted curves are provided for sensitivity ranging from 1 to 30, an upper limit for sensitivity in marine sediment (Richards, 1976; Locat & Lefebvre, 1986). Note that these predictions are for normal consolidation and ignore strengthening effects.

Considering the previous discussions concerning the effects of bioturbation on sediment density (and shear strength), it is not surprising to see that observed and predicted values are not in very good agreement at shallow burial depths. However, there is some convergence of the results with depth (Fig. 30), indicating that the initial differences due to alternate strengthening processes (e.g. bioturbation, cementation) are minimized, at least for the density and liquidity-index parameters. The strength values are indicative of well-structured sediment, with either a relatively high sensitivity (~15) or a relatively high degree of overconsolidation (Richards, 1976; Locat & Leroueil, 1988).

To check the applicability of these relationships to greater depths, liquidity-index data from core O550 (Eel Margin), Saguenay Fjord turbidite (Sag) and Osaka Bay Kansai clay, Japan (Tanaka & Locat, 1999) were compared (Fig. 31). The Osaka Bay profile represents a sequence of alternating sand and clay layers, and provides a good check because it extends to almost 400 m below the seafloor. An ash layer at a depth of about 250 m has been dated as ~700,000 yr BP, and the sedimentary history is complex due to interactions of basin filling and tectonic movements. Despite the complexity, the overall distribution of Osaka Bay data lies near or slightly above the SEDCON curves, and is roughly in line with the extension of the Saguenay Fjord profile. These results support the validity of Eq. 8.

#### *Sediment rheology*

In modelling mobilized sediment flows, the sediment and water mixture can be considered to be a fluid with a yield stress, so that the rheological behaviour of the matrix can be represented by a **yield strength** and **viscosity**. The Bingham model is routinely used to model debris flows (Johnson, 1970). It is defined by

$$\tau = \tau_y + \eta\gamma \quad (11)$$

where $\tau_y$ is the yield strength, $\eta$ is the viscosity, $\gamma$ is the shear rate and $\tau$ is the corresponding shear stress. According to the model, the flow moves as a plug surrounded by sheared fluid (Fig. 32) and progressively loses thickness. Motion ceases when the thickness of the sediment flow can no longer produce enough shear stress to exceed the yield strength. If the model assumptions are true, the thickness of a debris-flow deposit is a measure of its **rheology**. With an estimation of the viscosity ($\eta$) based upon rheometer tests of similar material, the degree of runout can be predicted. The simplicity of the Bingham model has been utilized many times by outcrop geologists seeking an estimation of travel distance for both subaqueous (Hiscott & James, 1985) and subaerial (Whipple & Dunne, 1992) debris flows.

The yield strength and viscosity can be related to the liquidity index (Locat & Demers, 1988; Locat, 1997) as long as the liquidity index is greater than 0 (i.e. for a water content above the plastic limit). Locat (1997) found that the yield strength contributes about 1000 times more than the viscosity to the resistance of the fluid to flow. These relationships have been represented numerically (Locat, 1997) and used by Elverhøi *et al*. (1997) to analyse the behaviour of debris flows along the coast of Norway.

In response to the complexities observed by many researchers (Coussot & Meunier, 1996), yield-strength models have been extended to several different generalized forms. The most common is the Herschel–Bulkley model (Hemphill *et al*., 1993)

$$\tau = \tau_c + K\gamma^n \quad (12)$$

where $\tau_c$ is the critical shear stress, $K$ is a linear coefficient analogous (although not identical) to viscosity and $n$ is an exponent describing the rate

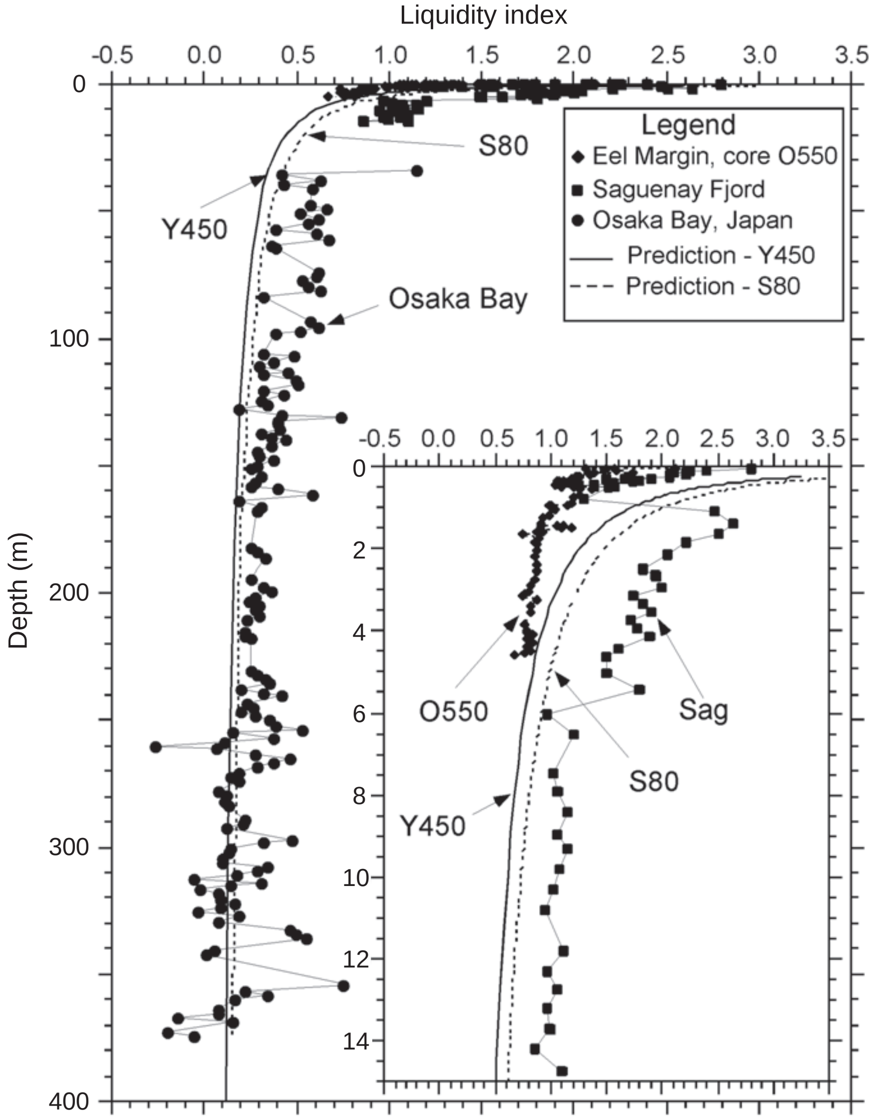


**Fig. 31** Application of sedimentation-consolidation predictive models derived from SEDCON tests Y450 and S80, to a deep profile from Osaka Bay, Japan, and to a long core from the Saguenay Fjord Central Basin (Sag). The insert panel expands the first 15 m, where an Eel margin sample (O550) is compared with the Saguenay Fjord sample (Sag) – all with reference to the sedimentation-consolidation models. (From Locat *et al.*, 2002.)

of change of the viscosity with the shear-imposed stress. If $n = 1$, Bingham behaviour is regained. If $K = 1$, the formulation is of a power-law fluid (another common rheological model). In most cases, the viscosity will depend on the shear rate. If the viscosity is decreased by increasing shear, the material is said to behave as a **shear-thinning fluid**; if viscosity is increased, it is **shear thickening**. Another possibility is the bilinear model

$$\tau = \tau_{ya} + \mu_{dh}\gamma - \frac{\tau_{ya}\gamma_0}{\gamma + \gamma_0} \qquad (13)$$

where $\tau_{ya}$ is an apparent yield strength, and $\mu_{dh}$ and $\gamma_0$ are coefficients that regulate behaviour at small shear rates. Equations 11–13 outline the three most common yield-strength models.

In addition to the above Bingham rheological models, Norem *et al.* (1990) proposed to analyse the mobility of subaqueous mass movements by using a visco-plastic model described by

$$\tau = \tau_c + \sigma(1 - r_u)\tan\phi' + \mu\gamma^n \qquad (14)$$

where $\sigma$ is the total stress, $r_u$ the pore-pressure ratio ($u/\gamma z$), $\mu$ is a viscosity-like term similar to $K$ in Eq. 12, $\phi'$ the friction angle and $n = 1$ for viscous flow and 2 for inertial or granular flow. This constitutive equation is a hybrid model, similar to that proposed by Suhayda & Prior (1978). The first

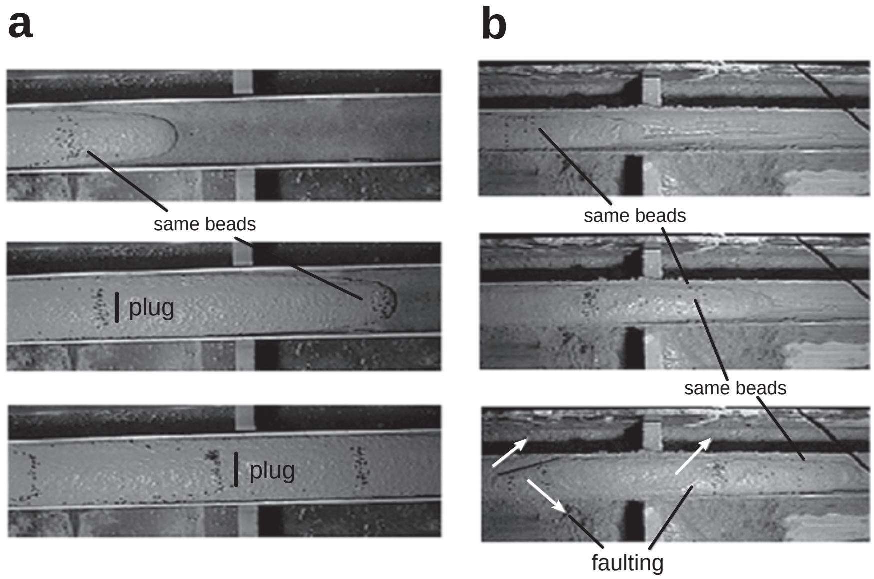


**Fig. 32** (a) Debris-flow experiment illustrating unsheared plug and shear bands (near sides of flow). The behaviour of the material is well described by a yield-strength model (shear thinning, Herschel–Bulkley). The sand content in the experiment was 50% by volume. The pipe diameter was 15 cm. (b) Coarse-grain experiment where frictional behaviour was observed. The snout in this flow was driven forward by accumulation of flowing material in the debris-flow body. The sand content in this experiment was 65% by volume. The pipe diameter was 10 cm. All frames were obtained approximately 1 s apart. (From Parsons *et al*., 2001.)

and third terms are related to the viscous components of the flow, as in Eqs 11–13. The second term is a plasticity term described by the effective stress and the friction angle. This approach can be adjusted to various flow conditions. For example, for a rapid (undrained) granular flow, the third term of Eq. 14 with $n > 1$ is most important. In the case of a mud flow (undrained), terms one and two would dominate with $n = 1$. For flows where the excess pore pressures can dissipate, the second term could dominate and the equation would approach the sliding-consolidation model proposed by Hutchinson (1986). For rock avalanches, the last two terms would be most significant.

Substantial criticism has been levelled against all of these yield-strength models in recent years (Iverson, 1997; Major, 2000). Large-scale experiments have shown that the interstitial pore pressure plays a key role in regulating the fluidity of a sediment mass (Iverson & LaHusen, 1993; Iverson, 1997). Once failure is initiated, pressures within the moving material are increased. Due to the low permeability of most natural materials, these pressures remain elevated and continue to fluidize the material (Major, 2000). The effects of heightened pore pressures are not easily incorporated into a Bingham model. As a result, Iverson (1997) proposed an alternative to the yield-strength-fluid model. The new model attempts to marry the clay-dominated Bingham behaviour with the pore-pressure-modulated granular dynamics observed in the large-scale experiments, incorporating both yield-strength and frictional behaviour. The model also recovers a yield-strength model for fine-grained systems. The only drawback is that it requires a partitioning of the grain-size distribution into granular material (grains) and matrix (slurry). As a result, experiments are required to characterize the transition of granular behaviour and assess the degree to which sand participates in the formation of a fluid phase.

Previous experiments to assess the rheology of natural materials have been performed in rheometers of various geometries. These devices typically impose shear onto the flow in an artificial manner (i.e. a central spindle turning within a larger cylinder), and have focused on coarser materials relevant to subaerial debris flows (Major & Pierson, 1992; Coussot & Piau, 1995). Major & Pierson (1992) discovered that as the percentage of sand is increased, the fluid becomes increasingly shear thinning. In addition, when shear rates are large ($\gamma > 10\ s^{-1}$), the material will behave more like a yield-strength fluid. However, using the results of O'Brien & Julien (1988) for shear rates in natural, subaerial flows, Major & Pierson (1992) concluded that debris flows with an excess of 20% sand by volume will behave frictionally.

Parsons *et al*. (2001) sought to examine the rheological transition of a fine-grained slurry to a frictionally dominated mass in a geometry similar to an actual flow. Using profiles of velocity across the surface and the flow rate of sediment in half-pipes of different size, they were able to vary the shear rate on a single sample and derive rheological behaviour (based upon Whipple, 1997). They also altered the grain-size distribution and the clay content to examine effects on rheology of natural materials. Contrary to earlier work in rheometers, the Bingham model predicted the flow rate of material (within experimental error) for all runs with sand contents less than about 50% by volume. Their experiments also showed that clay contents of 2.5% were adequate to produce yield-strength behaviour, while clay contents in excess of 5% produced a Bingham fluid.

Like earlier studies (Major & Pierson, 1992; Coussot & Piau, 1995), Parsons *et al*. (2001) found that frictional behaviour dominated for shear rates less than $10\ s^{-1}$, whereas strongly sheared flows behaved more like a yield-strength fluid. Unlike earlier studies (Major & Pierson, 1992), shear rates were observed directly within the flows and generally exceeded $10\ s^{-1}$, even for gentle gradients (i.e. $< 10°$), because the shear rate was associated with the shear bands bordering the half-pipes (Fig. 32). The plug did not participate in shearing, and was not used as the length scale in the calculation of the shear rate (unlike O'Brien & Julien, 1988). At the shear rates observed, shear-thinning behaviour was dominant and fine sand participated in the formation of the fluid phase. Within the plug, frictional behaviour most probably dominated, but this region did not regulate travel distances. These results indicate that the boundary between matrix and grain behaviour (Iverson, 1997) is highly complex and flow dependent.

The transition to frictional behaviour consistently began at the snout of the flow, which was found to coarsen and 'dry' quickly (Parsons *et al*., 2001). Coarse snouts are typical of both subaerial (Whipple & Dunne, 1992) and subaqueous (Hiscott & James, 1985) debris flows. However, the snouts observed by Parsons *et al*. (2001) did not form because of purely frictional processes. The flow itself caused coarse material to collect there, possibly due to internal circulation in the manner described by Suwa (1988). The bodies of flows remained fluid, so the flow rate caused material to pile up behind the snout and drive the flow forward (Fig. 32). It is uncertain how these mechanics interact with the dynamics of hydroplaning, which is a common dynamic process associated with subaqueous debris flows and is discussed at length in Parsons *et al*. (this volume, pp. 275–337).

A key question, which also applies to subaerial mass movement, is how sediment acquires these rheological properties. For example, Locat *et al*. (1996) indicated that the mobilized yield strength (or remoulded shear strength) back-calculated for Gulf of Mexico debris flows was up to three orders of magnitude lower than the minimum remoulded shear strength that was measured in the potential source area. There must be mechanical processes taking place during the transition from slide to flow that generate a mixture having a very low remoulded shear strength. Understanding this transition, which is accompanied by acceleration of the moving mass, remains one of the major challenges ahead in the study of mass movements.

### Submarine landslide geomorphology

Based on multibeam bathymetric data and GLORIA sidescan surveys, McAdoo *et al*. (2000) identified a total of 83 gravity flows, slides and slumps on the continental slopes of Oregon (Fig. 33a), central California (Fig. 33b), Texas (Fig. 33c) and New Jersey (Fig. 33d). The largest failures occur in the Gulf of Mexico, adjacent to Mississippi Canyon and between salt withdrawal basins (McGregor *et al*., 1993; Silva *et al*., 2004). Smaller landslides occur within the basins, and at the base of the Sigsbee Escarpment (Orange *et al*., 2003; Young *et al*., 2003). The smaller landslides tend to have higher headscarps than the larger ones and do not mobilize into mass flows as readily, indicating a stronger rheology. The Oregon section has the steepest slopes, but surprisingly few large failures for a seismically active margin, implying that slope angle and seismic activity may not be the most important slope-stability controls. A similar absence of failures in a comparable environment occurs in the Eel margin. The California continental slope is heavily incised, and this makes it difficult to identify landslides. Most of the landslides occur within larger canyons and adjacent to a pockmark field near Point Arena. The majority of the landslides on the New Jersey slope occur on the open slope between two major canyons. The slope in the Gulf of Mexico has the highest percentage (27%) of its surface area covered with failures, followed

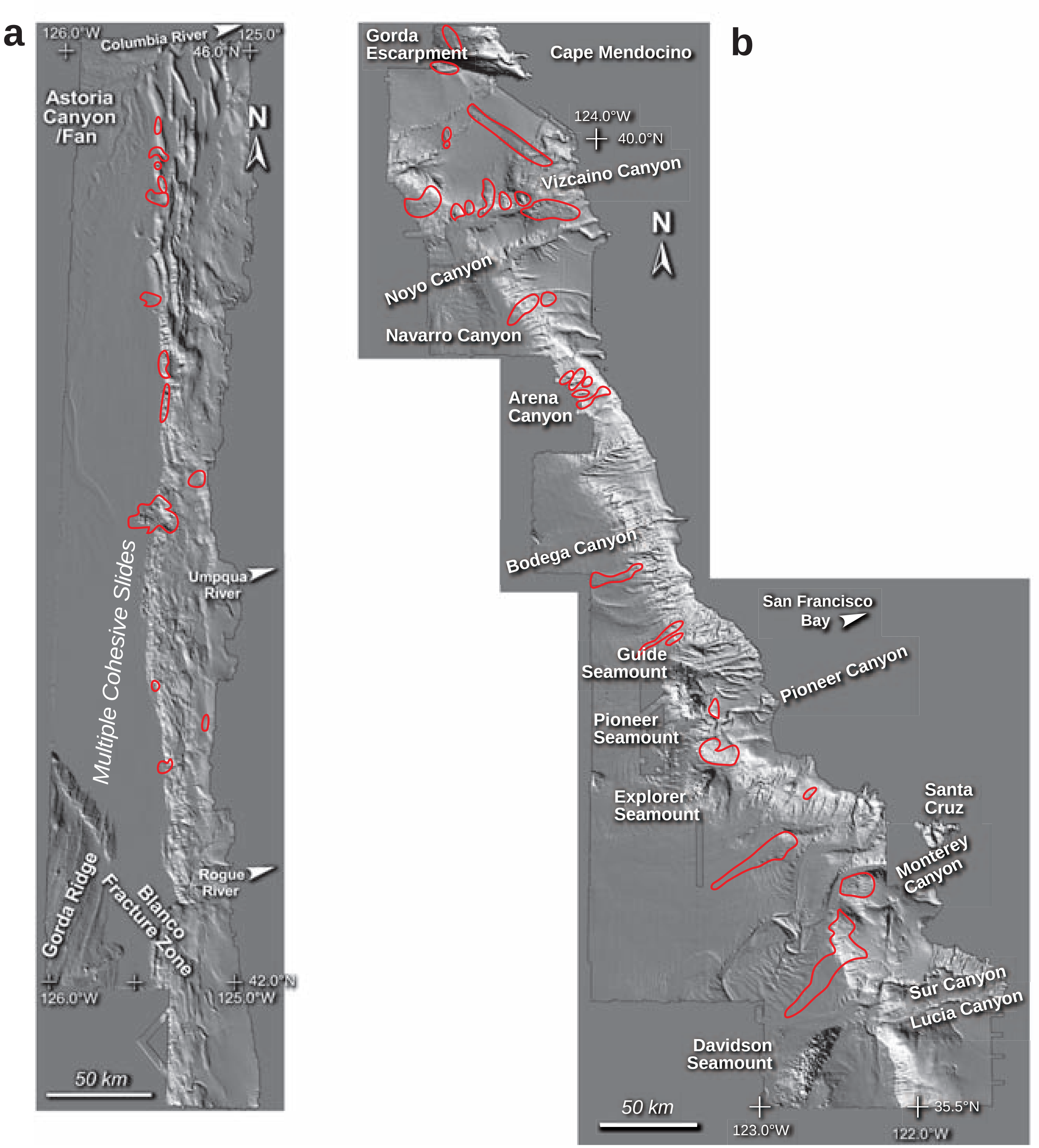


**Fig. 33** Gridded NOAA multibeam bathymetric data of the (a) Oregon, (b) California, (c) Gulf of Mexico and (d) New Jersey margins. Landslides are outlined in red. (After McAdoo *et al.*, 2000.)

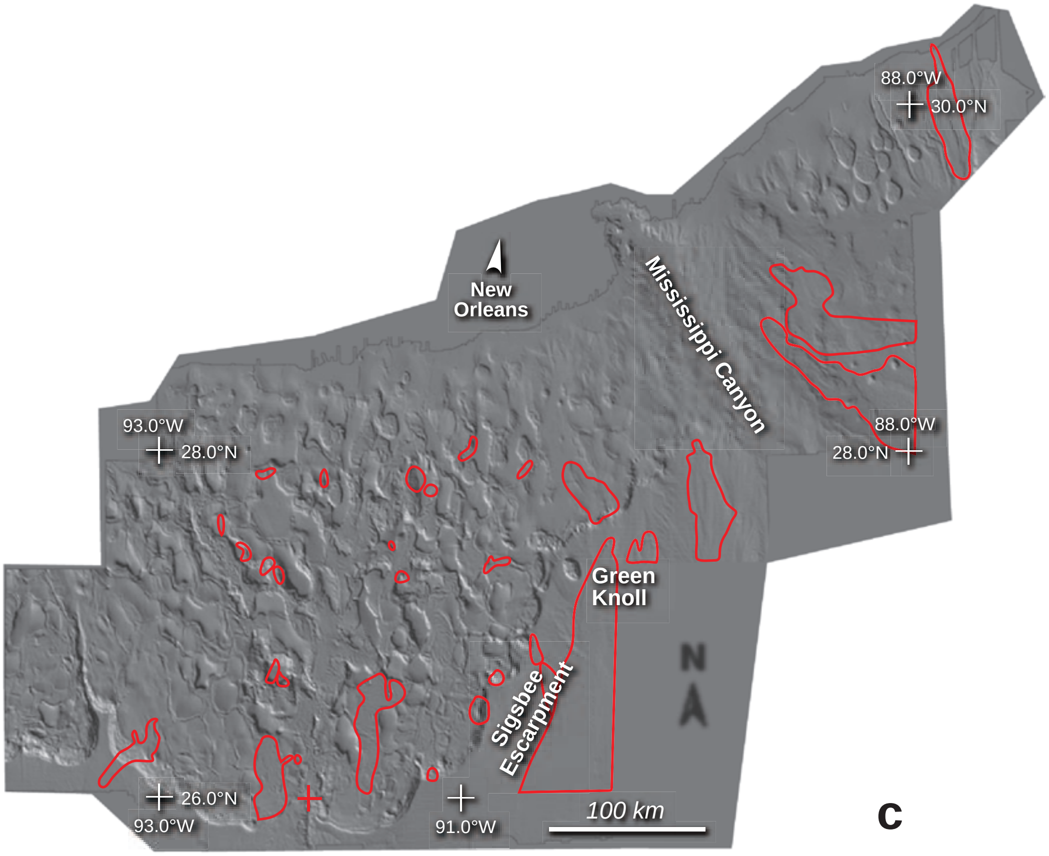
88.0°W
30.0°N
New Orleans
Mississippi Canyon
93.0°W
28.0°N
88.0°W
28.0°N
Green Knoll
Sigsbee Escarpment
N
26.0°N
93.0°W
91.0°W
100 km
c

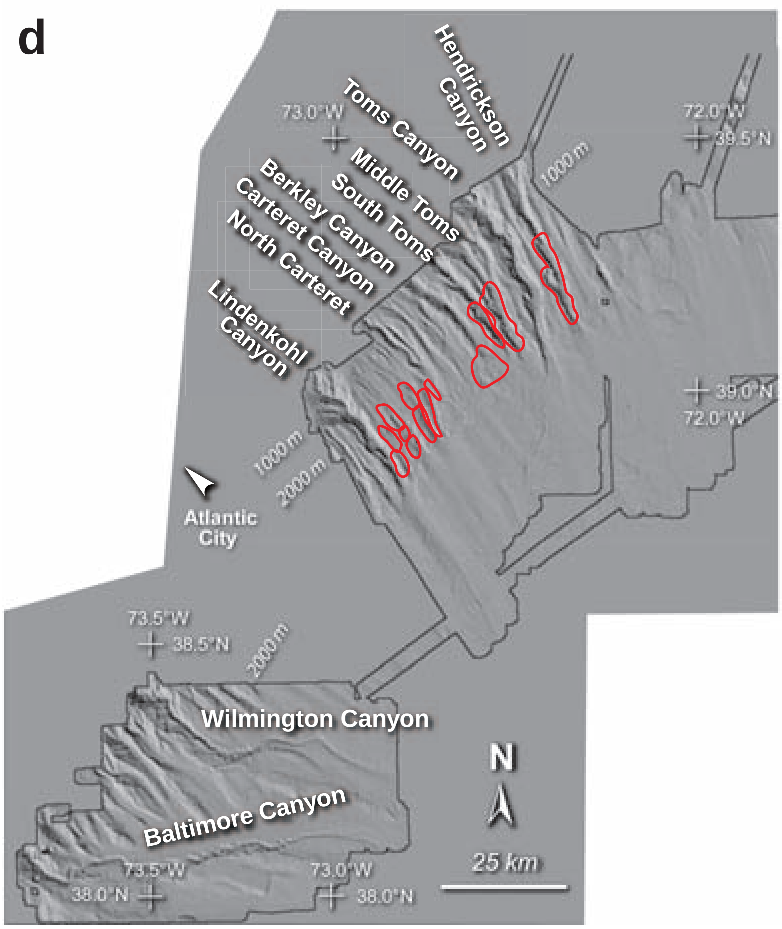
d
Hendrickson Canyon
Toms Canyon
73.0°W
72.0°W
39.5°N
1000 m
Middle Toms
South Toms
Berkley Canyon
Carteret Canyon
North Carteret
Lindenkohl Canyon
39.0°N
72.0°W
1000 m
2000 m
Atlantic City
73.5°W
38.5°N
2000 m
Wilmington Canyon
N
Baltimore Canyon
25 km
73.5°W
38.0°N
73.0°W
38.0°N

**Fig. 33** (*cont'd*)

by New Jersey (9.5%), California (7.1%) and Oregon (3%). Interestingly there is a rough inverse relation between the area covered by landslides and the local seismicity.

McAdoo *et al*. (2000) developed a set of morphometric statistics based on their synthesis. They found that most landslides occur on slopes with gradients < 10°, and that the steepness of the slope adjacent to the failure tends to be inversely proportional to the runout length. In both California and Oregon, slope failures tend to make the local slope steeper, whereas failures in the Gulf of Mexico and New Jersey slopes tend to make the local slope less steep. Landslides with rubble beneath the scar are generally small, deep seated and make the slope steeper. The ratio of headscarp height to runout length can be used as a measure of the failure's dynamic rheology. For submarine landslides, this ratio is orders of magnitude less than it is for subaerial landslides. McAdoo *et al*. (2000) noted that hydroplaning of the failed mass may be responsible for very long runout lengths.

#### Regional mapping of landslide susceptibility

Multibeam techniques provide detailed maps that describe seafloor topography with a high degree of precision. This information can be used to calculate the bathymetric gradient at any point, and compute gravitationally induced shear stresses throughout a region. This is a strong first step toward predicting the susceptibility of the seafloor to mass movement. In addition, multibeam systems often provide measures of backscatter intensity that contain information about lithology at the water–sediment interface and, in time, will allow evaluation of surface density and grain size. For now, bathymetry and surface character can be used to make predictions about the regional response of the seabed, including shallow-seated seabed stability. These sorts of analyses have been used productively on land (Carrara *et al*., 1991; Jibson *et al*., 1998). For the seafloor, several regional schemes to predict landslide susceptibility have been developed; the first of these originated out of the STRATAFORM programme.

##### *GIS mapping*

Lee *et al*. (1999, 2000) presented a methodology for applying the infinite-slope method to assess the regional variability of slope-failure potential. A series of layers were used that were operated upon by algorithms within the structure of a geographical information system (GIS). The first two layers were a map of bathymetric gradients from multibeam data (Goff *et al*., 1999) and a map of surface density derived from analyses of closely spaced sediment cores.

Conducting a regional slope-stability analysis requires estimating an appropriate shear strength, in this case, on the basis of a surface density map. Given that seismic loading may be the critical condition for slope failure, two factors were considered:

**1** the short duration of earthquakes will cause failure to occur without any flow of pore water (undrained loading);
**2** the cyclic nature of earthquake loading will cause pore-water pressures to increase or decrease and will alter the shear strength.

Both these factors are considered if the strength is evaluated using a **cyclic, undrained triaxial strength test**. In such a test, cylindrical samples are encased in a membrane and consolidated to an initial effective stress, $\sigma'_c$, which is equal to the overburden effective stress being simulated. Commonly, consolidation stresses applied in the laboratory are large enough (well beyond the maximum stresses measured) that the sediment sample is forced into the normally consolidated range. Following consolidation, repeated cycles of shear stress are applied in both extension and compression until failure (defined as 15% axial strain) is achieved. For a given sediment, the number of loading cycles required to reach failure varies inversely with the applied cyclic-shear-stress level.

On a semilog diagram, the **cyclic stress ratio** (CSR) is plotted versus the number of cycles to failure. If samples with the same lithology are tested at different levels of CSR, such a plot typically generates a nearly linear relation. Seed & Idriss (1971) reported that a representative number of cycles for a typical strong earthquake is approximately 10. Accordingly, the point at which CSR corresponds to failure in 10 cycles (designated as $CSR_{10}$) was chosen as a measure of cyclic shear strength in seismically active areas.

A previous geotechnical study of the Eel margin (Lee *et al*., 1981) included testing of six gravity cores for cyclic shear strength. The goal was to understand the strength properties in the vicinity of the 'Humboldt Slide'. Although 21 cyclic triaxial tests were performed as part of that study, these results do not represent the full variety of sediment lithologies in the study area and cannot be extrapolated to the entire Eel margin.

The previous Eel margin study was part of a much broader series of cyclic triaxial tests conducted at the USGS over a roughly ten-year period. Values of CSR at failure versus the number of cycles to failure were plotted for 144 tests (Fig. 34a). The complete data set forms a broad field with a range of $CSR_{10}$ extending from about 0.25 to 0.60. Data points were grouped according to initial water content with each group extending over a range of about 10% water content (Fig. 34a). Note that water content is defined in the engineering sense as the weight of interstitial water divided by the weight of solids. For each water-content group, a linear regression analysis was performed on the values of CSR versus the log of the number of cycles to failure. The intercept of these regression lines with

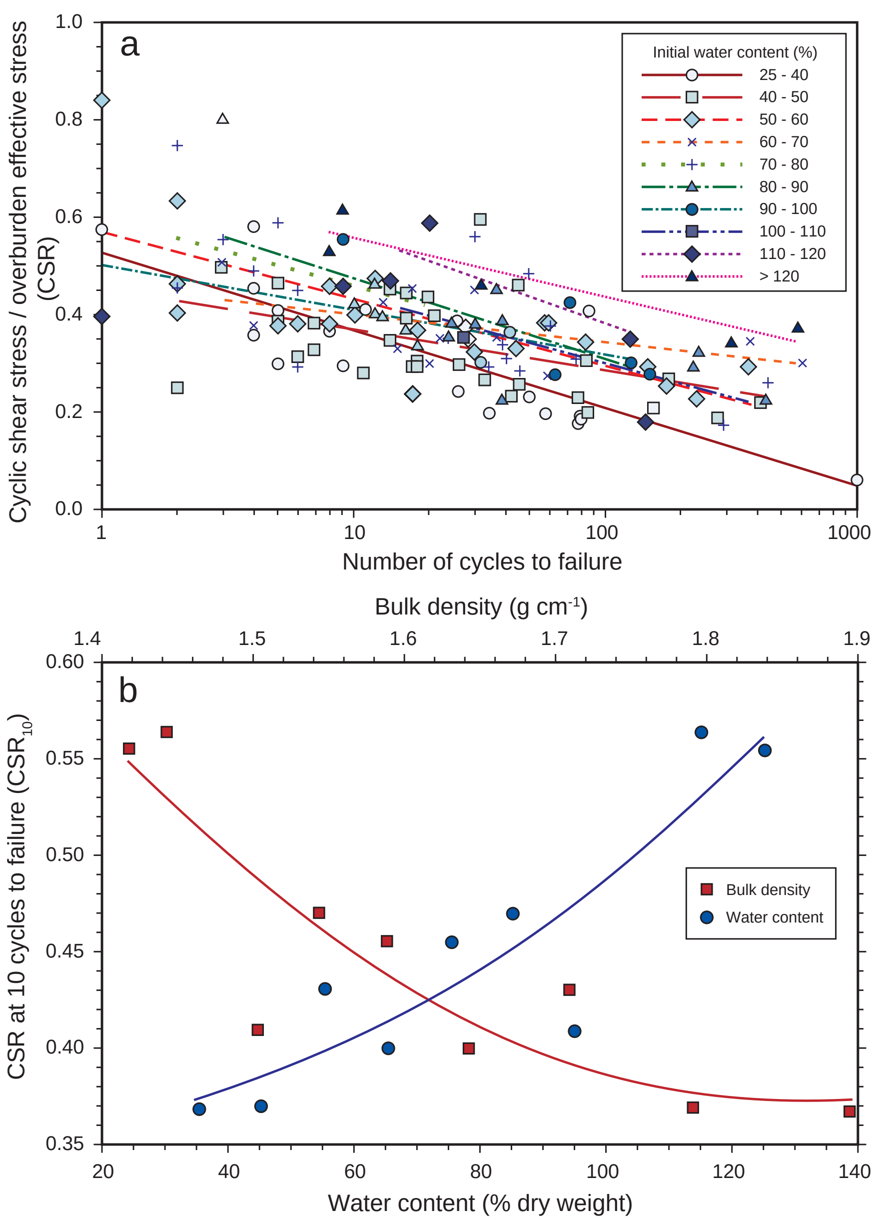


**Fig. 34** Laboratory test results used to derive cyclic shear strength from initial sediment-density measurements. (a) Cyclic shear stress normalized by laboratory consolidation stress (CSR) versus number of cycles to failure (15% strain) from 144 cyclic triaxial tests performed on sediment from 10 marine study areas distributed worldwide (see Lee *et al*. (1999) for more information). Data points are identified according to natural water content ($w$) of the sediment tested. (b) The cyclic stress ratio producing failure in 10 cycles versus initial sediment water content and bulk density. Plotted points were obtained from regression fits of data presented in (a).

a value of 10 cycles to failure ($CSR_{10}$) corresponds to the appropriate midpoint of the water-content range. For this set, $CSR_{10}$ varies consistently with water content and allows a parabolic regression fit of the data (Fig. 34b). For saturated marine sediment, water content and bulk density are directly related to each other at an assumed grain density of 2.7 g $cm^{-3}$. Accordingly, a parabolic relation between $CSR_{10}$ and bulk density can be obtained (Fig. 34b). This relation provides an algorithm for estimating the cyclic undrained shear strength from a measure of lithology, namely the sediment bulk density. This data synthesis provides a tool for regional mapping of sediment strength.

Acoustic backscatter cannot be used quantitatively to map physical properties at present, but it does allow identification of rock outcrops and overconsolidated sediment (Lee *et al*., 1999). These areas can often be excluded from consideration as locations for shallow-seated sediment failure.

Figure 35 shows an application of GIS regional mapping techniques to Santa Monica Bay, California (Lee *et al*., 2000). The GIS layers for slope gradient, density and a measure of anticipated level of seismic shaking ($a_p$, Frankel *et al*., 1996) are used in a series of algorithms to calculate $k_c$, the 'critical acceleration' to cause failure and a stability factor, $k_c/a_p$, which increases with level of predicted stability. Figure 35 indicates an association between areas that are predicted to be less stable (low $k_c/a_p$) and the locations of shallow-seated failures. A similar analysis was applied to the Eel margin (Fig. 36; Lee *et al*., 1999, 2000), where there are few, if any, classic examples of shallow slope failure (Fig. 36b). The 'Humboldt Slide' exists in the south-west part of the area mapped with multibeam, but even if this feature were a slide, it would be so deep seated that the regional mapping approach based on relatively short cores as described above would not be applicable. Elsewhere, the seafloor appears stable except for gullies. These are relatively diffuse and highly pockmarked in the north relative to those farther south, where sharper boundaries and steeper sides are present. The northern gullies are associated with the lowest values of $k_c/a_p$ (0.18–0.26) and those farther south are associated with higher values of $k_c/a_p$ (0.22–0.30). This suggests that the stability of the gully sidewalls is lower for the northern diffuse gullies than it is for the more sharply defined gullies farther south.

#### *Other regional mapping*

Mulder *et al*. (1994) presented an infinite-slope formulation of regional-slope stability analysis that is similar to that of Lee *et al*. (1999, 2000), although strength properties were handled differently and earthquake loads were not considered. A more advanced approach was given by Sultan *et al*. (2001), who considered failure planes that are not necessarily parallel to the seafloor, as is the case in infinite-slope stability analysis. Large numbers of arbitrary failure surfaces were evaluated throughout a finely spaced grid and minimum values for factors of safety were selected at each grid point. This method was applied to the same area considered by Mulder *et al*. (1994), and significant quantitative differences were observed in comparisons between the two sets of results. The Sultan *et al*. (2001) method does not consider seismic loads, and undrained-shear-strength properties are applied directly from a limited number of 2-m to 7-m long cores (as opposed to a model, such as the normalized-soil-property approach, Eq. 5).

## SUMMARY

This paper provides an introduction to the field of submarine landslides with an emphasis on recent advances due to the STRATAFORM programme.

### Overall occurrence and triggers

Much has been learned about submarine landslides over the past 100 yr, driven, in part, by events such as the 1929 Grand Banks earthquake, the 1964 Alaska Earthquake, Hurricane Camille in 1969, the 1979 failure of the Nice airport, the 1980 earthquake in northern California, and the Papua New Guinea tsunami of 1998. The field also has been driven by technological development, including sidescan sonar, GLORIA, multibeam swath mapping, and high-resolution sub-bottom seismic profiling. These studies show that submarine landslides are common in fjords, active river deltas, submarine canyons and the open continental slope. Landslides are triggered by increases in the driving stresses, decreases in the resisting strength, or a combination of the two. Among the important triggers are sediment accumulation, erosion, earthquakes, storm

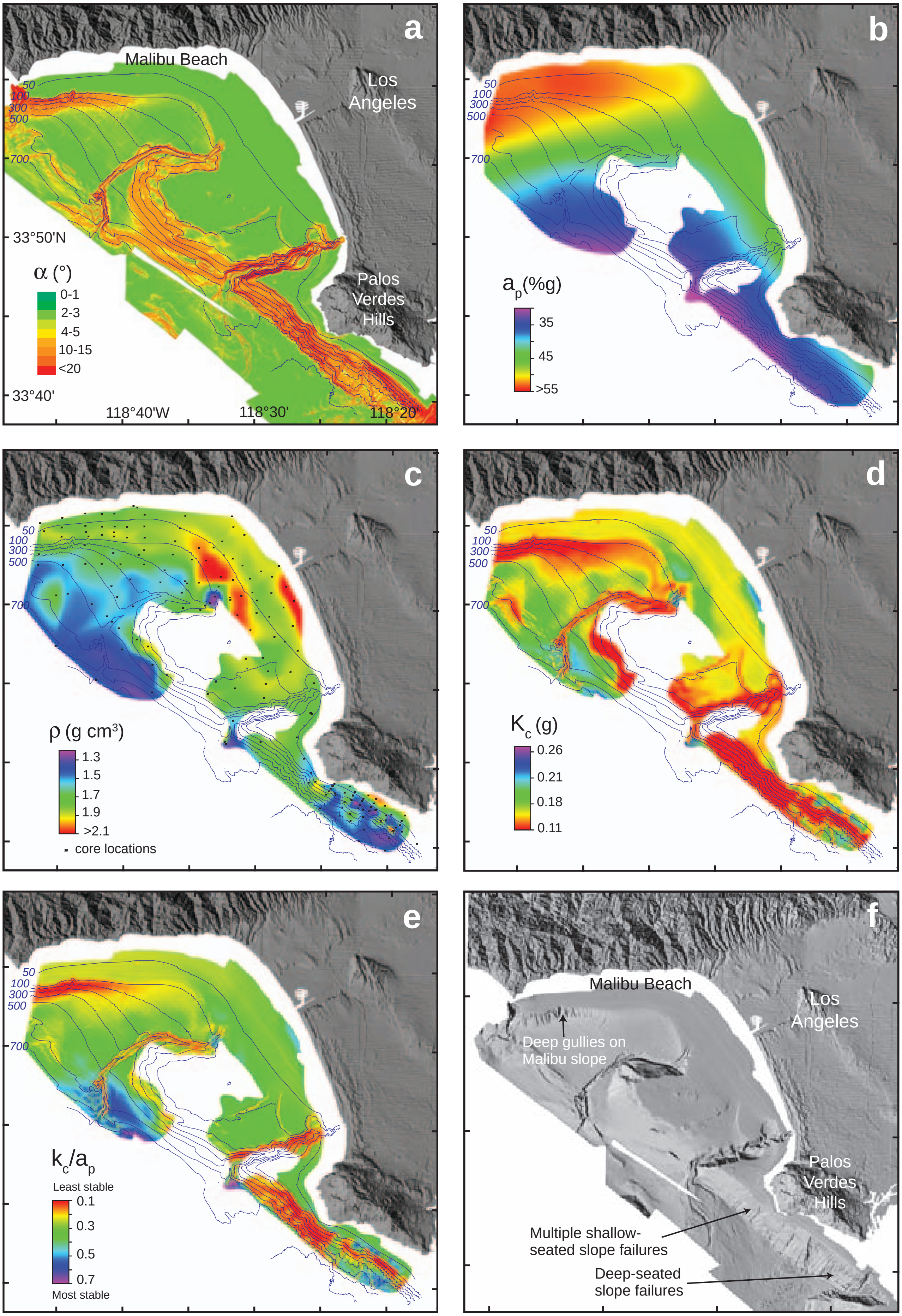
a
Malibu Beach
Los Angeles
Palos Verdes Hills
50
100
300
500
700
33°50'N
33°40'
118°40'W
118°30'
118°20'
α (°)
0-1
2-3
4-5
10-15
<20
b
$a_p$(%g)
35
45
>55
c
ρ (g cm³)
1.3
1.5
1.7
1.9
>2.1
core locations
d
$K_c$ (g)
0.26
0.21
0.18
0.11
e
$k_c/a_p$
Least stable
0.1
0.3
0.5
0.7
Most stable
f
Malibu Beach
Los Angeles
Deep gullies on Malibu slope
Palos Verdes Hills
Multiple shallow-seated slope failures
Deep-seated slope failures

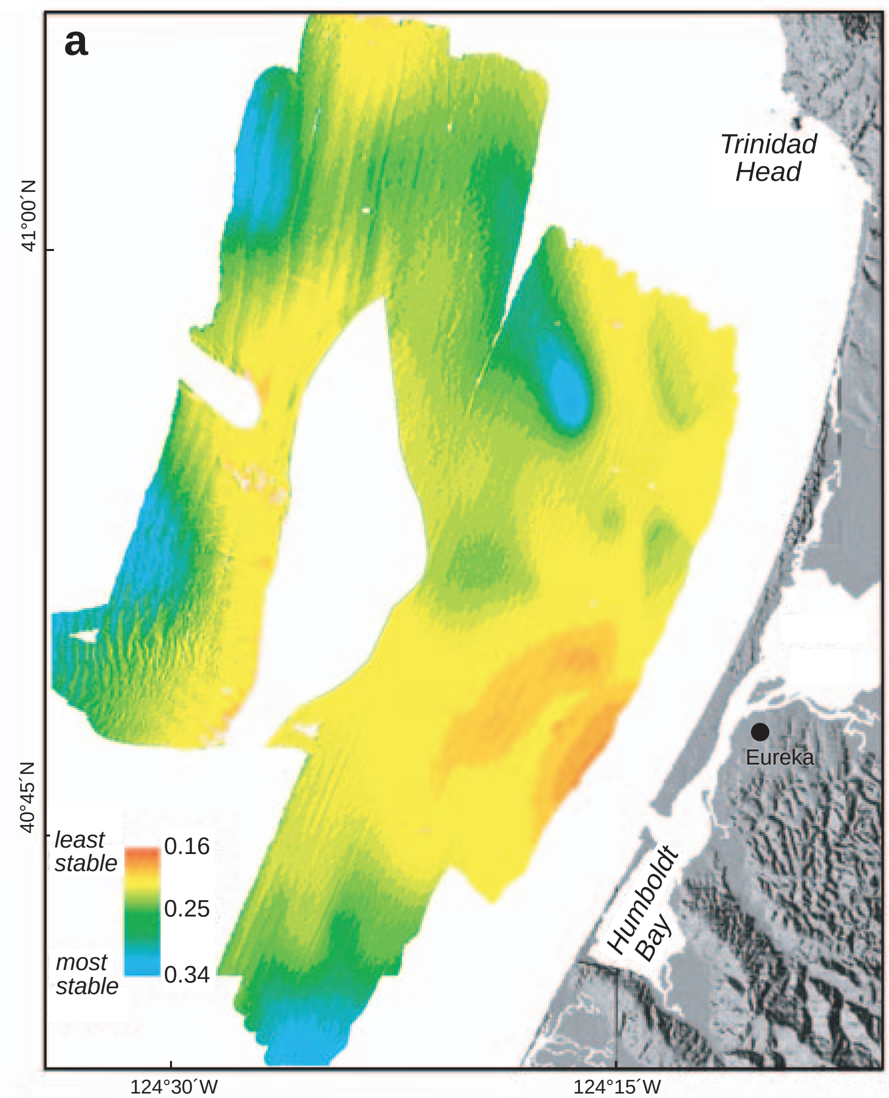


**Fig. 36** Sediment failure susceptibility and deformation in the Eel margin study area. (a) Calculated values of $k_c/a_p$. Lower values represent a greater susceptibility to failure during seismic loading. (b) Shaded bathymetric relief of the Eel margin study area; possible deformation features indicated. (From Lee *et al*., 1999.)

waves, volcanoes, gas and gas hydrates, groundwater seepage, diapirism and human activity.

Some elements of landslide occurrence are surprising. According to McAdoo *et al*. (2000), the greatest density of landslides occurs in the relatively aseismic Gulf of Mexico, whereas the seismically active Oregon and California margins have a much smaller percentage of their areas covered by landslide deposits. The Atlantic margin, with intermediate seismicity, has an intermediate occurrence of submarine landslides. Despite great seismicity, the Eel margin has few obvious slope-failure features, aside from the controversial 'Humboldt Slide'.

**Fig. 35** (*opposite*) Results of a GIS-based analysis of slope-failure susceptibility in Santa Monica Bay, California. (a) Seafloor gradient, $\alpha$, obtained from interpretations of multibeam bathymetric data. (b) Peak seismic acceleration (%$g$ ) with a 10% probability of exceedance in 50 yr, $a_p$ (Frankel *et al*., 1996). (c) Sediment bulk density, $\rho$, at 15 cm below the seafloor, interpreted from sediment core logs and contoured using a surface model. (d) Calculated values ($g$) of the critical horizontal earthquake acceleration, $k_c$, a measure of the shaking required to cause shallow slides. (e) Calculated values for the ratio of $k_c$ to $a_p$ (lower values represent a greater susceptibility to failure during seismic loading). (f) Shaded bathymetric relief of the Santa Monica Bay study area; possible landslide features noted. Isobaths are in metres. (From Lee *et al*., 2000.)

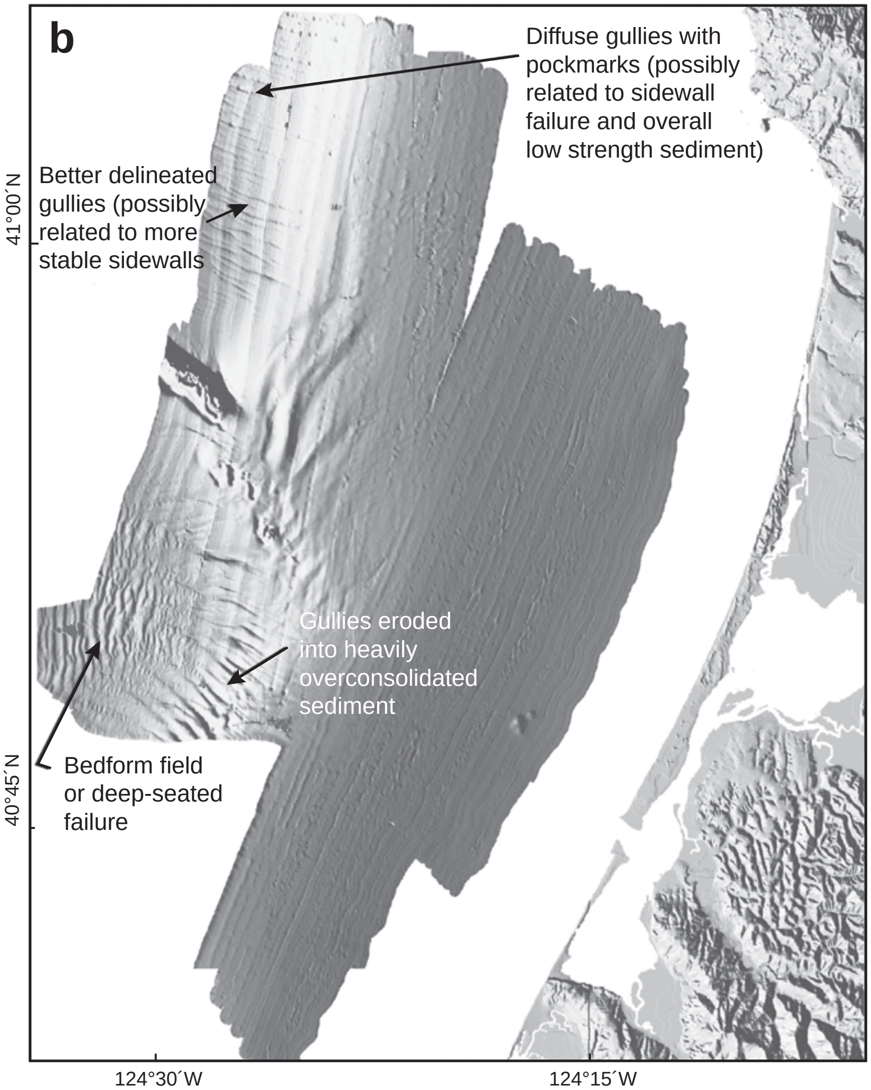


**Fig. 36** (*cont'd*)

**Controversies**

Considerable surface morphology and sub-bottom profile information is available on the 'Humboldt Slide', a large area of hummocky relief that some have interpreted as a large landslide. In profile, the feature seems to consist of a series of back-rotated blocks that have moved along discrete planes. However, the regularity of the hummocks, the continuity of beds, and the absence of a head scarp bear a great deal of resemblance to turbidity-current sediment waves observed in other areas around the world (Wynn *et al.*, 2000). Models have been formulated for the 'Humboldt Slide', as a landslide (Gardner *et al.*, 1999) and as a field of sediment waves (Lee *et al.*, 2002).

Controversy also surrounds the processes that led to the 1929 Grand Banks turbidity current. There were many small to medium-sized failures in fine-grained sediment at the source region. However, the deposit resulting from the turbidity current in the Sohm Abyssal Plain is mainly sand. No clear source of sand has been found. Landslides that involve human structures are also controversial in the cases of failures at both the Nice airport and the Skagway dock. In Papua New Guinea, a large landslide triggered by an earthquake is thought to be the cause for a tsunami, although the earthquake alone might have been sufficient cause (Geist, 2000).

#### Importance of the liquidity index

The liquidity index (a dimensionless number that relates the sediment water content to the Atterberg limits) is a good representation for the degree of openness in a sediment element, and is preferable to the water content itself or the porosity or void ratio. For normal consolidation, a plot of liquidity index versus depth seems to be almost independent of the sediment type, and one graph can be used to represent many different lithologies. Many important parameters needed for modelling debris flows and slope stability can be obtained from correlations with the liquidity index (Locat & Demers, 1988).

#### Pore pressures and the development of anomalously weak sediment

Failure occurs when the environmental stresses exceed the strength of the sediment. If the strength of the sediment is low, the tendency toward failure is increased. Low strengths often result from high excess pore pressures developed within the sediment fabric, which can be produced by a number of factors. The degradation of shear strength can be quantitatively determined for cyclic loading due to earthquakes or storm waves (Lee *et al*., 1999).

#### Development of anomalously high strength

Many seismically active environments, such as the Eel margin, do not display extensive submarine landsliding. A factor limiting slope failure may be the development of sediment strength. One mechanism for developing great strength (e.g. 50% increase) is repeated cyclic loading followed by pore-pressure dissipation. Certain types of bioturbation of surface sediment also seem to produce anomalously high strengths.

#### Slope stability analysis and regional assessment of landslide susceptibility

Slope stability analysis generally involves balancing the forces that tend to move sediment masses downslope against those that tend to resist such motion. Many methodologies have been developed (Syvitski *et al*., this volume, pp. 459–529) and can be used for regional assessment of landslide susceptibility. This application requires maps of the critical input parameters, including bathymetric gradients and geotechnical properties of the sediment. These maps can be operated upon within the context of a geographical information system (GIS) to calculate values of failure susceptibility or the factor of safety (Lee *et al*., 1999, 2000). Locations of actual failures appeared to be associated with areas calculated to have low values of relative susceptibility. Accordingly, these regional slope-stability assessment maps are recommended as an initial means of identifying the areas most vulnerable to shallow-seated slope failure.

#### An important contribution

Probably the most important contribution of the STRATAFORM programme to the field of submarine landslide research is the recognition that seafloor features that initially appear to be landslide deposits can in fact be ambiguous. That is, hummocky or crenulated bottom features may be suggestive of sediment failure, but closer examination may introduce questions concerning whether the features may rather be depositional, resulting from turbidity current deposition, or bottom-current modification. Resolving the conflicting interpretations can be a difficult process.

## ACKNOWLEDGEMENTS

The authors gratefully acknowledge the support of the Office of Naval Research and, in particular, the long-term encouragement of Dr Joseph Kravitz. The authors also acknowledge support from the US Geological Survey and Laval University. Finally we acknowledge helpful reviews by Charles Nittrouer, Richard Faas, Joseph Kravitz, David Mohrig, Beth Mullenbach, Andrea Ogston and Patricia Wiberg.

## NOMENCLATURE

| Symbol | Definition | Dimensions |
|---|---|---|
| $a, b$ | empirical constants in relation between $I_L$ and $\sigma'_v$ (Eq. 8) | $a$, mixed units, depending upon value of $b$; $b$ dimensionless |

| | | |
|---|---|---|
| $a_p$ | anticipated level of seismic shaking, expressed probabilistically (Frankel *et al.*, 1996) | portion of gravitational acceleration |
| $A_r$ | cyclic-loading strength-reduction factor | |
| CSR | cyclic stress ratio (cyclic shear stress/ ($\sigma'_v$ or $\sigma'_c$)) | |
| $Cu = s_u$ | undrained shear strength | $M\,L^{-1}\,T^{-2}$ |
| $c_v$ | coefficient of consolidation | $L^2\,T^{-1}$ |
| $d$ | water depth | L |
| $f_z$ | exp $(-2\pi z/L)$ (factor used in predicting wave-induced shear stress) | |
| $f_d$ | $0.5\,(1/\cosh(2\pi d/L))$ (factor used in predicting wave-induced shear stress) | |
| $h$, $z$ | depth below the seafloor | L |
| $H$ | wave height | L |
| $I_L$ | liquidity index $= (w - w_p)/I_p$ | |
| $I_p$ | plasticity index (liquid limit minus plastic limit) | |
| $K$ | linear coefficient analogous (though not identical) to viscosity used in the Herschel–Bulkley model | mixed units, depending upon value of $n$ |
| $k_c$ | critical acceleration (pseudo-static lateral acceleration needed to cause failure) | portion of gravitational acceleration |
| $L$ | wavelength | L |
| $m$ | sediment constant used in predicting normalized shear strength (commonly ~0.8) | |
| $n$ | exponent describing the rate of change of viscosity with imposed stress | |
| $(N_1)_{60}$ | a measure of the resistance to penetration from a standard penetration test | |
| OCR | overconsolidation ratio ($\sigma'_{vm}/\sigma'_v$) | |
| $r_u$ | pore-pressure ratio ($u/\gamma z$) | |
| $s_u = Cu$ | undrained shear strength | $M\,L^{-1}\,T^{-2}$ |
| $s_{ur}$ | remoulded shear strength | $M\,L^{-1}\,T^{-2}$ |
| $S$ | ratio of shear strength to vertical effective stress for normal consolidation | |
| $S_t$ | sensitivity ($s_u/s_{ur}$) | |
| $u$ | excess pore-water pressure (in excess of hydrostatic pressure) | $M\,L^{-1}\,T^{-2}$ |
| $w$ | water content (% dry weight) | |
| $w_p$ | plastic limit | |
| $z$ | depth below seafloor | L |
| $\alpha$ | seafloor gradient | degrees |
| $\gamma$ | shear rate or total unit weight of sediment | $T^{-1}$ or $M\,L^{-2}\,T^{-2}$ |
| $\gamma'$ | buoyant (submerged) unit weight of sediment | $M\,L^{-2}\,T^{-2}$ |
| $\gamma_0$ | coefficient that regulates rheological behaviour at small shear rates (bilinear model) | $T^{-1}$ |
| $\gamma_w$ | unit weight of water | $M\,L^{-2}\,T^{-2}$ |
| $\delta$ | empirical constant in relation between $I_L$ and $s_{ur}$ (Eq. 9) | $M\,L^{-1}\,T^{-2}$ |
| $\varepsilon$ | empirical constant in relation between $I_L$ and $s_{ur}$ (Eq. 9) | |
| $\eta$ | viscosity | $M\,L^{-1}\,T^{-1}$ |
| $\lambda$ | empirical constant in relation between $s_{ur}$ and $z$ (Eq. 10) | $M\,L^{-1}\,T^{-2}$ |

| | | |
|---|---|---|
| $\mu$ | viscosity-like term | mixed units depending on value of $n$ |
| $\mu_{dh}$ | coefficient that regulates rheological behaviour at small shear rates (bilinear model) | M L$^{-1}$ T$^{-1}$ |
| $\rho$ | total sediment mass density | M L$^{-3}$ |
| $\sigma$ | total stress | M L$^{-1}$ T$^{-2}$ |
| $\sigma'_c$ | consolidation stress | M L$^{-1}$ T$^{-2}$ |
| $\sigma'_v$, $\sigma_o$ | vertical effective overburden stress | M L$^{-1}$ T$^{-2}$ |
| $\sigma'_{vm}$ | maximum past stress | M L$^{-1}$ T$^{-2}$ |
| $\tau$ | shear stress | M L$^{-1}$ T$^{-2}$ |
| $\tau_{av}$ | average shear stress anticipated from a design earthquake | M L$^{-1}$ T$^{-2}$ |
| $\tau_c$ | cyclic shear stress | M L$^{-1}$ T$^{-2}$ |
| $\tau_c$ | critical shear stress (Herschel–Bulkley model) | M L$^{-1}$ T$^{-2}$ |
| $\tau_f$ | $\tau$ shear stress at failure | M L$^{-1}$ T$^{-2}$ |
| $\tau_s$ | downslope shear stress | M L$^{-1}$ T$^{-2}$ |
| $\tau_y$ | yield strength | M L$^{-1}$ T$^{-2}$ |
| $\tau_{ya}$ | apparent yield strength | M L$^{-1}$ T$^{-2}$ |
| $\phi'$ | friction angle | degrees |

## REFERENCES


Adams, J. (1984) Active deformation of the Pacific northwest continental margin. *Tectonics*, **3**, 449–472.

Atigh, E. and Byrne, P.M. (2004) Liquefaction flow of submarine slopes under partially undrained conditions: an effective stress approach. *Can. Geotech. J.*, **41**, 154–165.

Austin, J.A., Jr., Christie-Blick, N., Malone, M.J., *et al.* (1998) *Proceedings of the Ocean Drilling Program, Initial Reports*, **174A** (CD-ROM).

Barnard, W. (1978) The Washington continental slope: Quaternary tectonics and sedimentation. *Mar. Geol*, **27**, 79–114.

Bea, R.G., Wright, S.G., Sircar, P. and Niedoroda, A.W. (1983) Wave-induced slides in South Pass Block 70, Mississippi Delta. *J. Geotech. Eng.*, **109**, 619–644.

Bjerrum, L. (1955) Stability of natural slopes in quick clay. *Géotechnique*, **5**, 101–119.

Bohannon, R.G. and Gardner, J.V. (2004) Submarine landslides of San Pedro Escarpment, southwest of Long Beach, California. *Mar. Geol.*, **203**, 261–268.

Bokuniewicz, H.J., Gordon, R. and Rhoads, D.C. (1975) Mechanical properties of the sediment–water interface. *Mar. Geol.*, **18**, 263–278.

Booth, J.S. (1979) Recent history of mass wasting on the upper continental slope, northern Gulf of Mexico as interpreted from the consolidation states of the sediment. In: *Geology of Continental Slopes* (Eds O.H. Pilkey and L.J. Doyle), pp. 153–164. Special Publication 27, Society of Economic Paleontologists and Mineralogists, Tulsa, OK.

Booth, J.S. and Garrison, L.E. (1978) A geologic and geotechnical analysis of the upper continental slope adjacent to the Mississippi Delta. *Proceedings, 10th Offshore Technical Conference*, Houston, TX, pp. 1019–1028.

Booth, J.S., O'Leary, D.W., Popenoe, P. and Danforth, W.W. (1993) U.S. Atlantic continental slope landslides: their distribution, general attributes and implications. In: *Submarine Landslides: Selected Studies in the U.S. EEZ* (Eds W.C. Schwab, H.J. Lee and D.C. Twichell). *U.S. Geol. Surv. Bull.*, **2002**, 14–39.

Bornhold, B.D. and Prior, D.B. (1990) Morphology and sedimentary processes on the subaqueous Noeick River delta, British Columbia, Canada. In: *Coarse-grained Deltas* (Eds A. Colella and D.B. Prior), pp. 169–184. Special Publication 10, International Association of Sedimentologists. Blackwell Scientific Publications, Oxford.

Boulanger, E. (2000) *Comportement cyclique des sédiments de la marge continentale de la rivière Eel: une explication possible pour le peu de glissements sous-marins superficiels dans cette région*. MSc thesis, Department of Geology and Geological Engineering, Laval University.

Boulanger, E., Konrad, J.-M., Locat, J. and Lee, H.J. (1998) Cyclic behavior of Eel River sediments: a possible explanation for the paucity of submarine landslide features. *Eos* (*Trans. Am. Geophys. Union*), **79**, 254.

Bryn, P., Solheim, A., Berg, K., *et al.* (2003) The Storegga slide complex: repeated large scale sliding in response to climatic cyclicity. In: *Submarine Mass Movements and their Consequences* (Eds J. Locat and J. Mienert), pp. 215–222. Kluwer, Dordrecht.

Buffington, E.C. and Moore, D.G. (1962) Geophysical evidence on the origin of gullied submarine slopes, San Clemente, California. *J. Geol.*, **71**, 356–370.

Canals, M., Lastras, G., Urgeles, R., *et al.* (2004) Slope failure dynamics and impacts from seafloor and shallow sub-seafloor geophysical data: case studies from the COSTA project. *Mar. Geol.*, **213**, 9–72.

Carlson, P.R. (1978) Holocene slump on continental shelf off Malaspina Glacier, Gulf of Alaska. *Bull. Am. Assoc. Petrol. Geol.*, **62**, 2412–2426.

Carlson, P.R., Molnia, B.F. and Wheeler, M.C. (1980) Seafloor geologic hazards in OCS Lease Area 55, eastern Gulf of Alaska. *Proceedings, 12th Offshore Technology Conference*, Houston, TX, Vol. 1, pp. 593–603.

Carrara, A., Cardinali, M., Detti, R., *et al.* (1991) GIS Techniques and statistical models in evaluating landslide hazard. *Earth Surf. Process. Landf.*, **16**, 427–445.

Cashman, K.V. and Popenoe, P. (1985) Slumping and shallow faulting related to the presence of salt on the continental slope and rise off North Carolina. *Mar. Petrol. Geol.*, **2**, 260–272.

Cattaneo, A., Correggiari, A., Marsset, T., *et al.* (2004) Seafloor undulation pattern on the Adriatic shelf and comparison to deep-water sediment waves. *Mar. Geol.*, **213**, 121–148.

Christian, H.A. (1993) *In situ* measurement of consolidation and permeability of soft marine sediments. *Proceedings, 4th Canadian Conference on Marine Geotechnical Engineering*, St John's, Newfoundland, pp. 663–379.

Christian, H.A. (1998) *Excalibur Pore Pressure and Fluid Sampling STRATAFORM Wecoma 9807A Cruise*. Report to Laval University, Vol. 16.

Clague, D.A. and Denlinger, R.P. (1994) Role of olivine cumulates in destabilizing the flanks of Hawaiian volcanoes. *Bull. Volcanol.*, **56**, 425–434.

Clarke, S.H., Jr. (1992) Geology of the Eel River basin and adjacent region: implications for late Cenozoic tectonics of the southern Cascadia subduction zone and Mendocino triple junction. *Bull. Am. Assoc. Petrol. Geol.*, **76**, 199–224.

Clukey, E., Kulhawy, F.H., Liu, P.L.F. and Tate, G.B. (1985) The impact of wave loads and pore-water pressure generation on initiation of sediment transport. *Geo-Mar. Lett.*, **5**, 177–183.

Coleman, J.M. (1988) Dynamic changes and processes in the Mississippi River delta. *Geol. Soc. Am. Bull.*, **100**, 999–1015.

Coleman, J.M. and Garrison, L.E. (1977) Geological aspects of marine slope stability, northwestern Gulf of Mexico. *Mar. Geol.*, **2**, 9–44.

Coleman, J.M., Prior, D.B. and Garrison, L.E. (1980) Subaqueous sediment instabilities in the offshore Mississippi River delta. *U.S. Bur. Land Manag. Open-file Rep.*, **80–01**, 60.

Coleman, J.M., Prior, D.B., Garrison, L.E. and Lee, H.J. (1993) Slope failures in an area of high sedimentation rate: offshore Mississippi River Delta. In: *Submarine Landslides: Selected Studies in the U.S. EEZ* (Eds W.C. Schwab, H.J. Lee and D.C. Twichell). *U.S. Geol. Surv. Bull.*, **2002**, 79–91.

Correggiari, A., Trincardi, F., Langone, L. and Roveri, M. (2001) Styles of failure in late Holocene highstand prodelta wedges on the Adriatic shelf. *J. Sediment. Res.*, **71**, 218–236.

Coulter, H.W. and Migliaccio, R.R. (1966) Effects of the earthquake of March 27, 1964 at Valdez, Alaska. *U.S. Geol. Surv. Prof. Pap.*, **542-C**.

Coussot, P. and Meunier, M. (1996) Recognition, classification and mechanical description of debris flows. *Earth-Sci. Rev.*, **40**, 209–227.

Coussot, P. and Piau, J. (1995) A large-scale field coaxial cylinder rheometer for the study of the rheology of natural coarse suspensions. *J. Rheol.*, **39**, 105–124.

De Deckere, E.M., Tolhurst, T.J. and de Brouwer, J.F.C. (2001) Destabilization of cohesive intertidal sediments by infauna. *Estuar. Coast. Shelf Sci.*, **53**, 665–669.

Dietrich, J.H. (1988) Growth and persistence of Hawaiian rift zones. *J. Geophys. Res.*, **93**, 4258–4270.

Dill, R.F. (1964) Sedimentation and erosion in Scripps submarine canyon head. In: *Papers in Marine Geology* (Ed. R.L. Miller), pp. 232–248. MacMillan, New York.

Dugan, B., Olgaard, D.L., Flemings, P.B. and Gooch, M.J. (2002) Data report: bulk physical properties of sediments from ODP Site 1073. In: *Proceedings of the Ocean Drilling Program, Scientific Results*, Vol. 174A (Eds N. Christie-Blick, J.A. Austin, Jr. and M.J. Malone), pp. 1–62. College Station, TX.

Elverhøi, A., Norem, H., Andersen, E.S., *et al.* (1997) On the origin and flow behavior of submarine slides on deep-sea fans along the Norwegian–Barents Sea continental margin. *Geo-Mar. Lett.*, **17**, 119–125.

Embley, R.W. and Jacobi, R.D. (1977) Distribution and morphology of large submarine sediment slides and slumps on Atlantic continental margins. *Mar. Geotech.*, **2**, 205–228.

Emery, K.O., Uchupi, E., Phillips, J.D., *et al.* (1970) Continental rise of eastern North America. *Bull. Am. Assoc. Petrol. Geol.*, **54**, 44–108.

Esrig, M.I. and Kirby, R.C. (1977) Implications of gas content for predicting the stability of submarine slopes. *Mar. Geotech.*, **2**, 81–100.

Farrow, G.E., Syvitski, J.P.M. and Tunnicliffe, V. (1983) Suspended particulate loading on the macrobenthos in a highly turbid fjord: Knight Inlet, British Columbia. *Can. J. of Fisheries and Aquatic Sci.*, 40(suppl. 1), 273–288.

Faugères, J.-C., Gonthier, E., Mulder, T., *et al.* (2002) Multiprocess generated sediment waves on the Landes Plateau (Bay of Biscay, North Atlantic). *Mar. Geol.*, **182**, 279–302.

Field, M.E. (1981) Sediment mass-transport in basins: controls and patterns. In: *Short Course Notes Pacific Section* (Eds R.G. Douglas, E.P. Colburn and D.S.

Gorsline), pp. 61–83. Society of Economic Paleontologists and Mineralogists, Tulsa, OK.

Field, M.E. (1993) Liquefaction of continental shelf sediment: the northern California earthquake of 1980. In: *Submarine Landslides: Selected Studies in the U.S. EEZ* (Eds W.C. Schwab, H.J. Lee and D.C. Twichell). *U.S. Geol. Surv. Bull.*, **2002**, 143–150.

Field, M.E. and Barber, J.H., Jr. (1993) A submarine landslide associated with shallow sea-floor gas and gas hydrates off northern California. In: *Submarine Landslides: Selected Studies in the U.S. EEZ* (Eds W.C. Schwab, H.J. Lee and D.C. Twichell). *U.S. Geol. Surv. Bull.*, **2002**, 151–157.

Field, M.E. and Clarke, S.H. (1979) Small-scale slumps and slides and their significance for basin slope processes, Southern California Borderland. In: *Geology of Continental Slopes* (Eds O.H. Pilkey and L.J. Doyle), pp. 223–230. Special Publication 27, Society of Economic Paleontologists and Mineralogists, Tulsa, OK.

Field, M.E. and Edwards, B.D. (1980) Slopes of the southern California borderland: a regime of mass transport. In: *Proceedings, Quaternary Depositional Environments of the Pacific Coast: Pacific Coast Paleogeography, Symposium No. 4* (Eds M.E. Field, A.H. Bouma, I.P. Colburn, J.J. Douglas and J.C. Ingle), pp. 69–184. Pacific Section, Society of Economic Paleontologists and Mineralogists, Tulsa, OK.

Field, M.E. and Richmond, W.C. (1980) Sedimentary and structural patterns on the northern Santa Rosa–Cortes Ridge, southern California. *Mar. Geol.*, **34**, 79–98.

Field, M.E., Gardner, J.V. and Prior, D.B. (1999) Geometry and significance of stacked gullies on the northern California slope. *Mar. Geol.*, **154**, 271–286.

Field, M.E., Clarke, S.H., Jr. and White, M.E. (1980) Geology and geologic hazards of offshore Eel River Basin, northern California continental margin. *U.S. Geol. Surv. Open-file Rep.*, **80–1080**.

Fischer, J.A., Koutsoftas, D.C. and Lu, T.D. (1976) The behavior of marine soils under cyclic loading. *Proceedings, First International Conference, Behavior of Off-Shore Structures,* Trondheim, Norway, pp. 407–414.

Fisk, H.N., McFarlan, E., Jr., Kold, C.R. and Wilbern, L.J., Jr. (1954) Sedimentary framework of the modern Mississippi Delta. *J. Sediment. Petrol.*, **24**, 76–99.

Frankel, A., Mueller, C., Barnhard, T., *et al.* (1996) National seismic-hazard maps: documentation. *U.S. Geol. Surv. Open-file Rep.*, **96–532**.

Fulthorpe, C.S., Mountain, G.S., Austin, J.A., *et al.* (1996) STRATAFORM high-resolution MCS survey, Eel River basin, northern California margin: shelf/slope stratigraphy and processes (abstr.). *Eos* (*Trans. Am. Geophys. Union*), **77**, F330.

Gardner, J.V., Prior, D.B. and Field, M.E. (1999) Humboldt slide – a large shear-dominated retrogressive slope failure. *Mar. Geol.*, **154**, 323–338.

Garrison, L.E. (1977) The SEASWAB Experiment. *Mar. Geotech.*, **2**, 117–122.

Geist, E.L. (2000) Origin of the 17 July 1998 Papua New Guinea tsunami; earthquake or landslide. *Seism. Res. Lett.*, **71**, 344–351.

Gibson, R.E. (1958) The process of consolidation in a clay layer increasing in thickness with time. *Géotechnique*, **8**, 171–182.

Goff, J.A., Orange, D.L., Mayer, L.A. and Hughes Clarke, J.E. (1999) Detailed investigation of continental shelf morphology using a high-resolution swath sonar survey: the Eel margin, northern California, *Mar. Geol.*, **154**, 255–270.

Goff, J.A., Wheatcroft, R.A., Lee, H., *et al.* (2002) Spatial variability of shelf sediments in the STRATAFORM natural laboratory, *Cont. Shelf Res.*, **22**, 1199–1223.

Goldfinger, C., Nelson, C.H., Johnson, J.E. and Shipboard Scientific Party (2003) Holocene earthquake records from the Cascadia subduction zone and the northern San Andreas Fault based on precise dating of offshore turbidites. *Ann. Rev. Earth Planet. Sci.*, **31**, 555–577.

Greene, H.G., Maher, N.M. and Paull, C.K. (2002) Physiography of the Monterey Bay national Marine Sanctuary and implications about continental margin development. *Mar. Geol.*, **181**, 55–82.

Gregersen, O. (1981) The quick clay landslide in Rissa, Norway. *Proceedings, 10th International Conference on Soil Mechanics and Foundation Engineering*, Vol. 3, pp. 421–426.

Grozic, J.L.H., Robertson, P.K. and Morgenstern, N.R. (2000) Cyclic liquefaction of loose gassy sand. *Can. Geotech. J.*, **37**, 843–856.

Haflidason, H., Sejrup, H.P., Nygard, A., *et al.* (2004) The Storegga slide: architecture, geometry and slide development. *Mar. Geol.*, **213**, 201–234.

Hampton, M. (1972) The role of subaqueous debris flow in generating turbidity currents. *J. Sediment. Petrol.*, **42**, 775–993.

Hampton, M.A. and Bouma, A.H. (1977) Slope instability near the shelf break, western Gulf of Alaska. *Mar. Geotech.*, **2**, 309–331.

Hampton, M.A., Lee, H.J. and Beard, R.M. (1982) Geological interpretation of cone penetrometer tests in Norton Sound, Alaska. *Geo-Mar. Lett.*, **2**, 223–231.

Hampton, M.A., Lee, H.J. and Locat, J. (1996) Submarine landslides. *Rev. Geophys.*, **34**, 33–59.

Hampton, M.A., Karl, H.A. and Murray, C.J. (2002) Acoustic profiles and images of the Palos Verdes margin; implications concerning deposition from the White's Point outfall. *Cont. Shelf Res.*, **22**, 841–858.

Haner, B.E. and Gorsline, D.S. (1978) Processes and morphology of continental slope between Santa Monica and Dume submarine canyons, Southern California. *Mar. Geol.*, **28**, 77–87.

Heezen, B.C. and Drake, C.L. (1964) Grand Banks slump. *Bull. Am. Assoc. Petrol. Geol.*, **48**, 44–108.

Heezen, B.C. and Ewing, M. (1952) Turbidity currents and submarine slumps and the 1929 Grand Banks Earthquake. *Am. J. Sci.*, **250**, 849–873.

Hein, F.J. and Gorsline, D.S. (1981) Geotechnical aspects of fine-grained mass flow deposits: California Continental Borderland, *Geomar. Lett.*, **1**, 1–5.

Hemphill, T., Campos, W. and Pilehvari, A. (1993) Yield-power law model more accurately predicts mud rheology. *Oil & Gas Journal*. **91**, 45–50.

Henkel, D.J. (1970) The role of waves causing submarine landslides. *Géotechnique*, **20**, 75–80.

Hiscott, R.N. and James, N.P. (1985) Carbonate debris flows, Cow Head group, western Newfoundland. *J. Sediment. Petrol.*, **55**, 735–745.

Holcomb, R.T. and Searle, R.C. (1991) Large landslides from oceanic volcanoes. *Mar. Geotech.*, **10**, 19–32.

Hutchinson, J.N. (1986) A sliding-consolidation model for flow slides. *Can. Geotech. J.*, **23**, 115–126.

Iverson, R.M. (1995) Can magma-injection and groundwater forces cause massive landslides on Hawaiian volcanoes? *Jour. Volcan. Geother. Res.*, 66, 295–308.

Iverson, R.M. (1997) The physics of debris flow. *Rev. Geophys*, 35, 245–296.

Iverson, R.M. and LaHusen, R.G. (1993) Friction in debris flows: Inferences from large-scale flume experiments. *Hydraulic Engineering '93: Proceedings of the 1993 Conference, San Francisco, California, ASCE*, 1604–1609.

Jibson, R.W., Harp, E.L. and Michael, J.A. (1998) A method for producing digital probabilistic seismic landslide hazard maps: an example from the Los Angeles, California, area. *U.S. Geol. Surv. Open-file Rep.*, **98–113**, 17 pp.

Johnson, A.M. (1970) *Physical Processes in Geology*. Freeman, Cooper and Co., San Francisco.

Kachadoorian, R. (1965) Effects of the earthquake of March 27, 1964 at Whittier, Alaska, *U.S. Geol. Surv. Prof. Pap.*, **542-B**.

Kayen, R.E. and Lee, H.J. (1991) Pleistocene slope instability of gas hydrate-laden sediment on the Beaufort Sea margin. *Mar. Geotech.*, **10**, 125–141.

Knebel, H.J. and Carson, B. (1979) Small-scale slump deposits, Middle Atlantic Continental Slope, off eastern United States. *Mar. Geol.*, **29**, 221–236.

Kostaschuk, R.A. and McCann, S.B. (1983) Observations on delta-forming processes in a fjord-head delta, British Columbia. *Sediment. Geol.*, **36**, 269–288.

Kraft, L.M., Gavin, T.M. and Bruton, J.C. (1992) Submarine flow slide in Puget Sound. *J. Geotech. Eng., ASCE*, **118**, 1577–1591.

Ladd, C.C., Foott, R., Ishihara, K., Schlosser, F. and Poulos, H.G. (1977) Stress-deformation and strength characteristics. *Proceedings, Ninth International Conference on Soil Mechanics and Foundation Engineering*, Tokyo, Japan, Vol. 2, pp. 421–494.

Lambe, T.W. and Whitman, R.V. (1969) *Soil Mechanics*. John Wiley & Sons, New York, 553 pp.

Lee, H.J. (1985) State of the art: Laboratory determination of the strength of marine soils. In: *Strength Testing of Marine Sediments: Laboratory and In situ Measurements* (Eds R.C. Chaney and K.R. Demars), pp. 181–250. STP 883, American Society for Testing and Materials.

Lee, H.J. and Edwards, B.D. (1986) Regional method to assess offshore slope stability. *J. Geotech. Eng., ASCE*, **112**, 489–509.

Lee, H.J., Edwards, B.D. and Field, M.E. (1981) Geotechnical analysis of a submarine slump, Eureka, California. *Proceedings of the Offshore Technology Conference, Houston*, pp. 53–59.

Lee, H.J., Schwab, W.C., Edwards, B.D. and Kayen, R.E. (1991) Quantitative controls on submarine slope failure morphology. *Mar. Geotech.*, **10**, 143–158.

Lee, H.J., Locat, J., Dartnell, P., Israel and Wong, F. (1999) Regional variability of slope stability: application to the Eel margin, California. *Mar. Geol.*, **154**, 305–321.

Lee, H.J., Locat, J., Dartnell, P., Minasian, D. and Wong, F. (2000) A GIS-based regional analysis of the potential for shallow-seated submarine slope failure. *Proceedings, 8th International Symposium on Landslides*, Cardiff, Wales, pp. 917–922.

Lee, H.J., Syvitski, J.P.M., Parker, G., *et al*. (2002) Distinguishing sediment waves from slope failure deposits: field examples, including the 'Humboldt Slide' and modeling results. *Mar. Geol.*, **192**, 79–104.

Lee, K.L. and Focht, J.A. (1976) Strength of clay subjected to cyclic loading. *Mar. Geotech.*, **1**, 165–185.

Lehner, P. (1969) Salt tectonics and Pleistocene stratigraphy on continental slope of northern Gulf of Mexico. *Bull. Am. Assoc. Petrol. Geol.*, **53**, 2431–2479.

Lemke, R.W. (1967) Effects of the earthquake of March 27, 1964, at Seward, Alaska, *U.S. Geol. Surv. Prof. Pap.*, **542-E**.

Leroueil, S., Tavenas, F. and LeBihan (1983) Propriétés caractéristiques des argiles de l'est du Canada. *Can. Geotech. J.*, **20**, 681–705.

Leroueil, S., Vaunat, J., Picarelli, L., Locat, J., Lee, H. and Faure, R. (1996) Geotechnical characterization of slope movements. *Proceedings of the International Symposium on Landslides*, Trondheim.

Locat, J. (1982) *Contribution à l'étude de l'origine de la structuration des argiles sensibles de l'est du Canada. Unpublished PhD thesis*, Department of Civil Engineering, University of Sherbrooke, Sherbrooke, Quebec.

Locat, J. (1997) Normalized rheological behavior of fine muds and their flow properties in a pseudoplastic regime. In: *Debris-flow Hazards Mitigation: Mechanics, Prediction and Assessment*, pp. 260–269. Water Resources Engineering Division, American Society of Civil Engineers.

Locat, J. and Demers, D. (1988) Viscosity, yield stress, remolded shear strength and liquidity index relationships for sensitive clays. *Can. Geotech. J.*, **25**, 799–806.

Locat, J. and Lee, H.J. (2002) Submarine landslides: advances and challenges. *Can. Geotech. J.*, **39**, 193–212.

Locat, J. and Lefebvre, G. (1986) The origin of structuration of the Grande-Baleine marine sediments, Québec Canada. *Q. J. Eng. Geol.*, **19**, 365–374.

Locat, J. and Leroueil, S. (1988) Physicochemical and mechanical characteristics of recent Saguenay Fjord sediments. *Can. Geotech. J.*, **25**, 382–388.

Locat, J., Lee, H.J., Nelson, H.C., Schwab, W.C. and Twichell, D.C. (1996) Analysis of the mobility of far reaching debris flows on the Mississippi Fan, Gulf of Mexico. *Proceedings, 7th International Symposium on Landslides*, pp. 555–560.

Locat, J., Lee, H.J., Kayen, R., *et al.* (2002) Shear strength development with burial in Eel River Margin slope sediments. *Mar. Geotech.*, **20**, 111–135.

Locat, J., Desgagnés, P., Leroueil, S. and Lee, H.J. (2003) Stability analysis of the Hudson Apron slope, off New Jersey, U.S.A. In: *Submarine Mass Movements and their Consequences* (Eds J. Locat and J. Mienert), pp. 267–280. Kluwer, Dordrecht.

Mader, C.L. (1997) Modeling the 1994 Skagway tsunami. *Sci. Tsunami Haz.*, **15**, 41–48.

Major, J.J. (2000) Gravity-driven consolidation of granular slurries – Implications for debris-flow deposition and deposit characteristics. *J. Sediment. Res.*, **70**, 64–83.

Major, J.J. and Pierson, T.C. (1992) Debris flow rheology: Experimental analysis of fine grained slurries. *Water Resources. Res.*, **28**, 841–857.

Malahoff, A., Embley, R.W., Perry, R.B. and Fefe, C. (1980) Submarine mass-wasting of sediments on the continental slope and upper rise south of Baltimore Canyon: *Earth and Plan. Sci, Letters*, **49**, 1–7.

Malouta, D.N., Gorsline, D.S. and Thornton, S.E. (1981) Processes and rates of recent (Holocene) basin filling in an active transform margin: Santa Monica Basin, California Continental Borderland. *J. Sediment. Petrol.*, **51**, 1077–1095.

Marlow, M.S., Scholl, D.W., Buffington, E.C., Boyce, R.E., Alpha, T.R., Smith, P.J. and Shipek, C.J. (1970) Buldir Depression – a late Tertiary graben on the Aleutian Ridge, Alaska. *Mar. Geol.*, **8**, 85–108.

Marshall, N.F. (1978) Large storm-induced sediment slump reopens an unknown Scripps Submarine Canyon tributary. In: *Sedimentation in Submarine Canyons, Fans and Trenches* (Eds D.J. Stanley and G. Kelling, G.), pp. 73–84. Dowden, Hutchinson and Ross, Stroudsburg, PA.

Martin, R.G. and Bouma, A.H. (1982) Active diapirism and slope steepening, northern Gulf of Mexico continental slope. *Mar. Geotech.*, **5**, 63–91

Maslin, M., Owen, M., Day, S. and Long, D. (2004) Linking continental-slope failures and climate change; testing the clathrate gun hypothesis. *Geology*, **32**, 53–56

Maurice, F., Locat, J. and Leroueil, S. (2000) Caractéristiques géotechniques et évolution de la couche de sédiment déposée lors du déluge de 1996, dans la Baie des Ha! Ha! (fjord du Saguenay, Québec). *Proceedings of the 53rd Canadian Geotechnical Conference*, Montreal, Quebec.

McAdoo, B.G., Pratson, L.F. and Orange, D.L. (2000) Submarine landslide geomorphology, US continental slope. *Mar. Geol.*, 169, 103–136.

McGregor, B.A. (1977) Geophysical assessment of submarine slide northeast of Wilmington Canyon. *Mar. Geotech.*, **2**, 229–244.

McGregor, B.A., Bennett, R.H. and Lambert, D.N. (1979) Bottom processes, morphology and geotechnical properties of the continental slope south of Baltimore Canyon. *Appl. Ocean Res.*, **1**, 177–187.

McGregor, B.A., Rothwell, R.G., Kenyon, N.H. and Twichell, D.C. (1993) Salt tectonics and slope failure in an area of salt domes in the northwestern Gulf of Mexico. In: *Submarine Landslides: Selected Studies in the U.S. EEZ* (Eds W.C. Schwab, H.J. Lee and D.C. Twichell). *U.S. Geol. Surv. Bull.*, **2002**, 92–96.

Milliman, J.D. and Meade, R.H. (1983) World-wide delivery of river sediment to the oceans. *J. Geol.*, **91**, 1–21.

Mitchell, R.J. (1978) On the retrogression of landslides in sensitive muddy sediments, discussion. *Can. Geotech. J.*, **15**, 446–450.

Molnia, B.F., Carlson, P.R. and Bruns, T.R. (1977) Large submarine slide in Kayak Trough, Gulf of Alaska. *Geol. Soc. Am. Rev. Eng. Geol.*, **3**, 137–148.

Moore, J.G. (1964) Giant submarine landslides on the Hawaiian Ridge. *U.S. Geol. Surv. Prof. Pap.*, **501-D**, D95–D98.

Moore, J.G., Clague, D.A., Holcomb, R.T., *et al.* (1989) Prodigious submarine slides on the Hawaiian Ridge. *J. Geophys. Res.*, **94**, 17,465–17,484.

Morgenstern, N.R. (1967) Submarine slumping and the initiation of turbidity currents. In: *Marine Geotechnique* (Ed. A.F. Richards), pp. 189–210. University of Illinois Press, Urbana, IL.

Mucci, A. and Edenborn, H.M. (1992) Influence of an organic poor landslide deposit on the early diagenesis of iron and manganese in a coastal marine sediment. *Geochem. Cosmochim. Acta*, **56**, 3909–3921.

Mulder, T. and Cochonat, P. (1996) Classification of offshore mass movements. *J. Sediment. Res.*, **66**, 43–57.

Mulder, T. and Syvitski, J.P.M. (1995) Turbidity currents generated at river mouths during exceptional discharges to the world oceans. *J. Geol.*, **103**, 285–299.

Mulder, T., Tisot, J.-P., Cochonat, P. and Bourillet, J.-F. (1994) Regional assessment of mass failure events in the Baie des Anges Mediterranean Sea. *Mar. Geol.*, **122**, 29–45.

Mullenbach, B.I. and Nittrouer, C.A. (2000) Rapid deposition of fluvial sediment in the Eel Canyon, northern California. *Cont. Shelf Res.*, **20**, 2191–2212.

Mullenbach, B.I., Nittrouer, C.A., Puig, P. and Orange, D.L. (2004) Sediment deposition in a modern submarine canyon. *Mar. Geol.*, **211**, 101–119.

Nardin, T.R., Edwards, B.D. and Gorsline, D.S. (1979a) Santa Cruz Basin, California Borderland: dominance of slope processes in basin sedimentation. In: *Geology of Continental Slopes* (Eds O.H. Pilkey and L.J. Doyle), pp. 209–221. Special Publication 27, Society of Economic Paleontologists and Mineralogists, Tulsa, OK.

Nardin, T.R., Hein, F.J., Gorsline, D.S. and Edwards, B.D. (1979b) A review of mass movement processes, sediment and acoustic characteristics and contrasts in slope and base-of-slope systems versus canyon-fan-basin floor systems. In: *Geology of Continental Slopes* (Eds O.H. Pilkey and L.J. Doyle), pp. 61–73. Special Publication 27, Society of Economic Paleontologists and Mineralogists, Tulsa, OK.

Nelson, C.H. (1976) Late Pleistocene and Holocene depositional trends, processes and history of Astoria Deep-Sea Fan, northeast Pacific. *Mar. Geol.*, **20**, 129–173.

Norem, H., Locat, J. and Schieldrop, B. (1990) An approach to the physics and the modelling of submarine landslides. *Mar. Geotech.*, **9**, 93–111.

Normark, W.R., Hess, G.R., Stow, D.A.V. and Bowen, A.J. (1980) Sediment waves on the Monterey Fan Levee: a preliminary physical interpretation. *Mar. Geol.*, **37**, 1–18.

Normark, W.R., Moore, J.G. and Torresan, M.E. (1993) Giant volcano-related landslides and the development of the Hawaiian Islands. In: *Submarine Landslides: Selected Studies in the U.S. EEZ* (Eds W.C. Schwab, H.J. Lee and D.C. Twichell). *U.S. Geol. Surv. Bull.*, **2002**, 184–196.

O'Brien, J.S. and Julien, P.Y. (1988) Laboratory analysis of mudflow properties. *J. Hydraul. Eng., ASCE*, **114**, 877–887.

O'Leary, D.W. (1986) The Munson–Nygren slide, a major lower-slope slide off Georges Bank. *Mar. Geol.*, **72**, 101–114.

Orange, D.L. and Breen, N.A. (1992) The effects of fluid escape on accretionary wedges 2. seepage force, slope failure, headless submarine canyons and vents. *J. Geophys. Res.*, **97**, 9277–9295.

Orange, D.L., McAdoo, B.G., Moore, J.C., Tobin, H., Screaton, E., Chezar, H., Lee, H., Reid, M. and Vail, R. (1997) Headless submarine canyons and fluid flow on the toe of the Cascadia accretionary complex. *Basin Res.*, **9**, 303–312.

Orange, D.L., Yun, J., Maher, N., Barry, J. and Greene, G. (2002) Tracking California seafloor seeps with bathymetry, backscatter and ROVs. *Cont. Shelf Res.*, **22**, 2273–2290.

Orange, D.L., Saffer, D., Jeanjean, P., *et al*. (2003) Measurements and modeling of the shallow pore pressure regime at the Sigsbee Escarpment: successful prediction of overpressure and ground-truthing with borehole measurements. *Proceedings, Offshore Technology Conference (CD-ROM)*, 11 pp.

Parsons, J.D., Whipple, K.X. and Simoni, A. (2001) Experimental study of the grain-flow, fluid-mud transition in debris flows. *J. Geol.*, **109**, 427–447.

Perret, D. (1995) *Diagénèse mécanique précoce des sédiments fins du fjord du Saguenay*. Unpublished PhD thesis, Department of Geology and Geological Engineering, Laval University, 412 pp.

Perret, D., Locat, J. and Leroueil, S. (1995) Strength development with burial in fine-grained sediments from the Saguenay Fjord, Québec. *Can. Geotech. J.*, **32**, 247–262.

Piper, D.J.W. and Aksu, A.E. (1987) The source and origin of the 1929 Grand Banks turbidity current inferred from sediment budgets. *Geo-Mar. Lett.*, **7**, 177–182.

Piper, D.J.W. and Normark, W.R. (1982) Acoustic interpretation of Quaternary sedimentation and erosion on the channeled upper Laurentian Fan, Atlantic margin of Canada. *Can. J. Earth Sci.*, **19**, 1974–1984.

Piper, D.J.W., Cochonat, P. and Morrison, M.L. (1999) The sequence of events around the epicentre of the 1929 Grand Banks earthquake: initiation of debris flows and turbidity current inferred from sidescan sonar. *Sedimentology*, **46**, 79–97.

Ploessel, M.R., Crissman, S.C., Rudat, J.H., Son, R., Lee, C.F., Randall, R.G. and Norton, M.P. (1979) Summary of potential hazards and engineering constraints, proposed OCS Lease Sale No. 48, offshore Southern California. *Proceedings, 11th Offshore Technology Conference*, Houston, TX, pp. 355–363.

Poulos, S.G., Castro, G. and France, J.W. (1985) Liquefaction evaluation procedure. *J. Geotech. Eng., ASCE, 111*, 772–791.

Prior, D.B. (1984) Submarine landslides. *Proceedings of the IV International Symposium on Landslides*, Toronto, Vol. 2, pp. 179–196.

Prior, D.B. and Coleman, J.M. (1978) Disintegrating, retrogressive landslides on very low subaqueous slopes, Mississippi Delta. *Mar. Geotech.*, **3**, 37–60.

Prior, D.B. and Coleman, J.M. (1979) Submarine slope instability. In: *Slope Instability* (Eds D. Brunsden and D.B. Prior), pp. 419–455. John Wiley & Sons, Chichester.

Prior, D.B., Wiseman, W.J. and Gilbert, R. (1981) Submarine slope processes on a fan delta, Howe Sound, British Columbia. *Geo-Mar. Lett.*, **1**, 85–90.

Prior, D.B., Bornhold, B.D., Coleman, J.M. and Bryant, W.R. (1982a) Morphology of a submarine slide, Kitimat Arm, British Columbia. *Geology*, **10**, 588–592.

Prior, D.B., Coleman, J.M. and Bornhold, B.D. (1982b) Results of a known sea-floor instability event. *Geo-Mar. Lett.*, **2**, 117–122.

Prior, D.B., Bornhold, B.D. and Johns, M.W. (1986a) Active sand transport along a fjord-bottom channel, Bute Inlet, British Columbia. *Geology*, **14**, 581–584.

Prior, D.B., Yang, Z.S., Bornhold, B.D., *et al*. (1986b) Active slope failure, sediment collapse and silt flows on the modern subaqueous Huanghe (Yellow River) Delta. *Geo-Mar. Lett.*, **6**, 85–95.

Puig, P., Ogston, A.S., Mullenbach, B.L., Nittrouer, C.A. and Sternberg, R.W. (2003) Shelf-to-canyon sediment-transport processes on the Eel continental margin (northern California). *Mar. Geol.*, **193**, 129–149.

Puig, P., Ogston, A.S., Mullenbach, B.I., *et al*. (2004) Storm-induced sediment gravity flows at the head of the Eel submarine canyon, northern California margin. *J. Geophys. Res.*, **109** CO3019, doi: 10.1029/2003JC001918.

Puig, P., Ogston, A.S., Guillen, J., Fain, A. and Palanques, A. (In press) Sediment transport processes from the topset to the foreset of a crenulated clinoform (Adriatic Sea). *Cont. Shelf Res.*

Rabinovich, A.B., Thomson, R.E., Kulikov, E.A., *et al*. (1999) The landslide-generated tsunami November 3, 1994, in Skagway. *Geophys. Res. Lett.*, **26**, 3009–3012.

Reimnitz, E. (1972) Effects in the Copper River delta. In: *The Great Alaska Earthquake of 1964*, Vol. 6, *Oceanography and Coastal Engineering*, pp. 290–302. National Research Council, National Academy of Sciences, Washington, DC.

Reynolds, S. (1987) A recent turbidity current event, Hueneme Fan, California: reconstruction of flow properties. *Sedimentology*, **34**, 129–137.

Richards, A.F. (1976) Marine geotechnics of the Oslofjorden region. In: *Laurits Bjerrum Memorial Volume* (Eds N. Janbu, F. Jorsted and B. Kjaernasli), pp. 41–63. Norwegian Geotechnical Institute, Oslo.

Richardson, M.D., Young, D.K. and Briggs, K.B. (1983) Effects of hydrodynamic and biological processes on sediment geoacoustic properties in Long Island Sound, U.S.A. *Mar. Geol.*, **51**, 201–226.

Richmond, W.C. and Burdick, D.J. (1981) Geologic hazards and constraints of offshore northern and central California. *Proceedings, 13th Offshore Technology Conference*, Houston, TX, Vol. 4, pp. 9–17.

Robb, J.M. (1984) Spring sapping on the lower continental slope, offshore New Jersey. *Geology*, **12**, 278–282.

Saffer, D.M. and Bekins, B.A. (1999) Fluid budgets at convergent plate margins: Implications for the extent and duration of fault-zone dilation. *Geology*, **29**, 1095–1098.

Sangrey, D. (1977) Marine geotechnology – state of the art. *Mar. Geotech.*, **2**, 45–80.

Schwab, W.C. and Lee, H.J. (1983) Geotechnical analyses of submarine landslides in glacial marine sediment, northeast Gulf of Alaska. In: *Glacial Marine Sedimentation* (Ed. B.F. Molnia), pp. 145–184. Plenum press, New York.

Schwab, W.C., Lee, H.J. and Molnia, B.F. (1987) Causes of varied sediment gravity flow types on the Alsek prodelta, northeast Gulf of Alaska. *Mar. Geotech.*, **7**, 317–342.

Schwab, W.C., Lee, H.J., Twichell, D.C., *et al*. (1996) Sediment mass-flow processes on a depositional lobe, outer Mississippi Fan. *J. Sediment. Res.*, **66**, 916–927.

Schwehr, K. and Tauxe, L. (2003) Characterization of soft-sediment deformation; detection of cryptoslumps using magnetic methods. *Geology*, **31**, 203–206.

Schwehr, K., Driscoll, N., Tauxe, L. and Lee, H. (2003) Exploration of the Humboldt Slide using anisotropy of magnetic susceptibility comparison with the Gaviota slide. *Proceedings, American Geophysical Union Fall Meeting*, Abstract OS22A-1150.

Seed, H.B. (1968) Landslides during earthquakes due to soil liquefaction. *J. Soil Mech. Found. Div., ASCE*, **94**, 1055–1122.

Seed, H.B. and I.M. Idriss (1971) Simplified procedure for evaluating soil liquefaction potential. *J. Soil Mech. Found. Eng. Div., ASCE*, **97**, 1249–1273.

Seed, H.B. and Rahman, M.S. (1978) Wave-induced pore pressure in relation to ocean floor stability of cohesionless soils. *Mar. Geotech.*, **3**, 123–150.

Seed, H.B., Seed, R.B., Schlosser, F., Blondeau, F. and Juran, I. (1988) *The Landslide at the Port of Nice on October 16, 1979*. Report No. UCB/EERC-88/10, Earthquake Engineering Research Center, University of California, Berkeley, 68 pp.

Shepard, F.P. (1951) Mass movements in submarine canyon heads. *Eos* (*Trans. Am. Geophys. Union*), **32**, 405–418.

Shepard, F.P. (1955) Delta-front valleys bordering the Mississippi distributaries. *Geol. Soc. Am. Bull.*, **66**, 1489–1498.

Shepard, F.P. and Marshall, N.F. (1973) Storm-generated current in La Jolla Submarine Canyon, California. *Mar. Geol.*, **15**, Ml9–M24.

Shi, Y. and Wang, C.Y. (1988) Generation of high pore pressures in accretionary prisms: inferences from the Barbados subduction complex. *J. Geopys. Res.*, **93**, 8893–8910.

Shipboard Scientific Party (1995) Site 930. In: *Proceedings of the Ocean Drilling Program, Initial Reports*, Vol. 155 (Eds R.D. Flood, D.J.W. Piper, A. Klaus, *et al.*), pp. 87–122. College Station, TX.

Silva, A.J. (1974) Marine geomechanics: overview and projections. In: *Deep-Sea Sediments, Physical and Mechanical Properties* (Ed. A.L. Inderbitzen), pp. 45–76. Plenum Press, New York.

Silva, A.J., Baxter, C.D.P., LaRosa, P.T. and Bryant, W.R. (2004) Investigation of mass wasting on the continental slope and rise. *Mar. Geol.*, **203**, 355–366.

Silver, M.L., Chan, C.K., Ladd, R.S., *et al.* (1976) Cyclic triaxial strength of standard test sand. *J. Geotech. Eng. Div., ASCE*, **102**, 511–523.

Skempton, A.W. (1953) Soil mechanics in relation to geology. *Proc. York. Geol. Soc.*, **29**, 33–62.

Sterling, G.H. and Strohbeck, G.E. (1973) The failure of South Pass 70B Platform in Hurricane Camille. *Proceedings, 5th Offshore Technology Conference*, Vol. 1, pp. 123–150.

Suhayda, J.N. and Prior D.B. (1978) Explanation of submarine landslide morphology by stability analysis and rheological models. *Proceedings, 10th Annual Offshore Technology Conference*, Houston, TX.

Sultan, N., Cochonat, P., Bourillet, J.F. and Cayocca, F. (2001) Evaluation of the risk of marine slope instability: a psuedo–3D approach for application to large areas. *Mar. Geores. Geotech.*, **19**, 107–133.

Sultan, N., Cochonat, P., Foucher, J.P., *et al.* (2003) Effect of gas hydrates dissociation on seafloor slope stability. In: *Submarine Mass Movements and their Consequences* (Eds J. Locat and J. Mienert), pp. 103–111. Kluwer, Dordrecht.

Suwa, H. (1988) Focusing mechanism of large boulders to a debris-flow front. *Trans. Jpn. Geomorphol. Union*, **9**, 151–178.

Syvitski, J.P.M. and Farrow, G.E. (1983) Structures and processes in bayhead deltas: Knight and Bute Inlet, British Columbia. *Sediment. Geol.*, **36**, 217–244.

Syvitski, J.P.M., Burrell, D.C. and Skei, J.M. (1987) *Fjords: Processes and Products*. Springer-Verlag, New York, 379 pp.

Tanaka, H. and Locat, J. (1999) A microstructural investigation of Osaka Bay clay: impact of microfossils on its mechanical behavior. *Can. Geotech. J.*, **36**, 493–508.

Tappin, D.R., Matsumoto, T. and Shipboard Scientists (1999) Offshore surveys identify sediment slump as likely cause of devastating Papua New Guinea Tsunami 1998. *Eos* (*Trans. Am. Geophys. Union*), **80**, 329, 334, 340.

Tappin, D.R., Watts, P. and Matsumoto, T. (2003) Architecture and failure mechanism of the offshore slump responsible for the 1998 Papua New Guinea Tsunami. In: *Submarine Mass Movements and their Consequences* (Eds J. Locat and J. Mienert), pp. 383–389. Kluwer, Dordrecht.

Terzaghi, K. (1956) Varieties of submarine slope failures. In: *Proceedings, 8th Texas Conference of Soil Mechanics and Foundation Engineering*, pp. 1–41. Special Publication 29, Bureau of Engineering Research, Texas University.

Thornton, S.E. (1986) Origin of mass flow sedimentary structures in hemipelagic basin deposits: Santa Barbara Basin, California Borderland. *Geo-Mar. Lett.*, **6**, 15–19.

Traykovski, P., Geyer, W.R., Irish, J.D. and Lynch, J.F. (2000) The role of wave-induced density driven mud flows for cross-shelf transport on the Eel River continental shelf. *Cont. Shelf Res.*, **20**, 2113–2140.

Van Kessel, T. and Kranenburg, C. (1998) Wave-induced liquefaction and flow of subaqueous mud layers. *Coast. Eng.*, **34**, 109–127

Varnes, D.J. (1958) Landslide types and processes. In: *Landslides and Engineering Practice* (Ed. E.D. Eckel), pp. 20–47. Special Report 29, Highway Research Board, Washington, DC.

Whipple, K.X. (1997) Open-channel flow of Bingham fluids: applications in debris-flow research. *J. Geol.*, **105**, 243–262.

Whipple, K.X. and Dunne, T. (1992) The influence of debris-flow rheology on fan morphology, Owens Valley, California. *Geol. Soc. Am. Bull.*, **104**, 887–900.

Woodbury, H.O. (1977) Movement of sediments of the Gulf of Mexico Continental Slope and Upper Continental Shelf. *Mar. Geotech.*, **2**, 263–274.

Woodcock, N.H. (1979) Sizes of submarine slides and their significance. *J. Struct. Geol.*, **1**, 137–142.

Wynn, R.B., Weaver, P.P.E., Ercilla, G., Stow, D.A.V. and Masson, D.G. (2000) Sedimentary processes in the Selvage sediment-wave field, NE Atlantic; new insights into the formation of sediment waves by turbidity currents. *Sedimentology*, **47**, 1181–1197.

Xiao, H. and Suppe, J. (1992) Origin of rollover. *Bull. Am. Assoc. Petrol. Geol.*, **76**, 509–529.

Young, A.G., Bryant, W.R., Slowey, N.C., Brand, J.R. and Gartner, S. (2003) Age dating of past slope failures of the Sigsbee Escarpment within Atlantis and Mad Dog developments. *Proceedings of the Offshore Technology Conference* (CD-ROM).

Yun, J.W., Orange, D.L. and Field, M.E. (1999) Subsurface gas offshore of northern California and its link to submarine geomorphology. *Mar. Geol.*, **154**, 357–368.